A review of the fraction of four-coordinated boron in binary borate glasses and melts

OPEN ACCESS
IOP Publishing
Reports on Progress in Physics
Rep. Prog. Phys. **88** (2025) 076501 (58pp)
https://doi.org/10.1088/1361-6633/adc69c

Review

A review of the fraction of four-coordinated boron in binary borate glasses and melts

Oliver L G Alderman[1], Nagia S Tagiara[2], Ian Slagle[3], Rebecca M Gabrielsson[4], Piper Boggs[4], Molly Wagner[5], Aaron Rossini[5], Sophia John[4], Leilani Rocha[4], Robert M Wilson[4], Harry Hawbaker[4], Steve W Martin[6], Alex C Hannon[1], Efstratios I Kamitsos[2] and Steve A Feller[4,*]

[1] ISIS Facility, Rutherford Appleton Laboratory, Chilton, Didcot, Oxon OX11 0QX, United Kingdom
[2] Theoretical and Physical Chemistry Institute, National Hellenic Research Foundation, 48 Vassileos Constantinou Ave, 11635 Athens, Greece
[3] Department of Materials Science, Georgia Institute of Technology, Atlanta, GA 30332, United States of America
[4] Physics Department, Coe College, Cedar Rapids, IA 52402, United States of America
[5] Ames National Lab, Ames, IA 50011, United States of America
[6] Materials Science and Engineering Department, Iowa State University, Ames, IA 50011, United States of America

E-mail: sfeller@coe.edu

Received 20 November 2024, revised 11 March 2025
Accepted for publication 28 March 2025
Published 3 July 2025

Corresponding editor: Dr Mei-Yin Chou

Abstract

In borate materials, boron is found predominantly in either trigonal planar, or tetrahedral coordination states with oxygen, which are the two most ubiquitous building blocks of borate glasses. The fraction of tetrahedral boron, N_4, is found to vary considerably with both glass composition and applied pressure, as well as with fictive temperature – a result of its underlying dependence on temperature in the molten and supercooled liquid states. As such, the parameter N_4 is of fundamental structural importance, along with the mechanisms driving its evolution and its strong influence on thermophysical material properties. N_4 in glasses has been experimentally determined using a variety of means including nuclear magnetic resonance (NMR) spectroscopy, vibrational spectroscopy, and x-ray and neutron diffraction. In this review, we discuss how the techniques for the measurement of N_4 have evolved and improved since the pioneering x-ray diffraction measurements of the 1930s, up to the present day. A database is compiled of the available *high-quality* numerical experimental data for N_4, with a non-exclusive focus on binary borate glasses of the form RM_2O_z–B_2O_3 where R is the molar ratio of modifier to boron oxide and M is a metal cation of formal charge $z+$, other than boron. In addition, we

* Author to whom any correspondence should be addressed.

report new N_4 values for a series of strontium borate glasses, measured by ^{11}B magic angle spinning NMR, where a disparity in the literature is found. Based on the findings of the review, we are able to point to the gaps in our knowledge where future resources could best be focused, as well as summarizing overarching trends, the present state-of-the-art, and making recommendations for best practices.

Supplementary material for this article is available online

Keywords: borates, N_4, binary, diffraction, NMR, Raman, infrared

Contents

1. Introduction

In borate glasses, boron atoms commonly bond either to three oxygen atoms in a BO_3 trigonal planar arrangement, or to four oxygen atoms in a BO_4 tetrahedral arrangement. For pure boron oxide, B_2O_3, the ambient pressure forms are known to contain only trigonal BO_3 units. For example, in the ambient pressure crystal phase B_2O_3-I [1], each boron atom is bonded to three oxygen atoms with mean bond length of 1.369 Å and mean O–$\hat{B}$–O bond angle of 119.89°. There is considerable evidence to show that in B_2O_3 glass there are similar trigonal BO_3 sites [2]. However, as we will discuss in this review, the addition of a modifier (*i.e.* metal oxide, such as Li_2O) to B_2O_3, or the application of pressure, can result in a structure in which a fraction, N_4, of the boron atoms are tetrahedral. The main emphasis of this paper is to review the various methods of measuring N_4 in a wide variety of borate glass systems.

The mechanism for the formation of 4-coordinated borons is illustrated in this section. Figure 1(a) shows a fragment of a borate glass network formed of trigonal BO_3 units, as in pure, glassy B_2O_3. The addition of a modifier oxide, M_2O_z, (where M^{z+} is a modifier cation of valence z) to the material introduces surplus oxygen, which needs to be accommodated in the structure. Figure 1(b) shows how an additional oxygen atom can be incorporated into the borate network by breaking a B–O–B bridge (the oxygen forming the bridge is called a bridging oxygen (BO) Ø), and creating two non-BOs (NBOs). The breaking of bridges and the creation of NBOs is the normal mechanism for the incorporation of additional oxygen in systems such as silicates and phosphates. Alternatively, as shown in figure 1(c), an additional oxygen atom can be incorporated into the borate network by converting two boron atoms from three-coordination to four-coordination. For a binary borate of composition RM_2O_z-B_2O_3, the number of surplus oxygen atoms per boron atom is $Rz/2$, where z is related to the theoretical rate at which four-coordinated borons are formed. Thus, if all surplus oxygen atoms are incorporated by the mechanism shown in figure 1(c), the number of BO_4 units per boron atom is $N_4 = Rz$. For $z = 1$, the relation is $N_4 = R$, for z =3, it is $N_4 = 3R$. For $z = 2$ the glass composition is often written simply as RMO-B_2O_3 and so, again, $N_4 = R$, whilst for z =

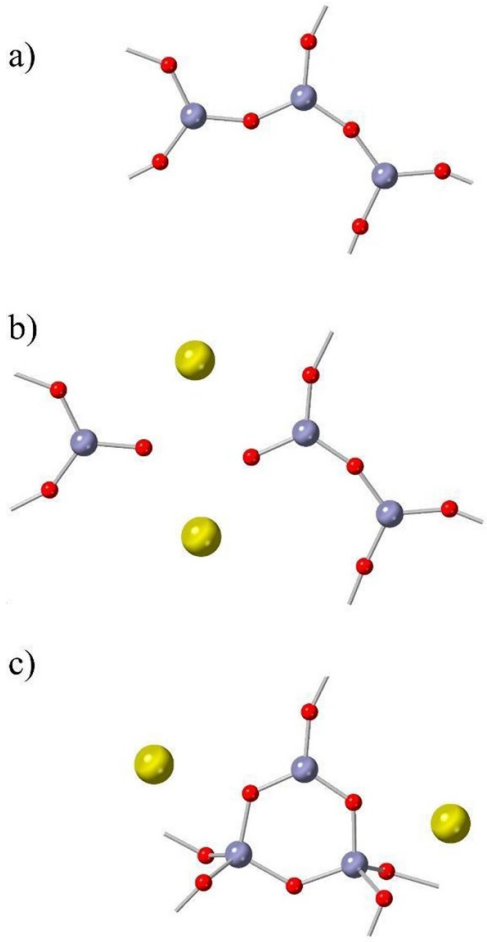

Figure 1. (a) A fragment of the borate network (larger blue spheres are boron atoms, and smaller red spheres are oxygen atoms). (b) The network fragment in figure (a) is shown after the incorporation of one unit of M_2O modifier by the conversion of one bridging oxygen to two NBOs (yellow spheres without bonds are modifier cations, M^+). (c) The network fragment in (a) is shown after the incorporation of one unit of M_2O modifier by the conversion of two BO_3 units to BO_4. (Note that this arrangement of atoms has been drawn to illustrate simply the way in which four-coordinated boron arises; it should not be taken to indicate whether or not BO_4 units exist in close proximity to each other, or to imply the presence of a particular superstructural unit).

4, defining the compositions as RMO_2-B_2O_3 leads to the relation $N_4 = 2R$. The point here is that the relationship between N_4 and composition parameter of course depends on how that parameter is defined.

The compositions of binary borate glasses are commonly expressed in terms of either the molar ratio, R, or the molar fraction of modifier, x (in which case the composition is xM_2O_z–(1-x)B_2O_3). These two parameters are related according to the following equations:

$$R = \frac{x}{1-x} \quad \text{and} \quad x = \frac{R}{1+R}. \tag{1.1}$$

There is interest in the behavior of N_4 due to its probable relation to the borate anomaly (also called the boron anomaly). The composition dependence of most thermophysical properties of borate glasses shows a maximum or minimum, typically at ∼15–30 mol% $M_{2/z}O$. The physical property measurements reported by Shelby [3] are an excellent example of this behavior in alkali borate glasses. This behavior has been known for many decades (for example, see Gooding and Turner [4]), and it is in sharp contrast to the monotonic behavior for silicate glasses, which has led to it being regarded as anomalous. The first evidence for the evolution of four-coordinated boron in borate glass was reported by Biscoe and Warren [5], who used x-ray diffraction on sodium borate glasses to show an increase in the boron-oxygen coordination number (CN) as Na_2O is added to B_2O_3. It was proposed that the property maxima and minima could be explained in terms of the change in boron CN. However, the extrema of different properties occur at different compositions, and a more modern view is that the change in boron CN is one of several factors that govern the borate anomaly [3].

As we show in this review, most experimental evidence for binary borate glass systems shows that for low modifier content, the measured values of N_4 are commonly close to the ideal $N_4 = R$ relation. Then, as the modifier content increases, the measured values of N_4 generally reach a maximum and subsequently decrease, exhibiting a behavior that is similar to the changes in physical properties associated with the borate anomaly. This behavior is evidence that BO_4 formation (figure 1(c)) is the dominant mechanism for incorporation of modifiers for low values of R, but that NBO formation is the dominant mechanism for high values of R.

In principle, other structural mechanisms are possible. For example, the high pressure crystal phase B_2O_3-II [6] has only tetrahedral BO_4 units (*i.e.* it has $N_4 = 1$, even though $R = 0$); each boron atom is bonded to four oxygen atoms with mean bond length 1.476 Å and mean O–$\hat{B}$–O bond angle 109.35°. To understand how this higher CN arises, it is useful to note that the O–B and B–O CNs are necessarily related:

$$n_{O-B} = n_{B-O}\frac{c_B}{c_O} \tag{1.2}$$

where c_B and c_O are the atomic fractions of boron and oxygen. Thus, for pure B_2O_3, a B–O coordination of four corresponds to an O–B CN of 8/3 ≈ 2.67. In B_2O_3-II, two thirds of the oxygen atoms are three-coordinated by boron, rather than acting as BOs between two boron atoms (as in figure 1(a)). Thus, the formation of three-coordinated oxygen causes an increase in the value of N_4, and can lead to values greater than predicted by the $N_4 = R$ relation. On the other hand, linear BO_2 units are rare, but not unknown, in crystal structures [7]. Topologically, a BO_2 unit can be formed in a network of BO_3 units (as in figure 1(a)) by breaking a single B–O bond; in that case, the presence of BO_2 units leads to an increase in the number of NBOs.

Borates are unusual in that they have superstructural units (well-defined rings formed by a small number of boron triangles and tetrahedra, most commonly three). It is well established that the structure of pure B_2O_3 glass includes a large number of $B_3O_3Ø_3$ boroxol groups [2] (highly planar rings of three BO_3 units). The structure of B_2O_3 glass in terms of the fraction of B atoms in boroxol-rings has been found to corresponds to the majority of boron atoms; that is ∼0.82–0.85

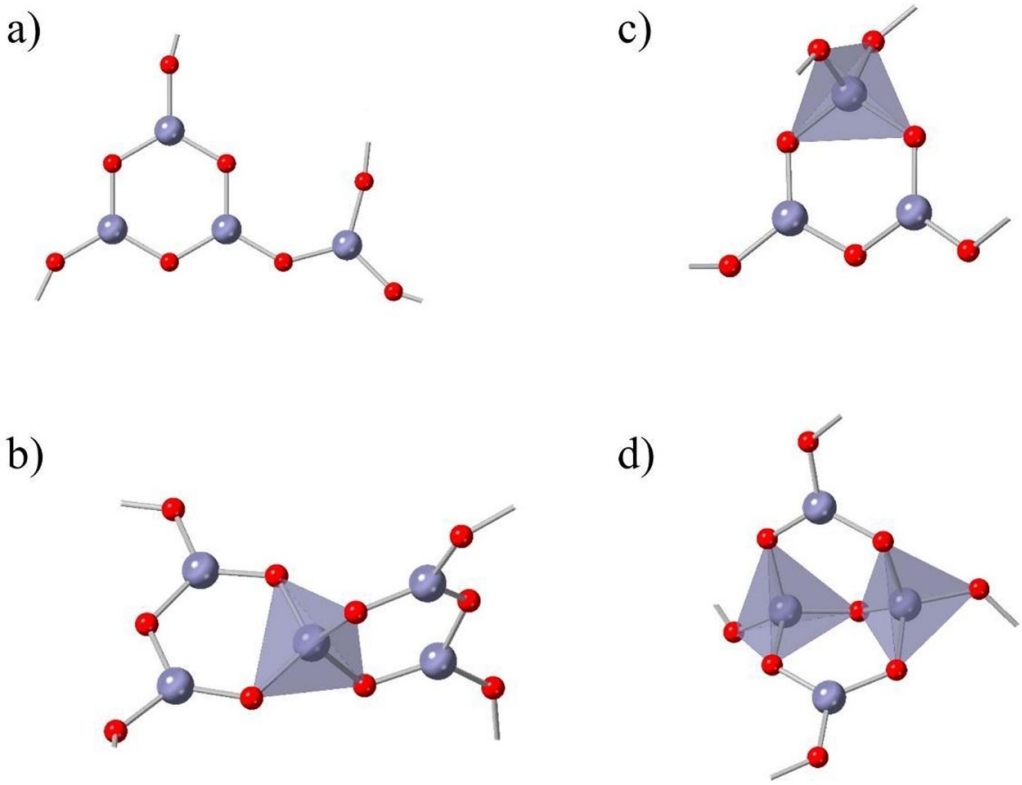

Figure 2. Some of the more important superstructural units in borates, shown for increasing concentration of BO_4 tetrahedra. Larger blue spheres are boron atoms, and smaller red spheres are oxygen atoms. Four-coordinated boron atoms are shown surrounded by a tetrahedron. (a) A boroxol ring, shown bonded to an independent BO_3 unit, (b) a pentaborate ring, (c) a triborate unit, (d) a diborate unit.

based on ^{10}B, ^{11}B and ^{17}O NMR [8, 9] and the nuclear quadrupole resonance (NQR) studies of Bray and coworkers [10, 11], 0.80 ± 0.05 according to neutron diffraction and inelastic neutron scattering studies of Hannon *et al* [12], 0.72 based on the NMR study by Kroeker and Stebbins [13], 0.73 ± 0.01 by ^{11}B double rotation (DOR) NMR spectroscopy [14] and by other means such as inelastic neutron scattering which determined the fraction to be very close to 2/3 [2]. The remainder of the boron atoms are arranged in independent BO_3 units, as shown in figure 2(a). As the modifier content is increased, and the number of BO_4 units increases and then declines, a succession of different superstructural units occurs. Figure 2 shows some of the more important superstructural units in borates. A comprehensive consideration of the superstructural units in borate structures has been given by Wright [15]. The number of basic units (BO_3 or BO_4) in the rings of the superstructural units is relatively small (usually three) compared to the rings that occur in other glass forming systems, due to the relatively large O–$\hat{B}$–O bond angle of 120° in the BO_3 units [2, 16]. As a result of the small size of the rings, they are well defined and often planar, leading to sharp vibrational modes that are detectable by Raman spectroscopy [16, 17].

Recently, it has been discovered that edge-sharing can occur between two BO_4 tetrahedra in some crystalline borates (see figure 3). This structural feature was first observed in the high-pressure phase of $Dy_4B_6O_{15}$ [18], where it involves a very short B…B distance of 2.098 Å. Then it was found to occur in additional high-pressure phases, before subsequently being discovered in ambient pressure phases, starting with $KZnB_3O_6$ [19]. Typically, it has been found in metaborate crystals (*i.e.* 50 mol% B_2O_3). Figure 3 shows the sharing of an edge between two BO_4 tetrahedra in the ambient pressure crystal phase of $Li_4Na_2CsB_7O_{14}$ [20]. It should be noted that BO_2 units and edge-shared BO_4 tetrahedra have only been discovered relatively recently in crystalline compounds, and to our knowledge evidence has not currently been found for the presence of these structural features in glasses. It will be interesting to see if such evidence emerges in the future. The occurrence of edge-shared tetrahedra does not have a direct effect on the value of N_4, but it would be likely to have an indirect influence.

Now, we shift our attention to the fact that borates are not the only glass-forming system in which the glass former cation can change CN. For example, the average Ge CN can become larger than four in germanate glasses [21], whilst the Te CN may become less than four in tellurite glasses [22]. However, the exact nature of the structural changes in germanates and tellurites is still under discussion. In contrast, it has been thoroughly established that ambient B_2O_3 glass involves only three-coordinated boron, and that there are two possible boron CNs in borates, either three or four. We can represent the coordination change by the relationship: $B\text{Ø}_3 + {}^1/_2\,O^{2-} \rightarrow [B\text{Ø}_4]^-$, where Ø is a BO. Also, the creation of NBOs (O^-) is a possibility by the following formula: $B\text{Ø}_3 + {}^1/_2\,O^{2-} \rightarrow [B\text{Ø}_2O]^-$. Thus there is an equilibrium relationship, $[B\text{Ø}_2O]^- \rightleftarrows [B\text{Ø}_4]^-$. It is observed that the formation of $[B\text{Ø}_4]^-$ is energetically preferred at low modifications of the

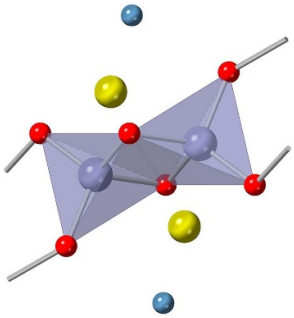

Figure 3. The pair of edge-sharing BO_4 tetrahedra in the ambient pressure crystal phase $Li_4Na_2CsB_7O_{14}$ [20]. Boron atoms are shown by the larger gray spheres at the center of a tetrahedron of four oxygen atoms, shown as smaller red spheres. Spheres without bonds show sodium (larger yellow spheres) and lithium (smaller blue spheres) atoms.

borate network (see further discussion below). Thus, borates are ideally suited to the study of the phenomenon of changing CNs in glasses.

In this review, we mostly restrict our attention to binary borate systems. Nevertheless, the structural study of these systems is of direct relevance to glasses with more complex compositions (for example the commercial borosilicate Pyrex® [23] or to thioborates based on the glass former B_2S_3).

We will now discuss the various methods that have been used to measure N_4: NMR, vibrational spectroscopy, and neutron and x-ray scattering techniques.

2. Nuclear magnetic resonance methods

2.1. Introduction

NMR spectroscopy principally relies on the interaction of the magnetic dipole moments of atoms' nuclei with an external magnetic field (Zeeman effect). Various additional interactions give rise to a spectrum with rich structural implications. These interactions include the magnetic dipole-dipole interaction (the alteration of the magnetic field seen by a given nucleus due to neighboring dipole moments), the chemical shift (the shielding effect due to the electrons opposing the external magnetic field), and for nuclei with a spin greater than or equal to 1 ($I \geqslant 1$), the quadrupole interaction (the changes in the energy levels due to the interaction of the quadrupole moment of the nucleus with the gradient of the electric field from bonding electrons) [24].

^{11}B, the most common isotope for determining N_4 by NMR has a spin of 3/2. This results in quadrupolar perturbed transitions including a central transition ($-1/2 \rightarrow 1/2$) and two satellite transitions ($1/2 \rightarrow 3/2$ and $-3/2 \rightarrow -1/2$). In static NMR, it was usually the case that the central transition was observed. In magic angle spinning (MAS) NMR, effects due to the satellite transitions are perceived and must be accounted for.

MAS NMR allows for the elimination of the dipole-dipole interaction. To accomplish this, the sample is spun at tens of kilohertz at the magic angle of 54.74 degrees. The result is a narrowing and sharpening of the resulting NMR spectrum, allowing for more precise determination of N_4, particularly at high magnetic fields.

For ^{11}B MAS NMR the chemical shift results in an isotropic shift that is different for three- and four-coordinated borons. For relatively large fields, 14.1 T or greater, substantial separation occurs between the three- and four-coordinated borons, allowing clear separation and quantification of each. This magnetic field strength dependence of the separation between three-and four-fold boron resonances arises due to the quadrupolar interaction, which gives rise to both quadrupole induced shifts and broadenings, even under MAS conditions.

The quadrupole interaction is characterized by two parameters: the quadrupole coupling constant C_Q, which is proportional to the z-component (largest component) of the electric field gradient tensor, and the asymmetry parameter η, which is a measure of the cylindrical symmetry in the xy-plane (η may take values between 0, completely cylindrically symmetric, and 1). Trigonal borons with either three BOs or three NBOs have η near 0. For trigonal borons with one or two NBOs, η is typically greater than 1/2. The C_Q of the three- and four-coordinated ^{11}B in borate glasses are roughly 2.5 MHz and 0.5 MHz respectively. For ^{10}B, these values are approximately doubled.

Boron NMR is notable for its use to determine N_4 due to its inherently quantitative results: in the integrated NMR spectrum, the areas of the peaks associated with the three- and four-coordinated borons are nearly proportional to the population of each of the species:

$$N_4 = \frac{n_4}{n_3 + n_4} \approx \frac{A_4}{A_3 + A_4} \tag{2.1}$$

where n is the population of the nth species, and A_n is the relative area of the peak corresponding to the nth species. Equation (2.1) is subject to usually small corrections due to the effects of the spinning sidebands on the areas of the three- and four-coordinated boron resonances, as described by Massiot *et al* [25]. The CN dependent C_Q leads to a different shape of the two peaks arising from the two different coordinations of boron, aiding identification. Specifically, the larger C_Q of the trigonal sites leads to broader spectral features, as compared to the relatively sharper ones arising from the tetrahedral sites.

2.2. Historical determination of N_4 by NMR

In 1958, Arnold Silver and Phil Bray published pioneering work on NMR in borate glasses [26]. Figure 4(a), obtained from glassy B_2O_3, depicts the first derivative of a classic second order quadrupole line shape characteristic of trigonal planar boron. The spectrum was observed using a permanent magnet of field strength just over 0.5 T (^{11}B radiofrequency of 7.177 MHz), and the measured C_Q was 2.76 MHz.

In the same paper, Silver and Bray also explored sodium borate glasses [26]; figure 4(b) shows a boron spectrum, composed of the quadrupolar broadened second order response due to trigonal boron, as well as a narrow symmetric response near

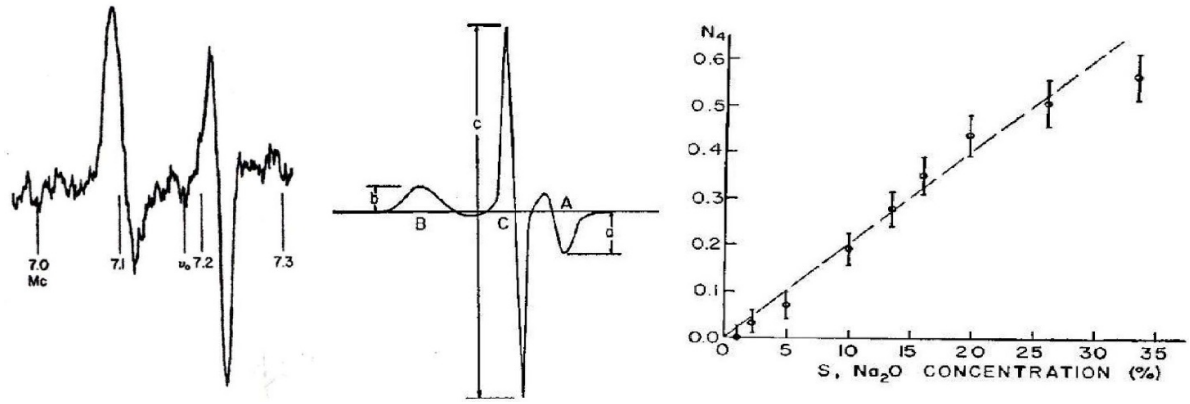

Figure 4. All figures above are from Silver and Bray [26], ((a), left) ^{11}B NMR derivative spectrum from boron oxide glass, ((b), middle) Typical NMR derivative response from a sodium borate glass that shows three and four coordinated boron, ((c), right) The fraction of four-coordinated boron as a function of sodium oxide content in sodium borate glasses. Reprinted from Silver, A.; Bray, P. Nuclear Magnetic Resonance Absorption in Glass. I. Nuclear Quadrupole Effects in Boron Oxide, Soda-Boric Oxide, and Borosilicate Glasses. J. Chem. Phys. 1958, 29 (5), 984–990, https://doi.org/10.1063/1.1744697 with the permission of AIP Publishing.

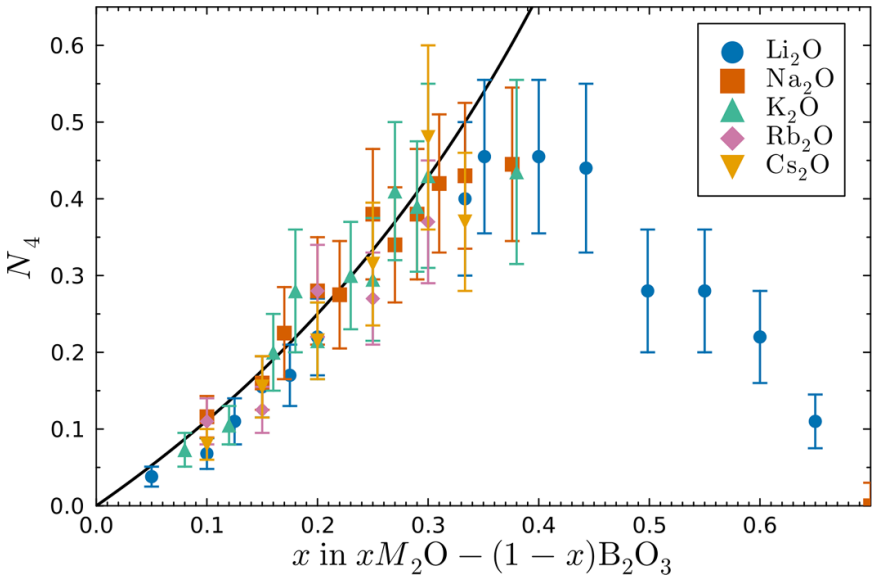

Figure 5. The fraction of four-coordinated boron in alkali borate glasses as found by Bray and O'Keefe [27]. The black curved line is the relation $N_4 = x/(1\text{-}x)$ where x is the molar fraction of alkali oxide.

the Larmor (operating) frequency. This new line was identified as originating from tetrahedral boron that resulted from sodium oxide modifying the borate network. This peak was narrower due to the reduced quadrupolar coupling constant, though later it was found to still be quadrupolar broadened [25], just to a lesser extent than the response from the trigonal borons [28].

Silver and Bray did not integrate the spectrum computationally; rather they assumed the normalized shape of the peaks to be constant, used the height as a proxy for area, and utilized the observation that B_2O_3 is fully three-coordinated. By this methodology, Silver and Bray found N_4 as a function of sodium oxide concentration, as shown in figure 4(c) [26].

By 1963, Bray and O'Keefe [27] determined the fraction of four-coordinated boron in alkali borate glasses, see figure 5. In this paper, the fraction of four-coordinate boron was found by a comparison of the NMR intensity to a standard. This standard was chosen to be crystalline sodium borohydride because N_4 in this crystal is equal to one [29]. This resulted in a relative error in N_4 of about ± 0.04; this is similar to the relative error in Silver and Bray's 1958 paper [26]. However, there is additional systematic error in the 1958 paper due to the broadening of the wide line part of the spectrum, resulting in an overestimation of N_4. In fact, the authors themselves discussed this bias at some length [26, 27].

By 1970, computerized techniques began to be used; before this time, chart recorders were employed for the output. With digital computers, spectra could be signal averaged and programs could be written to automatically determine numerical integrals or areas under curves (see figure 6(a) for part of the experimental spectrometer setup for doing solid state wideline NMR during this time period). The fitting program

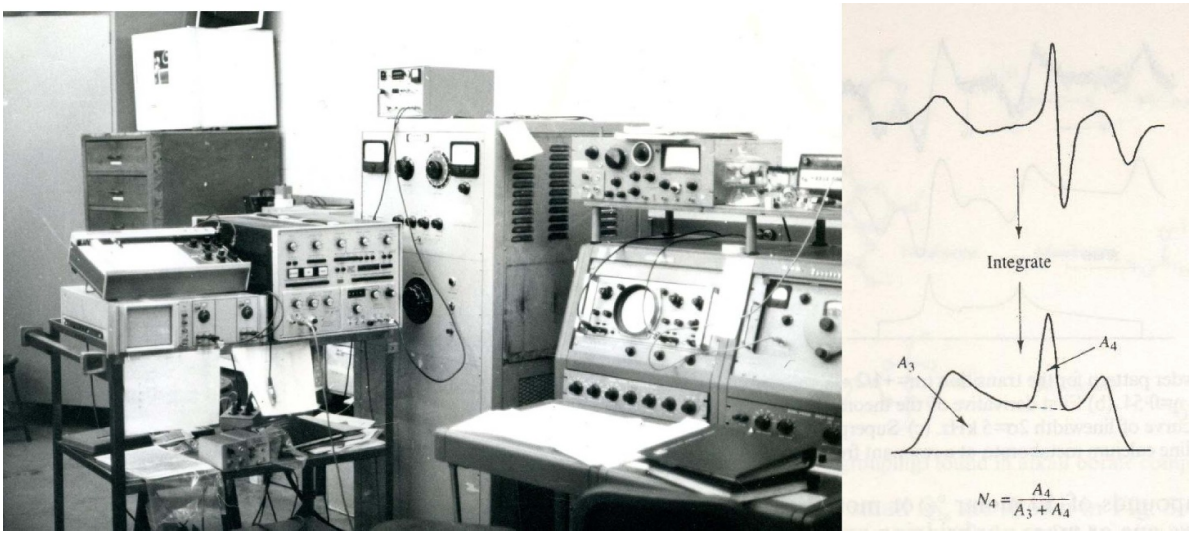

Figure 6. (a) Wideline NMR spectrometer for measuring N_4 circa 1975 from Prof. Phil Bray's lab at Brown University. The chart recorder sits on an oscilloscope and is the furthest instrument to the left. The computerized signal averager is to the right of the chart recorder. The magnet power supply is to the right of the signal averager. In this *Continuous Wave* (CW) setup the magnetic field was swept by varying the magnet's electric current for a fixed Larmor NMR radio frequency, (b) signal averaged wide line NMR derivative spectrum circa 1975–1980. Shown below the experimental spectrum is the numerical integration from which areas were determined digitally.

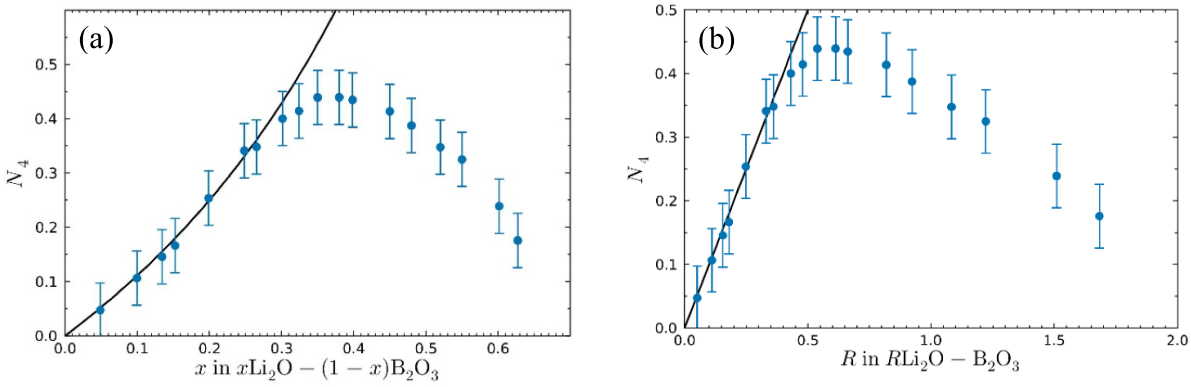

Figure 7. (a) Jellison, Feller, and Bray [30] reported N_4 versus mole fraction Li_2O, x, from lithium borate glasses. (b) N_4 as a function of R, the molar ratio of lithium oxide to boron oxide. Note the resulting linear regions that simplify modeling.

of Taylor and Bray allowed NMR line shapes to be simulated [31, 32]; however, a significant practical drawback was that it used a mainframe computer that required batch jobs. Another approach allowed for the derivative spectrum, a result of modulation, output from the signal averager to be numerically integrated, allowing area to be measured directly (see figure 6(b)). The first to employ this methodology for binary borate glasses was the group of Werner Müller-Warmuth, and Bray employed this in 1976 [33, 34].

Such techniques were employed by Jellison *et al* [30] to find more precise values for N_4 in lithium borate glasses, as shown in figure 7(a). The error in N_4 was reduced to about ± 0.01, considerably better than earlier results. As shown earlier in 1963 [27], for lithium borate glasses, N_4 initially closely follows the $N_4 = x/(1\text{-}x) = R$ curve shown in figure 7(a). It is often useful to plot N_4 also as a function of R, see figure 7(b), because in this representation, N_4 tends to follow linear trends, not only in the low R region prior to the maximum where it is increasing, but also in the high R region, after the maximum, where it declines.

In 1989, another study of N_4 for alkali borates was conducted by Zhong and Bray [35] who found an alkali dependence *of* N_4 above $R = 0.2$ as shown in figure 8(a). An alternative method of acquiring the experimental data, known as adiabatic fast passage, was employed in this work. At $R = 0.167$, the N_4 from each of the alkali borate glasses was essentially the same at $N_4 = 0.16$ [31, 32]. Above $R = 0.4$, the N_4 values were found to be alkali dependent with N_4 decreasing as atomic number of the modifier increases.

In 1990, MAS was first applied to binary borate glasses [37, 38], and most N_4 measurements since have been made using MAS NMR. MAS eliminates effects due to dipolar and 1st order quadrupolar broadening, narrowing the spectra, allowing for more precise N_4 determination. However, the correction required to account for the satellite transitions [25] in MAS NMR measurements was first applied in

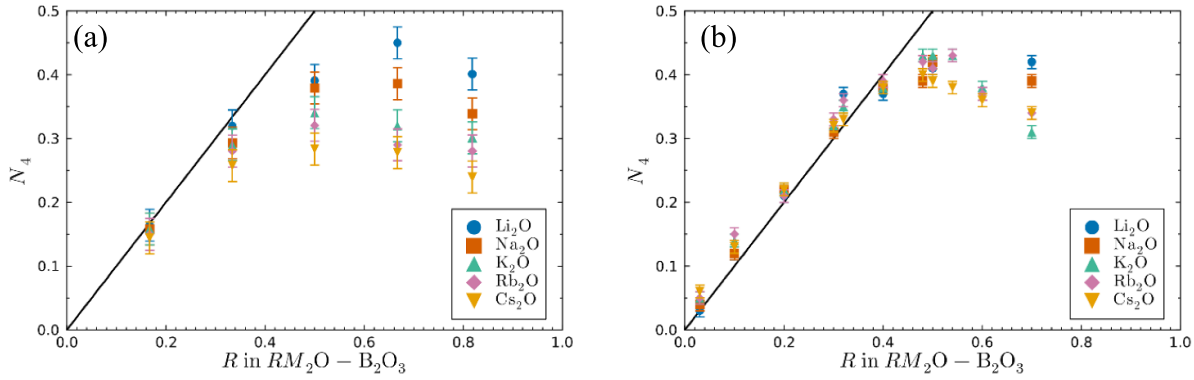

Figure 8. (a) Zhong and Bray's N_4 for alkali borate glasses [35]. We note that the figure in the original paper is discrepant compared to the text of that paper, in that data at $R = 0.2$ are shown in the figure, whereas the text states sample compositions of $R = 0.167$. We have plotted at this latter composition in our reproduction above. (b) N_4 for alkali borate glasses after Kroeker *et al* [36]. The plot represents results from ^{11}B MAS NMR taken at 14.1 T.

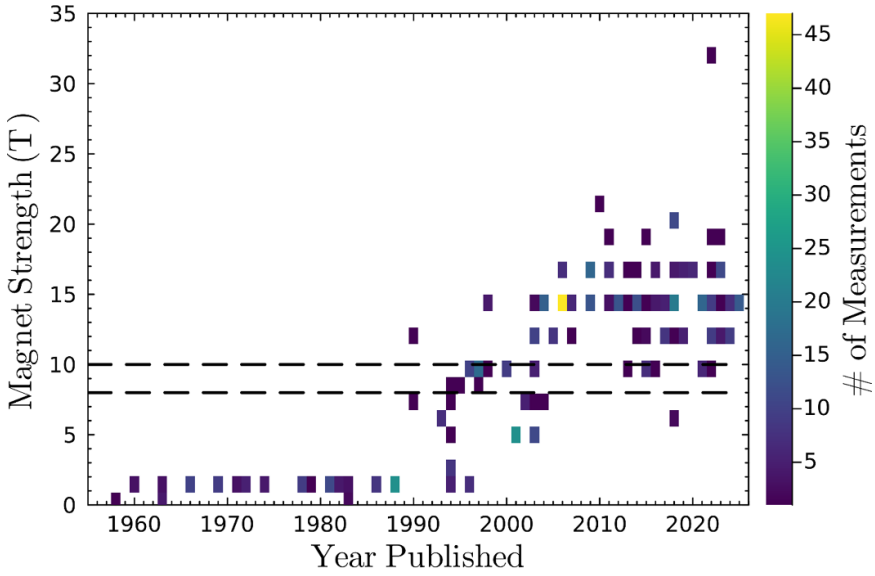

Figure 9. The historical distribution of the magnet strength of N_4 measurements where the magnet strength is unambiguously specified, and the measurements are otherwise high quality [6, 27, 32, 36–38, 40–171]. Dashed horizontal lines indicate 8 and 10 T, the range of magnetic field strength for which N_4 determinations cannot be considered high quality, see main text.

2000 [39], and is unfortunately not ubiquitous in modern MAS NMR N_4 determinations. Due to the narrowing of the spectra, N_4 determination from MAS NMR benefits from increasing the magnetic field, and that has also taken off since 1990 (figure 9).

One issue that arose in this transition to higher fields is that between 8–10 T, the four-coordinated boron resonance overlaps with one of the peaks in the second order quadrupolar lineshape arising from the three-coordinated borons, which causes their separation to require computer simulation, and even then, there are enough degrees of freedom in the fitting that the N_4 determination can be unreliable. The first binary borate glass measurement, with the four-coordinated environment resolved from that of the three-coordinated was published in 1998 and used a 14.1 T field [40], which has become a popular field strength for such measurements, although the commonly used 11.7 T is also sufficient to resolve the two resonances. The increased magnetic fields (in the most extreme case exceeding 30 T [41]) have allowed ^{11}B MAS NMR to yield rapid and precise measurements of the fraction of four-coordinated boron, though higher fields do limit the information that can be gained regarding the quadrupolar interactions, due to their diminished influence.

In 2005, Kroeker *et al* [36] studied alkali borates using MAS NMR performed at 14.1 T. At that magnetic field, the chemical shift difference between the three- and four-coordinated boron is enough to nearly completely separate the respective spectral features, figure 10(a), making determination of N_4 easier.

The resulting N_4 fractions are shown in figure 8(b). Like the Zhong and Bray results [35], N_4 is initially independent of alkali. Above $R \approx 0.5$, N_4 is alkali dependent, in the same direction as, but to a lesser extent than reported by Zhong and Bray [35]. Also, whereas the data of Zhong and Bray initially

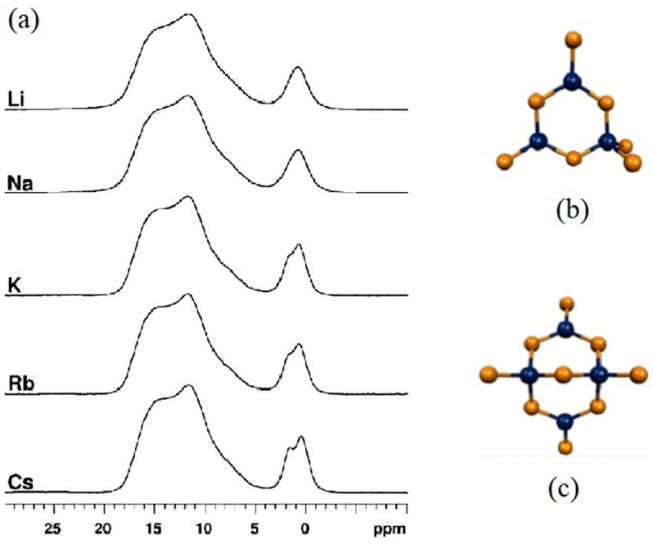

Figure 10. (a) ^{11}B MAS NMR from alkali borate glasses with $R = 0.1$ at a 14.1 T field [36] (b) triborate superstructural unit, and (c) diborate superstructural unit. (a) Reproduced with permission from Kroeker, S.; Aguiar, P.; Cerquiera, A.; Okoro, J.; Clarida, W.; Doerr, J.; Olesiak, M.; Ongie, G.; Affatigato, M.; Feller, S. A. Alkali Dependence of Tetrahedral Boron in Alkali Borate Glasses. Phys. Chem. Glasses-Eur. J Glass Sci. Tech Proc. Fifth Int. Conf. Borate Glass Cryst. Melts 2006, 47 (4), 393–396.

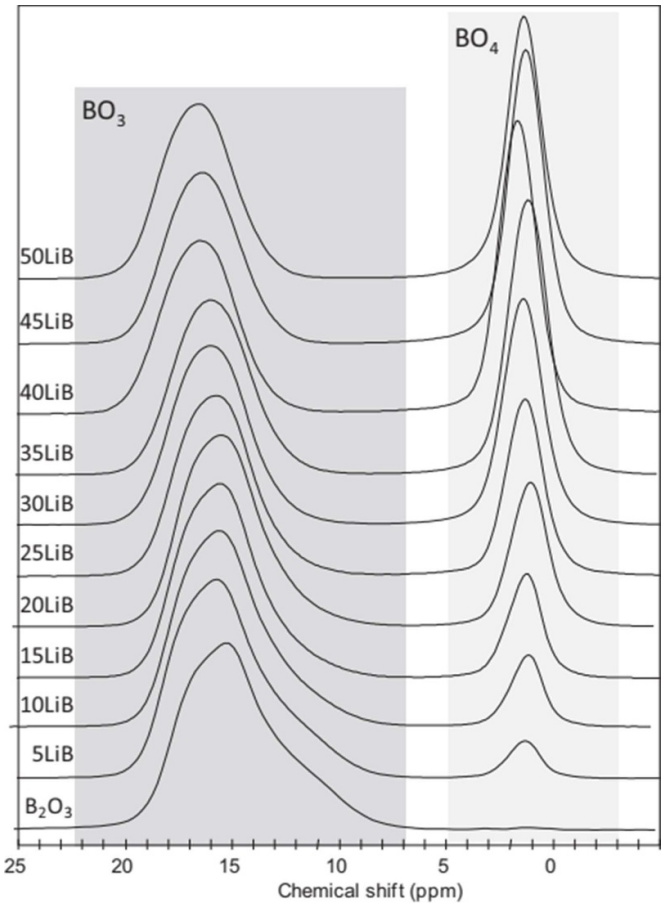

Figure 11. ^{11}B MAS NMR spectra of lithium borate glasses obtained at 20 T [42]. Reprinted from Montouillout, V.; Fan, H.; del Campo, L.; Ory, S.; Rakhmatullin, A.; Fayon, F.; Malki, M. Ionic Conductivity of Lithium Borate Glasses and Local Structure Probed by High Resolution Solid-Sate NMR. J. Non-Cryst. Solids 2018, 484, 57–64. https://doi.org/10.1016/j.jnoncrysol.2018.01.020 Copyright 2018 with permission from Elsevier.

fell below $N_4 = R$, at low R, the data of Kroeker *et al* initially very slightly exceeded $N_4 = R$ [36].

Additionally, due to the high magnet strength, a new feature was resolved in the four-coordinated boron peak (manifold). Two tetrahedral boron environments are apparent for K, Rb, Cs, and possibly for Na borate glasses. Kroeker *et al* [36] show that this was due to distinct chemical shifts of tetrahedral boron in different superstructural groups, see figures 10(a)–(c). Kroeker *et al* further speculated that it is likely that the high frequency component is due to the diborate or di-triborate groups and the low frequency feature is due to the triborate superstructural grouping.

In 2018 ^{11}B MAS NMR was performed on the lithium borate system at 20 T (Larmor frequency of 272.8 MHz) [42]. The boron-free rotor was spun at 20 kHz. With stronger fields, the chemically shifted trigonal and tetrahedral boron features separate yet further, figure 11. Notice the superb signal to noise ratio and the complete separation of the three and four-coordinated boron species resonances in figure 11. The corresponding plot of N_4 vs R is provided in figure 12 and shows that $N_4 = \mathrm{R}$ up to approximately $R = 0.38$.

2.3. Review of NMR measurements of N_4

A survey of the literature was conducted for N_4 measurements of binary borate glasses [26, 27, 32, 34, 36–38, 40–141, 144–146, 160–162, 164–181]. In total, 646 high-quality measurements were collected, covering 25 different modifying oxides. The distribution of modifiers as found in the literature is shown in figure 13(a). This table is color coded to indicate the number of N_4 values reported for each modifying element oxide.

Figure 13(b) displays the full compilation of the N_4 values from binary borate glasses found using NMR indicated in figure 13(a). High-quality measurements means, for our purposes, that the method of analyzing the spectra is appropriate, no crystallization was observed, the magnet strength was not between 8 and 10 T (or unspecified and published 1990 or later), the glass was not pressurized, and either the glass synthesis was a solution technique, or the melting container is specified and is not silica or alumina without measuring for this material contaminating the glass. It is likely that these criteria err on the side of being too strict, as many older papers do not specify the melting container, for example. That said, these criteria *do not* reject measurements made using MAS NMR without accounting for spinning sideband corrections. Two studies have been excluded for being otherwise unexplained severe outliers [50, 142]. One study with binary alumina borates is excluded, as the melting temperature is substantially below the reported liquidus [182, 183]. The N_4 for strontium borate glasses, which are anomalously high in the work of Park and Bray [50], were checked by synthesizing new glasses and measuring them for this paper.

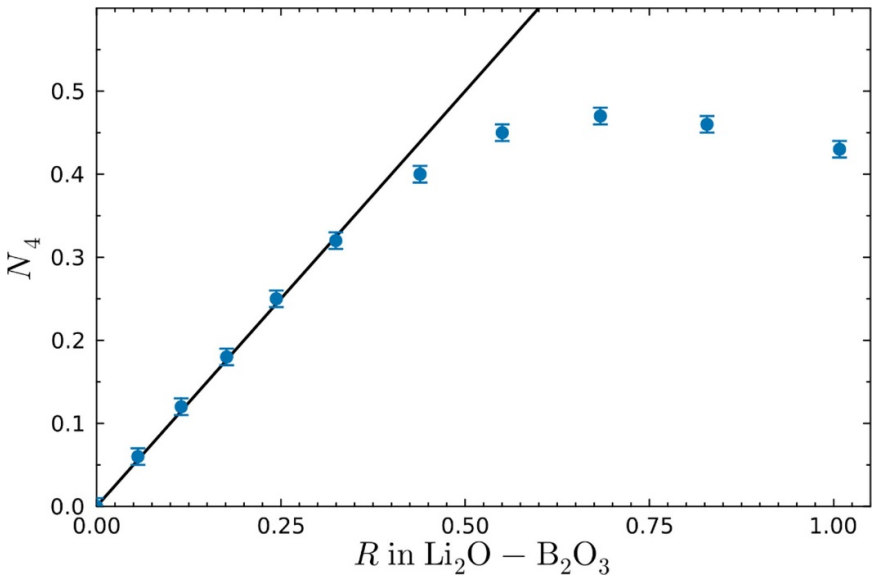

Figure 12. N_4 vs R for lithium borates from the study of Montouillout *et al* [42].

We recognize that other criteria might be considered necessary to fully satisfy the statement that the data are of 'high quality'. This includes the influence of fictive temperature, the possible composition change due to volatilization of one or more components of the glass, and possible nanoscale phase separation or unobserved crystallization in otherwise clear glasses. However, we have chosen out of necessity to proceed without further consideration of these effects. The supplemental section provides further details pertinent to the quality of the N_4 data. Several of these binary borate glass systems contain immiscibility regions, where two liquids are present in the melt. In some situations, the glasses were melted in this immiscibility region, which could lead to unobserved phase separation. In other cases, the quench passes through the immiscibility region, which again may lead to unobserved phase separation, depending on the quenching rate. In some studies, the melting temperature is not reported, but where it is, we have included that information in the table in our supplemental information. Subliquidus (metastable) immiscibility regions have not been considered here by us. The authors were not able to find published phase diagrams for SnO–and Sb_2O_3–B_2O_3, and so we were unable to check for the presence of immiscibility regions, or for use of inappropriate (subliquidus) melting temperatures used for glass making in the literature. The phase diagrams of the alkali borates [183–195], and SiO_2– [196, 197], P_2O_5– [198], and Ag_2O–B_2O_3 [184, 199] glasses do not contain immiscibility regions. The phase diagrams of GeO_2– [198], PbO– [183, 200], Bi_2O_3– [183, 201] and Y_2O_3–B_2O_3 [202] glasses contain immiscibility regions, but only for compositions where there are not any high-quality NMR N_4 measurements. For the remaining modifiers (alkaline earth [183, 203–207], ZnO [183, 208], TeO_2 [209], La_2O_3 [183, 210], CdO [183, 211], MnO [212], Tl_2O [84, 213]), there are glasses formed in those regions, with otherwise high-quality NMR N_4 measurements. For this paper, we will still consider those points high quality but we have not used these points in the analysis below for checking the hypothesis of $N_4 = R$ in low-modifier alkaline earth borate glasses. Additionally, the glasses melted in or through an immiscibility region are noted in the table in the supplemental information.

We can investigate statistically the hypothesis that N_4 is equal to R at low modification for alkali and alkaline earth borate glasses. Linear regressions were performed on $N_4(R)$ for both alkali and alkaline earth borate systems to determine the slope below $R = 0.4$, see figures 14(a) and (b). The intercept was fixed at zero during fitting, as this is likely the most agreed-upon point in all of borate glass NMR [38, 42, 43, 48, 59, 62, 68, 116], but unmodified $x = 0$ glasses are not used in this analysis. Figures 14(a) and (b) and table 1 show the regression results. While the analysis of the alkali borate glasses rejects the hypothesis that $N_4 = R$ in this region, the slope being only slightly higher may instead be explained by the systematic errors caused by not correcting for spinning sideband effects, for example.

2.4. An example of a discrepancy between strontium borate results

As can be seen from figure 15(b) there is a discrepancy between literature values for N_4 from the strontium borate system. In particular, the values reported by Park and Bray [50] are significantly higher than other reported values in the literature [61] in the x $>$ 35 mol% SrO region. In order to investigate this, a series of strontium borate glasses were prepared by plate quenching from the melt and ^{11}B MAS NMR was performed on the samples.

The strontium borate glasses ($R = 0.5$, 0.6, 0.7, 0.8, 0.9, and 1.0) were prepared by melting appropriate amounts of reagent grade or better $SrCO_3$ and H_3BO_3 at 1200 °C in platinum crucibles. The samples were heated for a total of 25 min, a weight loss measurement was performed after 15 min, and the melts were then plate quenched after a final 10 min in the

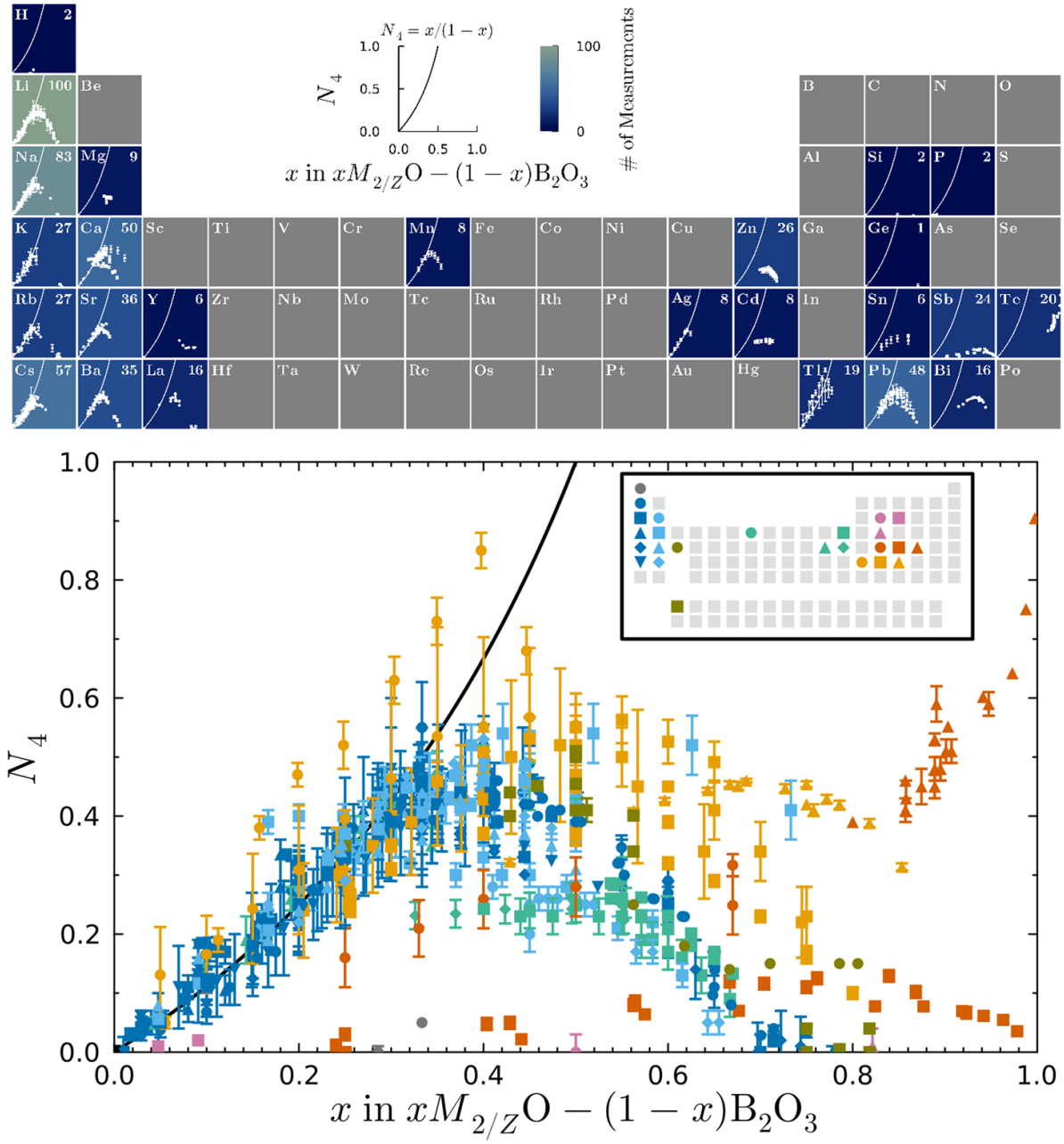

Figure 13. (a) Number of high-quality NMR data points for N_4 for each modifying element (oxide), as found in the literature. The data are color coded by the number of reported values, according to the color bar in the legend. Small plots of N_4 vs. x are overlaid to give the general shape of the trend for each modifier (b) N_4 values as determined by NMR measurements from the literature [26, 27, 32, 34, 36–38, 40–141, 144–146, 160–162, 164–181]. Color and shape of the symbols indicate the modifier as depicted on the periodic table inset, and the black curve shows $N_4 = x/(1\text{-}x)$. Compositions are normalized to a single oxygen per x moles of modifier oxide, so that a single $N_4 = R$ curve is appropriate for all data sets.

furnace. Weight loss measurements on 6 gram batches were within between 0.04 g to 0.10 g of expectations, indicating the reactions proceeded to completion, evolving all of the volatile CO_2 and H_2O side products. The samples were crushed to a powder for subsequent ^{11}B MAS NMR experiments. No further treatment was applied to the samples.

Solid-state NMR spectroscopy experiments were performed on a 14.1 T (ν_0 (^{1}H) = 600 MHz; $\nu_0(^{11}\text{B}) = 192.51$ MHz) Bruker wide-bore magnet equipped with a Bruker Neo console and a 2.5 mm triple resonance MAS NMR probe configured in double resonance (^{1}H-^{11}B) mode. The ^{1}H and ^{11}B channels were isolated with bandpass filters.

The ^{11}B central transition (CT)-selective $\pi/2$ and π pulse lengths were 15 μs and 30 μs, respectively, corresponding to an 8.3 kHz RF field and 16.7 kHz CT nutation frequency. Quantitative $\pi/18$ single-pulse ^{11}B NMR spectra were recorded with a pulse duration of 1.4 μs and recycle delay of 7.5 s. DM-FIT was used to fit the spectra. Corrections for spinning sideband intensities were made [25].

An example of a spectrum and resulting fit is shown in figure 15(a) and the N_4 results are shown below in figure 15(b).

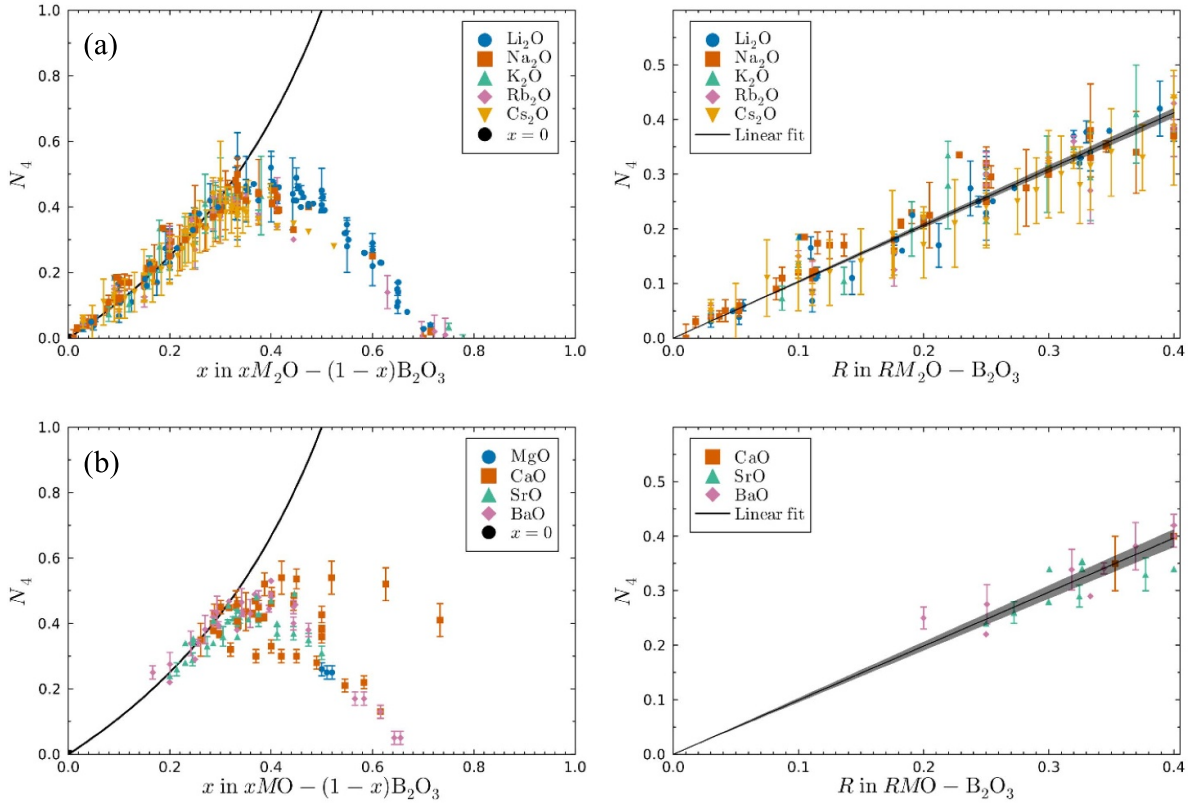

Figure 14. N_4 values as determined by NMR measurements of ((a), upper panels) alkali borate glasses in literature [6, 27, 32, 36, 38, 40–43, 46, 48, 49, 55, 59, 60, 62, 64, 65, 68–72, 74, 77, 81–83, 85, 88, 90, 93, 97–99, 102, 104–106, 108, 111, 112, 116–118, 120, 123, 128–130, 132–138, 141, 144, 161, 162, 164–168, 170–172, 176–178, 180, 181] and ((b), bottom panels) alkaline earth borates [38, 42, 43, 45, 48, 50, 53, 59, 61, 62, 68, 79, 87, 90, 92, 95, 96, 101, 107, 110, 115, 116, 122, 126, 127, 130, 131, 160, 173, 176, 179].

Table 1. Linear regression results for the $0 < R \leqslant 0.4$ alkali and alkaline earth borate systems with intercept 0. The p-value is for a comparison against the null hypothesis of $N_4 = R$.

System	n	Slope	Standard error	p-value	Reject/fail to reject H_0 of $N_4 = R$ with 95% confidence
Alkali	147	1.031	0.011	0.0070	Reject
Alkaline Earth	21	0.991	0.020	0.6609	Fail to reject

Clearly the new data do not support the results of Park and Bray [50], whereas those of Yang, Torimoto, Jin and Moon *et al* were closely replicated and verified with increased precision [61, 107, 110, 122]. We have also been able to extend the range of $N_4(R)$ measurements to higher R in the Sr borate glass system, clearly showing the decline in $N_4(R)$ as NBOs become increasingly abundant.

2.5. Summary of NMR-determined N_4 measurements

We have collated a large number of NMR determinations of N_4 by performing a thorough literature review. One example of the utility of this approach was discussed in section 2.4 where strontium borate NMR results were reviewed. Based on the literature there was a large discrepancy between reported values (Park and Bray vs Yang, Torimoto, Jin and Moon *et al*) [50, 61, 107, 110, 122]. This discrepancy was resolved by making a series of strontium borate glasses and independently determining N_4 using ^{11}B MAS NMR. The results of Park and Bray were confirmed to be outliers, and should be discarded, at least for x > 35 mol% SrO.

N_4 may also be found by other spectroscopic techniques including infrared (IR) and Raman as well as x-ray and neutron scattering. In the next part of the paper, we examine vibrational techniques that have been used to determine N_4, and in the subsequent section, x-ray and neutron scattering methods are used for N_4 determiantion.

3. Vibrational spectroscopy methods

3.1. Introduction

IR and Raman are complementary techniques of vibrational spectroscopy, and are well-known analytical tools for

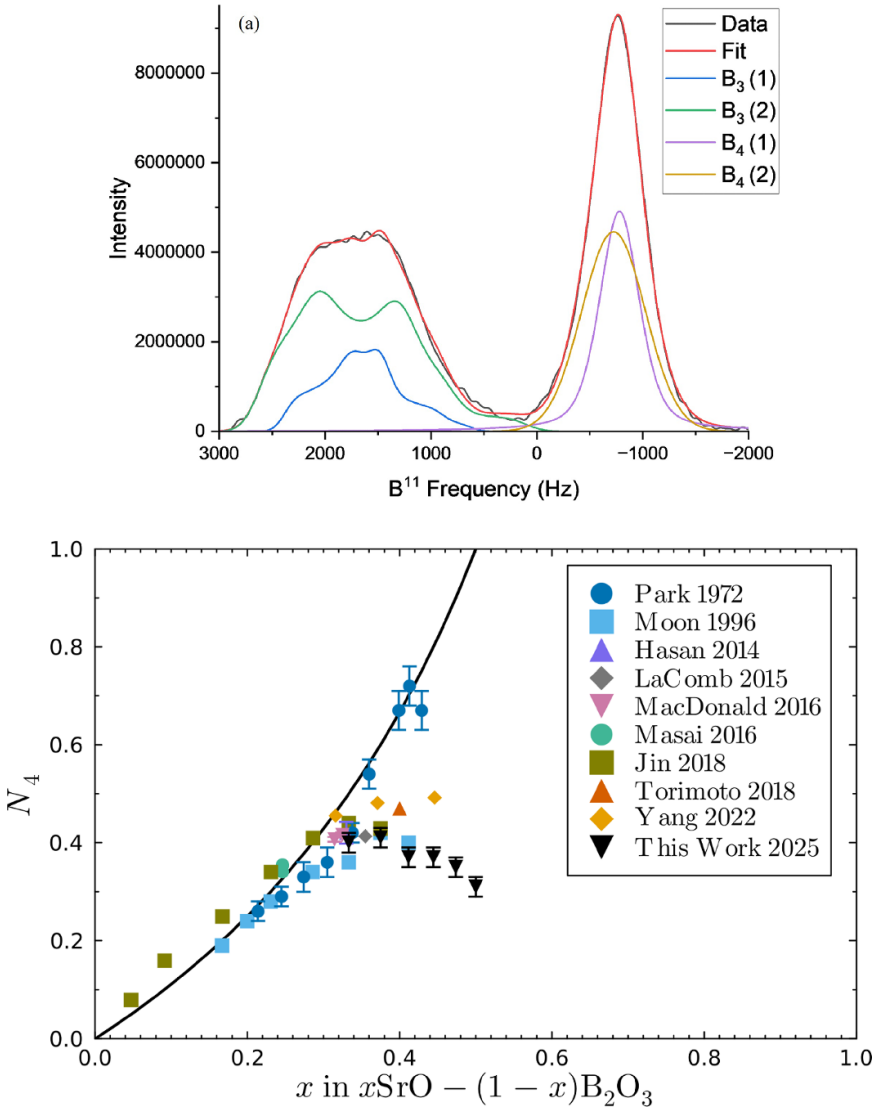

Figure 15. (a) NMR spectra from the 0.7SrO-B_2O_3 ($x = 0.41$) glass sample produced for this study. It is composed of two B_3 and two B_4 peaks, as specified in the legend, and corresponds to an N_4 value of 0.37, (b) new N_4 values from strontium borates performed for this study compared to values from past studies [50, 61, 87, 92, 95, 96, 107, 110, 122].

structural studies of glasses, since bonds constituting the glass structure can vibrate in a broad part of the spectrum covering the far-IR (10–500 cm^{-1}) and mid-IR (500–5000 cm^{-1}) frequency ranges [214–216]. While both techniques are important for structural studies, this section focuses on IR spectroscopy because it is more effective than Raman in quantifying the borate structure in terms of the fraction of four-coordinated boron atoms, N_4.

Early comprehensive studies by IR spectroscopy on crystalline anhydrous borates were reported by Weir and Lippincott [217], Hart and Smallwood [218] and Weir and Schroeder [219], and concern mainly borate compounds with relatively high modification levels. IR spectra were recorded on thin films produced in a diamond cell [217], on powdered materials dispersed in KBr pressed disks [218], and on films deposited on KBr and CsBr windows by evaporating suspensions in light petroleum oil, i.e. the mull sampling technique [219]. Measured IR bands were assigned to borate anionic species like metaborates, $[BO_2]^-$, pyroborates, $[B_2O_5]^{4-}$ and orthoborates, $[BO_3]^{3-}$. Also, absorption bands tabulated for more than 80 borate compounds allowed the identification of IR bands characteristic of boron in 3-fold and 4-fold coordination [219]. More recent studies include the IR spectra of crystalline metaborates with infinite chain structures, $(BO_2)_n^{n-}$, using dispersions in KBr discs [220], and the combination of Raman with IR reflectance spectroscopy to classify metaborate crystals according to their tendency to form chain-, $(BO_2)_n^{n-}$, or ring-type, $[B_3O_6]^{3-}$, metaborate structures [221].

Applications of IR spectroscopy to borate glasses go back to the fifties and earlier, and refer to glasses such as boron oxide and soda borates [222], alkali borates [223], boron oxide and lithium borates [224], and vitreous B_2O_3-xH_2O [225]. These early IR investigations were conducted on powdered glasses using the KBr disk technique [222], on polished glass samples employing the reflectance technique [223], on thin film specimens drawn from the melt by dipping a platinum ring or by blowing bulbs with very thin walls [224], and by the Nujol mull technique [225]. The study of Anderson *et al*

[222] showed that hydrogen bonds play an important role in the atomic arrangement of the B_2O_3 and the low soda content glasses. For the B_2O_3 glass in particular, it was suggested that it consists of $[B_9O_{14}]^-$ complexes held together by hydrogen bonds between oxygen atoms [222]. One of the nine borons in the complex is tetrahedrally coordinated and the other borons are triangularly coordinated to oxygen. When Na_2O is added to the glass, the number of $[B\emptyset_4]^-$ tetrahedra and B–O–B bridges increase. Other IR studies suggested a structure for B_2O_3 glass made up of boron-oxygen triangles, $B\emptyset_3$, where each oxygen atom is shared by two boron atoms in adjacent triangles [223–225], noting that weak absorption measured at about 1000–1110 cm^{-1} was taken to indicate the presence of a small proportion of $[B\emptyset_4]^-$ tetrahedral units [224]. Also, water was detected in boron oxide glass as manifested by strong IR absorption at 3300 cm^{-1} due to the O–H stretching vibration [224], and was suggested to lead to hydrogen bonding between oxygen atoms [224, 225]. The IR absorption spectra of alkali borate glasses showed a lower proportion of water than that retained in boron oxide glass. Addition of alkali oxides to B_2O_3 was found to decrease the intensity of bands attributed to $B\emptyset_3$-containing units (400, 719, 885, 1250, 1430 cm^{-1}) in favor of new bands (950, 1055, 1330 cm^{-1}) associated with $[B\emptyset_4]^-$-containing units [224].

In his pioneering studies [226, 227], Krogh–Moe showed that the IR spectra of alkali borate glasses are consistent with the group model where the borate triangular and tetrahedral units are arranged into superstructural groups similar to those found in crystalline borates like pentaborate (K_2O–$5B_2O_3$), triborate (Cs_2O-$3B_2O_3$), and diborate (Li_2O–$2B_2O_3$), see figure 2 of the introduction section. For boron oxide glass, Krogh–Moe reviewed previous IR studies and concluded that the $B\emptyset_3$ triangles are arranged in planar boroxol rings (see ring in figure 2(a)) which form the glass network [226, 227]. Raman spectroscopy provided strong support to the group structural model of Krogh-Moe. For B_2O_3 glass, the Raman spectrum is dominated by a strong and highly polarized band at 806 cm^{-1}; this band was shown to arise from the symmetric breathing mode of the boroxol ring and involves only the motion of the three oxygen atoms in the ring [228–231]. We note in particular the Windisch and Risen Raman study of v-B_2O_3 with different isotopic substitutions for both B and O, which beautifully identified the breathing mode of oxygens in the boroxol ring as responsible for the sharp Raman peak at 806 cm^{-1} [231].

The presence of superstructural groups in modified borate glasses is supported also by more recent Raman and IR studies, with some of these superstructural entities containing directly linked $[B\emptyset_4]^-$ units [232–237]. A review of the earlier literature on the structural peculiarities of borate glasses has been reported by Griscom [238], while an extensive review on the different models and superstructural groups proposed for borate glasses was given by Wright [15].

The earlier IR studies provided valuable qualitative information for the evolution of the borate structure as metal oxides are added to B_2O_3, but gave no quantitative measure of the borate structure such as the fraction of four-coordinated boron atoms. This difficulty is related to the fact that most of the earlier IR measurements were made by transmission on pellets of powdered glasses dispersed in non-absorbing matrix materials such as alkali metal halides. However, this technique often leads to sample hydrolysis [235] and ion-exchange [239] during glass grinding and pellet processing at high pressures. As a result, frequency shifts of absorption bands are observed as well as the appearance of bands which are not representative of the pristine glass. The use of alkali halide salts as matrices also causes spectral distortions and non-reproducible intensities of absorption bands because they represent a combination of transmission and reflection phenomena, the extent of which depends on the size and aggregation of glass particles and on the dielectric constant of the salt matrix [240, 241]. An alternative method is to measure IR transmission on thin films, if the viscosity of the molten borate permits the preparation of such films [242]. It is noted though that the quantitative assessment of the IR spectra of glass films is more complicated compared to bulk glasses. This is because thin films may exhibit the Berreman effect under oblique incidence of the IR radiation, and this causes the mixing of transverse optical (TO) and longitudinal optical (LO) modes [243], or could suffer from band distortions caused by a strong interference wave which develops under nearly perpendicular incidence of the IR radiation [244].

Among the various IR sampling techniques, IR reflectance spectroscopy on bulk glasses is advantageous for quantitative studies. First, the same glass sample, i.e. a polished slab, is used for data acquisition over a broad frequency range covering the entire IR spectrum. Second, the capabilities of modern Fourier-transform spectrometers, combined with the availability of software for analysis of reflectivity data, allow for the quantitative determination of the frequency-dependent optical and dielectric properties of the glass. This is because the true shapes and relative intensities of IR bands related to vibrational modes can be obtained and, thus, can permit the quantitative analysis of glass structure. These features make IR reflectance a powerful tool in glass science, as manifested by the steadily increasing interest in the field [215, 245]. It is noted that in early studies by IR reflectance [223], no quantification of the borate structure was discussed. This is because the measured reflectance, $R(\nu)$, depends both on the real, $n(\nu)$, and the imaginary, $k(\nu)$, parts of the complex refractive index, in comparison to the absorption coefficient $\alpha(\nu)$ which depends only on the extinction coefficient $k(\nu)$ [215, 235]. Here ν is the IR frequency in wavenumbers, cm^{-1}. It is noted that glasses absorb strongly the IR radiation, especially in the mid-IR region where the stretching vibrations of the glass network are active. For example, the absorption coefficient for the strong IR band at 1370 cm^{-1} for glass of composition $0.33Li_2O$–$0.67B_2O_3$ (see figure 17 below) is $\alpha = 13.0 \times 10^3$ cm^{-1}, suggesting that the penetration depth of the IR radiation into the glass is limited to $d_p = 1/\alpha = 0.77$ μm. This indicates that IR reflectance spectroscopy is a surface-sensitive technique and, thus, is very capable for studying surface corrosion effects [245]. For this reason, the evaluation of structure of bulk glasses by IR reflectance spectroscopy requires measurements on flat and fresh glass surfaces to avoid hydrolysis phenomena. Therefore, IR

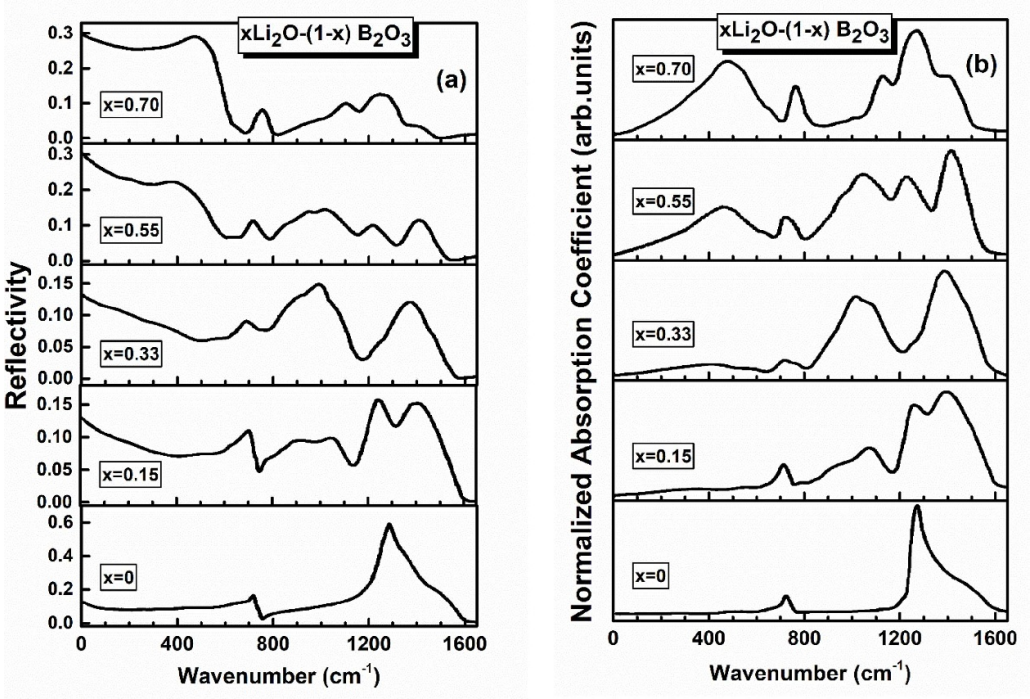

Figure 16. (a) Infrared reflectance spectra (left), and (b) calculated absorption coefficient spectra (right) of lithium-borate glasses $x\mathrm{Li_2O}$-(1-x)$\mathrm{B_2O_3}$ with $0 \leqslant x \leqslant 0.70$ (reproduced from [235]).

reflectance spectra are useful for the quantitative assessment of the bulk glass structure, provided that proper analysis is made to separate the $n(\nu)$ and $k(\nu)$ contributions to $R(\nu)$. For a review on IR reflectance spectroscopy of glasses and techniques for analyzing the $R(\nu)$ spectra see 'Infrared Spectroscopy of Glasses' by Kamitsos [215].

In the following sections, we will review applications of IR reflectance spectroscopy to evaluate N_4 in different families of modified borate glasses. A case of IR transmission measurements on borate thin films will be presented to highlight precautions to be taken when applying this technique for quantitative studies. Semi quantitative descriptions of the borate structure from Raman spectroscopy will be also given.

3.2. *Lithium borate glasses, $x\mathrm{Li_2O}$-(1-x)$\mathrm{B_2O_3}$*

The transmittance of bulk glasses is practically zero in the region of their fundamental vibrational modes, because glasses are strong absorbers of IR radiation. This facilitates the measurement of good quality reflectance spectra on bulk glasses and allows for their quantitative treatment. Lithium borate glasses, $x\mathrm{Li_2O}$-(1-x)$\mathrm{B_2O_3}$ with $0 \leqslant x \leqslant 0.73$, were studied by specular reflectance in the continuous spectral region 30–4000 $\mathrm{cm^{-1}}$. Figure 16(a) shows reflectance spectra, $R(\nu)$ [235] for some lithium borate glass compositions. The reflectance spectra were analyzed by the Kramers–Krönig (KK) transformation to calculate the corresponding $n(\nu)$ and $k(\nu)$ spectra [215, 235], as well as the absorption coefficient spectra using the expression $\alpha(\nu) = 4\pi\nu k(\nu)$ where ν is the frequency in wavenumbers ($\mathrm{cm^{-1}}$). The calculated $\alpha(\nu)$ spectra are shown in figure 16(b) and demonstrate a progressive evolution with $\mathrm{Li_2O}$ addition. To understand the origin of the induced spectral changes, we will briefly review the assignments for the main absorption profiles and employ the experimental IR data to obtain N_4.

As discussed in the original study [235], absorption in the range 800–1200 $\mathrm{cm^{-1}}$ can be attributed to the B-Ø stretching vibrations in structural groups containing $[\mathrm{BØ_4}]^-$ tetrahedra, with anhydrous $\mathrm{B_2O_3}$ glass naturally showing no absorption in this spectral range ($x = 0$, figure 16(b)). The high frequency absorption profile (ca. 1200–1650 $\mathrm{cm^{-1}}$) originates from the stretching vibration of B–Ø and B–$\mathrm{O^-}$ bonds in borate triangular units, which are of the $\mathrm{BØ_3}$ and $[\mathrm{BØ_2O}]^-$ type for glasses below the metaborate stoichiometry, $x = 0.5$. At higher $\mathrm{Li_2O}$ contents, $x > 0.5$, asymmetric stretching vibrations of the pyro-borate $[\mathrm{B_2O_5}]^{4-}$ and ortho-borate $[\mathrm{BO_3}]^{3-}$ units also contribute to the high frequency envelope. Thus, the evolution of the ca. 800–1200 $\mathrm{cm^{-1}}$ envelope with x in the range $0 < x \leqslant 0.40$ shows the progressive change of boron CN from three to four. For higher $\mathrm{Li_2O}$ contents ($x \geqslant 0.45$), the decrease of the relative intensity of the $[\mathrm{BØ_4}]^-$ absorption envelop denotes the destruction of $[\mathrm{BØ_4}]^-$ units in favor of borate triangles with increasing number of NBO atoms, and this leads to the change of boron CN from four back to three. Deformation modes of the borate units give rise to weaker absorption bands in the ca. 550–800 $\mathrm{cm^{-1}}$ range, while absorption in the far-IR range (below 550 $\mathrm{cm^{-1}}$) is due to Li ion-site vibrations and exhibits increasing intensity and frequency with $\mathrm{Li_2O}$ content (figure 16(b)).

To quantify the effect of $\mathrm{Li_2O}$ on the borate structure, the $\alpha(\nu)$ spectra were fitted and the component bands were assigned to borate species ($\mathrm{BØ_3}$, $[\mathrm{BØ_4}]^-$, $[\mathrm{BØ_2O}]^-$, $[\mathrm{B_2O_5}]^{4-}$

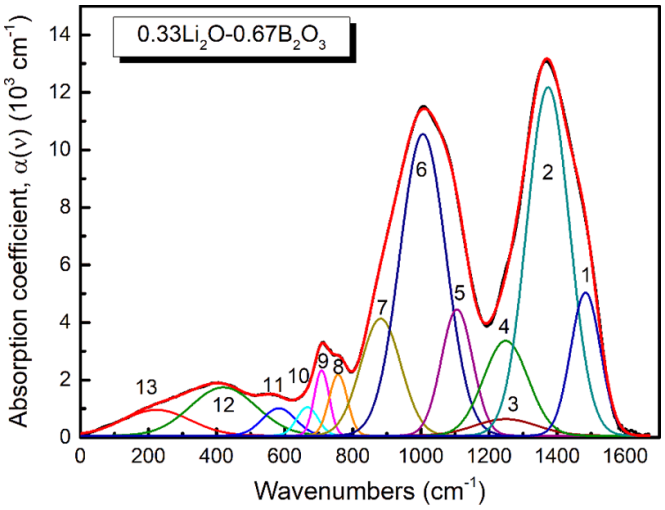

Figure 17. Fitting of Gaussian component bands of the absorption coefficient spectrum of glass $0.33Li_2O$–$0.67B_2O_3$. Black solid line represents the experimental spectrum, the red line is the simulated spectrum and the Gaussian component bands are labeled 1–13.

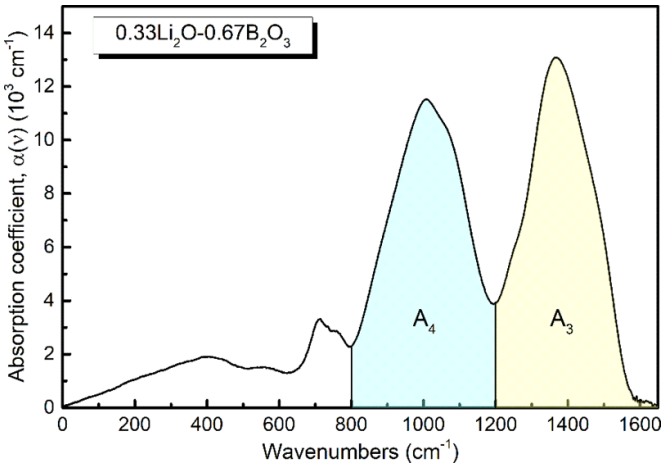

Figure 18. Example of spectral integration for the infrared absorption bands of borate tetrahedral units (800–1200 cm^{-1}, A_4) and triangular units (1200–1600 cm^{-1}, A_3) for glass $0.33Li_2O$-(1-x)B_2O_3.

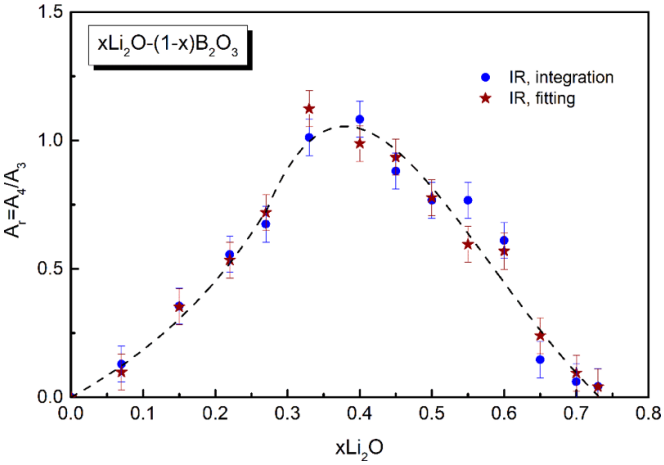

Figure 19. Relative integrated absorption $A_r = A_4/A_3$ as a function of Li_2O content obtained by fitting or integration of the absorption profiles corresponding to borate tetrahedral (A_4) and triangular (A_3) units for lithium-borate glasses. The line through the data points is drawn to guide the eye.

and $[BO_3]^{3-}$) and to Li ion-site vibrations [235]. This allowed the mapping of the network structure in the entire glass-forming range in terms of the relative integrated intensities of borate species; however, no attempt was made to calculate N_4 from the IR data. In a subsequent study on alkali diborate glasses, M_2O–$2B_2O_3$ with M = Li, Na, K, Rb, Cs, the total integrated intensity A_4 of $[B\emptyset_4]^-$ units was found to vary linearly with the fraction N_4 determined from NMR measurements [246]. In the following, we revisit the IR data of lithium-borate glasses to calculate N_4.

The integrated IR intensities of borate tetrahedral (A_4) and triangular (A_3) units can be obtained by spectral fitting or integration. Examples are shown in figures 17 and 18 for the $x = 0.33$ glass, noting that the spectral fitting involved 13 Gaussian component bands as performed earlier for the $x = 0.55$ composition [235].

From spectral fitting, A_4 is obtained as the sum of the integrated intensities of bands 5–7 and A_3 is the sum of the integrated intensities of bands 1–4 (figure 17). From spectral integration, A_4 is calculated as the total integrated intensity of the absorption envelope at ca. 800–1200 cm^{-1} and A_3 corresponds to the total integrated intensity of the ca. 1200–1650 cm^{-1} absorption envelope (figure 18).

Denoting by $[B_4]$ and $[B_3]$ the concentrations of borate tetrahedral and trigonal units, then $N_4 = [B_4]/([B_4]+[B_3])$ with $[B_4] = A_4/\alpha_4$ and $[B_3] = A_3/\alpha_3$, where α_4 and α_3 are the absorption coefficients of boron tetrahedral and triangular units. Combination of these relations gives the following simple expression for the fraction of boron atoms in four-fold coordination:

$$N_4 = \frac{A_r}{\alpha_r + A_r} \tag{3.1}$$

where $A_r = A_4/A_3$ and $\alpha_r = \alpha_4/\alpha_3$ is the relative absorption coefficient of boron tetrahedra versus triangles [247]. The composition dependence of A_r as obtained by fitting and integration is presented in figure 19 and demonstrates the change of boron coordination number from three to four up to about $x = 0.40$ and then back to three at higher Li_2O contents.

The use of the A_r data to calculate N_4 through equation (3.1) requires the knowledge of the relative absorption coefficient, α_r. As presented in figure 7(a) of the NMR section, the structural modification of glasses with Li_2O contents below ca. 27 mol% involves only the transformation of $B\emptyset_3$ into $[B\emptyset_4]^-$ units and, thus, the relation $N_4 = x/(1-x)$ is obeyed. Then, equation (3.1) can be rewritten in the following form for $x < 0.27$:

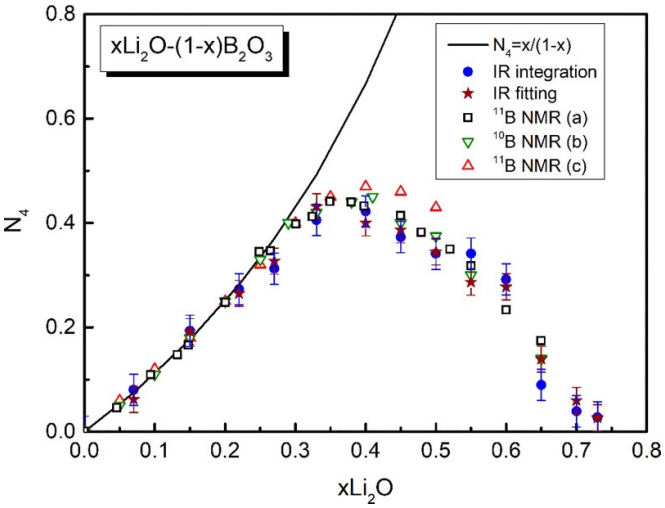

Figure 20. Fraction of four-coordinated boron atoms, N_4, for glasses xLi$_2$O-(1-x)B$_2$O$_3$. N_4 was calculated from the IR data using equation (3.1) where A_r was derived by integration or fitting of the absorption profiles for borate tetrahedral and triangular units (figures 17 and 18). Comparison is made with N_4 from NMR, (a) [30], (b) [249, 250] and (c) [42], and the x/(1-x) values when each oxygen atom from the added Li$_2$O converts two triangular BØ$_3$ units into two tetrahedral [BØ$_4$]$^-$ units (Ø = bridging oxygen atom).

$$\alpha_r = \frac{A_r\ (1-N_4)}{N_4} = \frac{A_r\ (1-2x)}{x}. \qquad (3.2)$$

The A_r data for glasses $x = 0.07$, 0.15 and 0.22 and equation (3.2) lead to the average value of the relative absorption coefficient $<\alpha_r> = 1.48 \pm 0.07$. The obtained value is in good agreement with that reported for lithium-metaborate glass ($\alpha_r = 1.50$, x = 0.5) [247], and the value $<\alpha_r> = 1.6 \pm 0.1$ found for ternary glasses in the system yLi$_2$O-(1-y)[x(2TeO$_2$)-(1-x)B$_2$O$_3$] with $y = 0.33$ and 0.40 and $0 \leqslant x \leqslant 1$ [248].

Therefore, we use the obtained value $<\alpha_r> = 1.48 \pm 0.07$ for lithium borate glasses in the entire glass-forming range and apply equation (3.1) to convert the A_r data into N_4 values. The N_4 results from the IR analysis are shown in figure 20 in comparison with N_4 data from earlier ^{11}B [30] and ^{10}B NMR [249, 250] and more recent ^{11}B NMR [42] studies. It is observed that the agreement between IR and NMR results is good in the entire glass-forming range, indicating the utility of IR reflectance spectroscopy to quantify the borate glass structure.

3.3. Silver borate glasses, xAg$_2$O-(1-x)B$_2$O$_3$

Silver borate glasses, xAg$_2$O-(1-x)B$_2$O$_3$, have attracted interest because they form the basis of fast-ion-conducting glasses like those in the ternary system AgI–Ag$_2$O–B$_2$O$_3$ [251, 252]. The structure of the borate network of the binary glasses xAg$_2$O-(1-x)B$_2$O$_3$ ($0 \leqslant x \leqslant 0.33$) was studied by IR reflectance and Raman spectroscopy [253]. The absorption coefficient spectra were calculated by KK transformation of the specular reflectance spectra and are shown in figure 21. Comparison with figure 16(b) shows that the lithium and silver borate glasses exhibit similar spectral evolutions suggesting the presence of similar short-range order borate units. Therefore, the same approach is applied here for the derivation of N_4 from the IR data.

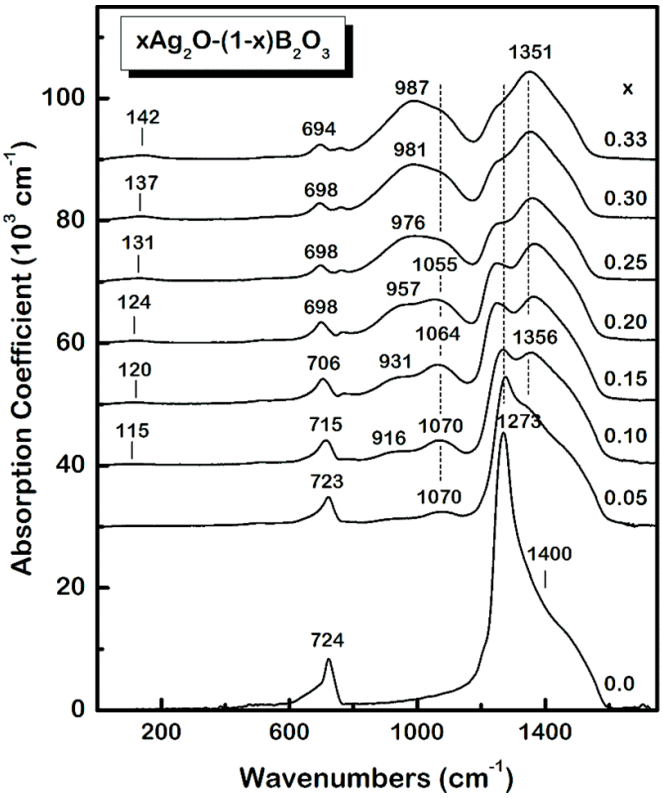

Figure 21. Infrared absorption coefficient spectra of glasses xAg$_2$O-(1-x)B$_2$O$_3$ (reproduced from [253]). The spectra for $x = 0.05$ to $x = 0.33$ have been offset to allow comparison.

The integrated intensities A_4 (800–1200 cm^{-1}) and A_3 (1299–1550 cm^{-1}) were calculated and their ratio $A_r = A_4/A_3$ is presented in figure 22(a), demonstrating the progressive change in boron CN. Application of equation (3.2) for glasses $x = 0.05$ and 0.07 gives the average value for the relative absorption coefficient $<\alpha_r> = 1.25$, which is then used to calculate N_4 from the A_r data. The results in figure 22(b) show good agreement between the IR-based N_4 data and those derived from the NMR study of Kim and Bray [51] and from neutron diffraction of Wright *et al* [254]. Clearly, N_4 follows the theoretical curve x/(1-x) up to about $x = 0.25$ and deviates from this curve at higher Ag$_2$O contents, indicating the formation of NBO atoms on triangular metaborate units, [BØ$_2$O]$^-$.

3.4. Alkaline earth borate glasses, xMO-(1-x)B$_2$O$_3$

Compared to alkali borate glasses, less structural information is available for alkaline-earth borates (xMO-(1-x)B$_2$O$_3$, M = Mg, Ca, Sr, Ba) including, for example, the M-dependence of N_4 (see figure 14(b)). In this context, results obtained by IR spectroscopy will be reviewed in this section and compared to those obtained by other techniques.

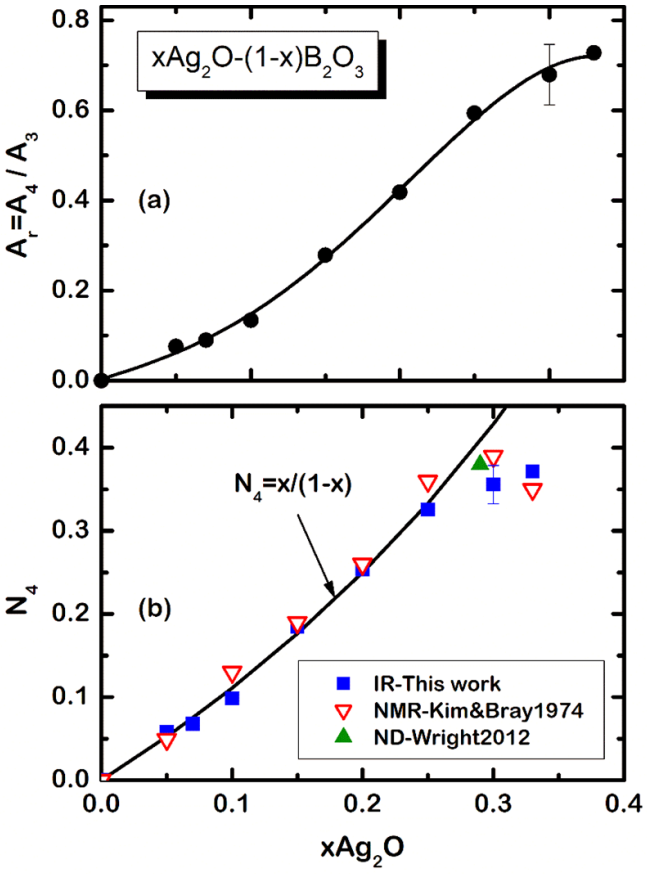

Figure 22. Effect of Ag_2O content on the relative integrated intensity $A_r = A_4/A_3$ (a), and the fraction N_4 calculated from equation (3.1) using $\alpha_r = 1.25$ (b) for glasses xAg$_2$O-(1-x)B$_2$O$_3$. The line in (a) is a guide to the eye and in (b) is the theoretical value $N_4 = x/(1\text{-}x)$. Comparison is made with experimental N_4 data from NMR spectroscopy [51] and neutron diffraction [254].

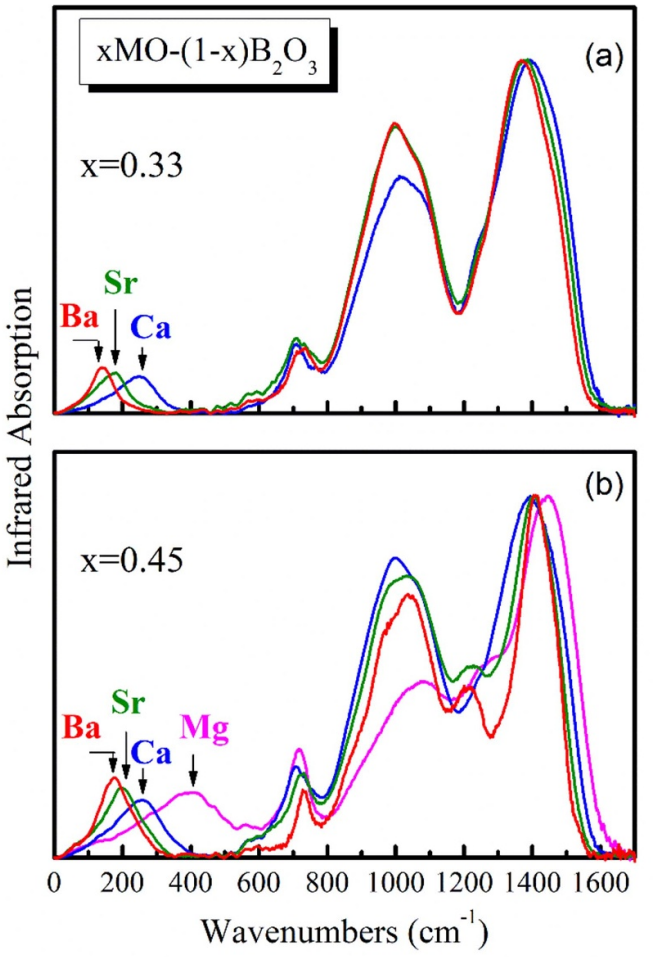

Figure 23. Infrared absorption spectra of alkaline earth borate glasses, xMO-(1-x)B$_2$O$_3$, with composition $x = 0.33$ (a) and $x = 0.45$ (b), reproduced from [255, 256]. For each composition, the spectra have been normalized on the height of the strongest high-frequency band at 1370–1450 cm^{-1} to facilitate comparison.

Absorption coefficient spectra, obtained by KK analysis of the measured reflectance spectra [255, 256], are shown in figure 23 for MO contents $x = 0.33$ and 0.45. To facilitate spectral comparison, the spectra of glasses with the same MO content were scaled at the high frequency absorption band. It is clear that the absorption profiles depend not only on the MO content but also on the type of alkaline-earth metal.

To quantify the effects on the short-range order structure by IR spectroscopy, we have calculated the integrated intensity of the absorption envelopes 800–1150 cm^{-1} (A_4, borate tetrahedral units) and 1150–1550 cm^{-1} (A_3, borate triangular units), noting that the frequency ranges for absorption of the triangular and tetrahedral borate units depend slightly on the modifier cation i.e. the cation mass and the strength of interactions between the cation and the borate unit. The relative integrated intensity, $A_r = A_4/A_3$, is shown in figure 24 as a function of MO content and type. The change in boron coordination from three to four as the MO content increases towards the metaborate composition ($x = 0.50$) is illustrated in this figure, noting that the x value at which A_r exhibits its maximum is a function of the type of alkaline-earth oxide. Also, for glasses of the same MO content the value of A_r decreases in the order Ba >Sr >Ca≫Mg for x up to ca. $x = 0.45$, and changes to Ca > Sr > Ba≫Mg for x >0.45.

The relative integrated intensities A_r can be used to calculate N_4 from equation (3.1), once the relative absorption coefficients, α_r, are known for all four glass systems. We note that the glass-forming ranges of alkaline earth borates made by splat quenching are considerably narrower than those of the alkali borates, i.e. Mg: $0.45 \leqslant x \leqslant 0.55$, Ca: $0.33 \leqslant x \leqslant 0.50$, Sr: $0.20 \leqslant x \leqslant 0.47$ and Ba: $0.15 \leqslant x \leqslant 0.47$. Therefore, only the low modification Ba- and Sr-borate glasses offer the possibility to apply equation (3.2) for the evaluation of α_r. Application of this approach to Ba-borate glasses with $x = 0.20$ and $x = 0.25$ gives the average value α_r(Ba) $= 1.32 \pm 0.05$, while the $x = 0.20$ Sr-borate glass composition gives α_r(Sr) $= 1.36 \pm 0.05$. For Ca-borates the IR data (A_r) have been scaled with the NMR data of Wu and Stebbins [90] at $x = 0.5$ ($N_4 = 0.383$) to obtain α_r(Ca) $= 1.40 \pm 0.05$. For Mg-borate glasses Dell and Bray [131] reported $N_4 = 0.20$ for the 0.45MgO-0.55B$_2$O$_3$ glass and this gives α_r(Mg) $= 1.90 \pm 0.075$. These findings show

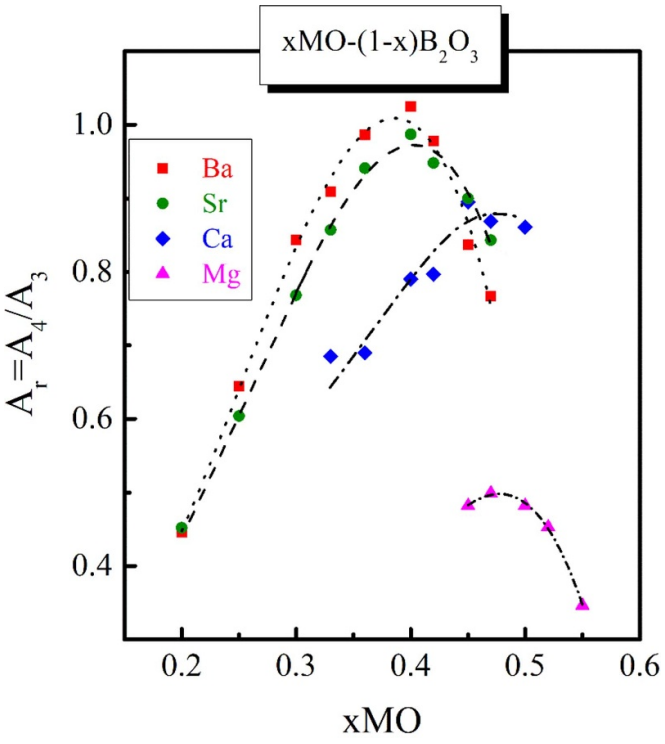

Figure 24. Relative integrated IR absorption $A_r = A_4/A_3$ as a function of the MO content and type in alkaline earth borate glasses xMO-(1-x)B_2O_3 (M = Mg, Ca, Sr, Ba) [255, 256].

that α_r increases with increasing cation field strength, noting that in earlier studies the average value $\alpha_r = 1.30$ was employed for M = Ba, Sr and Ca [255, 256].

The results for the IR-based N_4 values are shown in figure 25 versus MO content and are compared with the theoretical curve x/(1-x), as well as with N_4 values obtained by other techniques including neutron diffraction [254], NMR [61, 90, 107, 122, 127, 131, 160, 176], neutron diffraction and molecular dynamics [257] and x-ray diffraction [258].

The following observations can be made from figure 25: (i) In general, there is good agreement between the IR results and those of other techniques, noting the presence of scattering in the N_4 values among various techniques. IR reflectance spectroscopy is shown again to be a useful tool for the quantification of the borate glass structure; (ii) For Ba- and Sr-glasses of low MO contents (up to ca. $x = 0.25$) the N_4 value follows the theoretical x/(1-x) curve, but it deviates for M = Ca and Mg; (iii) The MO content at which N_4 attains its maximum value shifts to higher x values as the field strength of the M^{2+} ion increases, in line with the earlier observations of Holland *et al* for various borate systems [68]; (iv) Borate glasses of the same alkaline-earth content exhibit a decreasing trend in N_4 with increasing field strength of the M^{2+} ion, i.e. from Ba to Mg. Note that this N_4 trend with M^{2+} cation field strength is opposite to that found for alkali borate glasses for compositions $x > 0.3$ [36].

As presented above, the relative absorption coefficient of boron tetrahedra versus triangles, $\alpha_r = \alpha_4/\alpha_3$, depends on the type of alkaline-earth cation. To quantify this effect, we consider the role of the cation field strength, F, defined according to Dietzel [259] as follows:

$$F = \frac{Z}{(r_C + r_O)^2}. \tag{3.3}$$

Here Z is the cation valence ($Z = 2$ for M^{2+} cations), r_C is the cation radius for an assumed CN and r_O is the oxygen radius. We take here $r_O = 1.35$ Å [260] for two-fold coordination of oxygen in all alkaline-earth borate compositions studied in this work. While this is an approximation, a constant r_O value has been employed in other studies as well [261]. In any case, the oxygen coordination is expected to have a small effect on the cation-oxygen distance, and so on the values of F. Taking CN = 4 for Mg^{2+}, CN = 6 for $Ca^{2+}$and Sr^{2+} and CN = 8 for Ba^{2+}, the corresponding ionic radii are $r(Mg^{2+}) = 0.57$ Å, $r(Ca^{2+}) = 1.00$ Å, $r(Sr^{2+}) = 1.18$ Å, and $r(Ba^{2+}) = 1.42$ Å [260]. The relative IR absorption coefficient (α_r) and cation field strength (F) values for M = Ba, Sr, Ca and Mg cations are presented in table 2 and plotted figure 26, where the correlation between α_r and F can be described by the quadratic equation:

$$\alpha_r = 1.75\ (\pm 0.14) - 3.41\ (\pm 0.74)\ F + 6.79\ (\pm 0.90)\ F^2 \tag{3.4}$$

To test the predictive value of equation (3.4), we consider here the case of lead-borate glasses, xPbO-(1-x)B_2O_3, for which A_r data are available from IR reflectance measurements [262], and N_4 data have been obtained by NMR spectroscopy [27, 73, 78, 80, 119, 143] and neutron diffraction [263, 264]. For lead ions with a network-modifier role, i.e. with primarily ionic Pb–O bonds, we assume CN = 6 [73, 78, 80, 119, 143, 263–265], and take $r(Pb^{2+}) = 1.19$ Å [260], which result in the cation field strength value $F(Pb^{2+}) = 0.31$ Å^{-2} and then in $\alpha_r(Pb^{2+}) = 1.35$ by application of equation (3.4). Thus, the A_r IR data [262] can be converted to N_4 data by equation (3.1) and compared in figure 27 with N_4 obtained from other experimental techniques [27, 73, 78, 80, 119, 143, 263, 264].

The agreement between the N_4-IR, and the N_4 data from other techniques [27, 73, 78, 80, 119, 143, 160, 263, 264], found in figure 27 for Pb-borates demonstrates the utility of equation (3.4) and equation (3.1) for predicting N_4 from IR spectra of borate glasses containing divalent cations, and implies applicability to other cations, such as Zn^{2+}. With $\alpha_r(Zn^{2+}) = 1.85$ (table 2) one expects a similar evolution of the IR spectra and structure of Zn- and Mg-borate glasses; for example, N_4(Zn) = 0.26 for $x = 0.54$ [125] in comparison to N_4(Mg) = 0.20 for $x = 0.50$ [131] and N_4(Mg) = 0.25 for $x = 0.50$ [160] in figure 25, which are indeed similar. Futhermore, equation (3.4) should be helpful for glasses with paramagnetic ions for which no NMR data are available [266]; predicted values for α_r are given in table 2 for Mn^{2+}, Fe^{2+} and Cu^{2+} ions and can be employed in future structural studies to

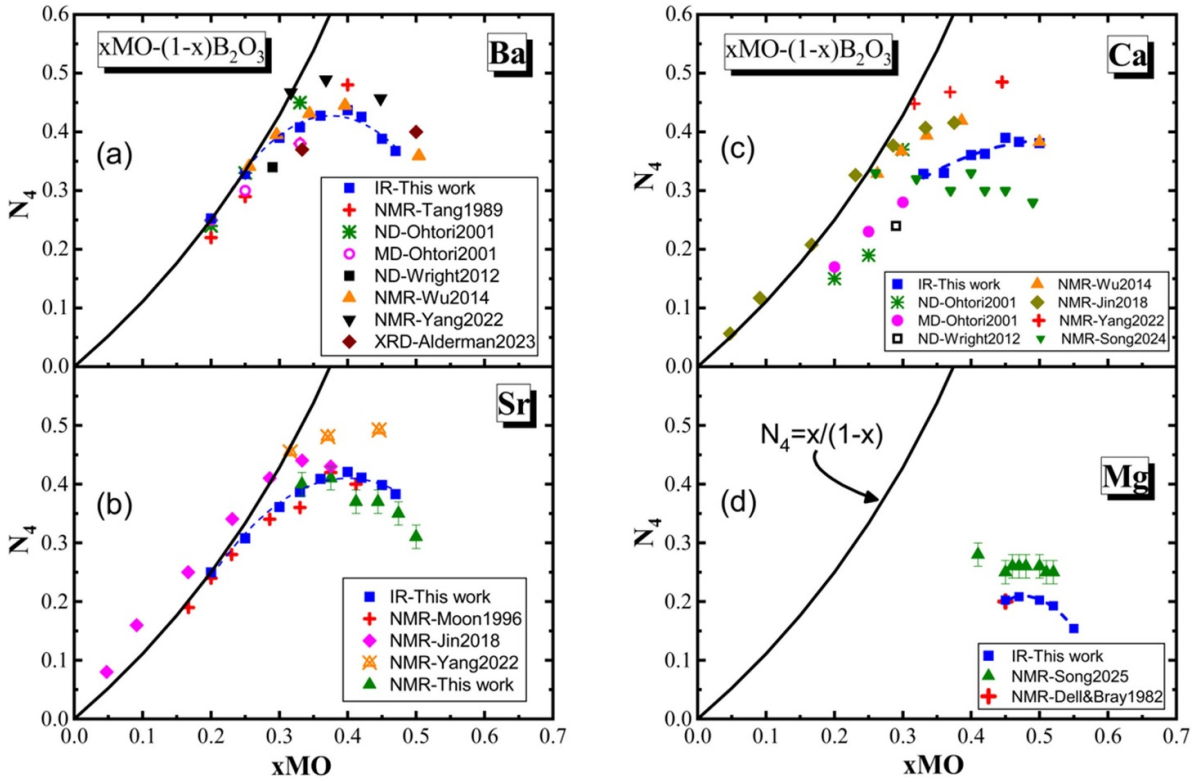

Figure 25. Composition dependence of N_4 in alkaline earth borate glasses xMO-(1-x)B_2O_3 (M = Ba (a), Sr (b), Ca (c) and Mg (d)) obtained by IR, NMR, neutron diffraction (ND), molecular dynamics (MD), and x-ray diffraction (XRD) studies [61, 90, 107, 122, 127, 131, 176, 254, 257, 258]. Dashed lines through IR data points are guides to the eyes. The figures were compiled from those in [255, 256] by using the new $\alpha_r(M)$ values and adding recent N_4 data from other techniques.

Table 2. Assumed coordination number (CN), ionic radius (r_C), cation field strength (F) calculated by equation (3.3) with r_O = 1.35 Å [260], and relative IR absorption coefficient ($\alpha_r = \alpha_4/\alpha_3$) for the divalent M^{2+} cations considered in this work.

Cation	CN	r_C (Å)	F (Å^{-2})	α_r
Mg^{2+}	4	0.57	0.54	1.90 ± 0.07[a]
Ca^{2+}	6	1.00	0.36	1.40 ± 0.05[a]
Sr^{2+}	6	1.18	0.31	1.36 ± 0.05[a]
Ba^{2+}	8	1.42	0.26	1.32 ± 0.05[a]
Pb^{2+}	6	1.19	0.31	1.35[b]
Mn^{2+}	4	0.66	0.50	1.74[b]
Mn^{2+}	6	0.67	0.49	1.71[b]
Fe^{2+}	4	0.63	0.51	1.78[b]
Fe^{2+}	6	0.77	0.44	1.56[b]
Cu^{2+}	4	0.57	0.54	1.89[b]
Cu^{2+}	6	0.73	0.46	1.62[b]
Zn^{2+}	4	0.60	0.53	1.85[b]

[a] Obtained in this work.
[b] Calculated by equation (3.4).

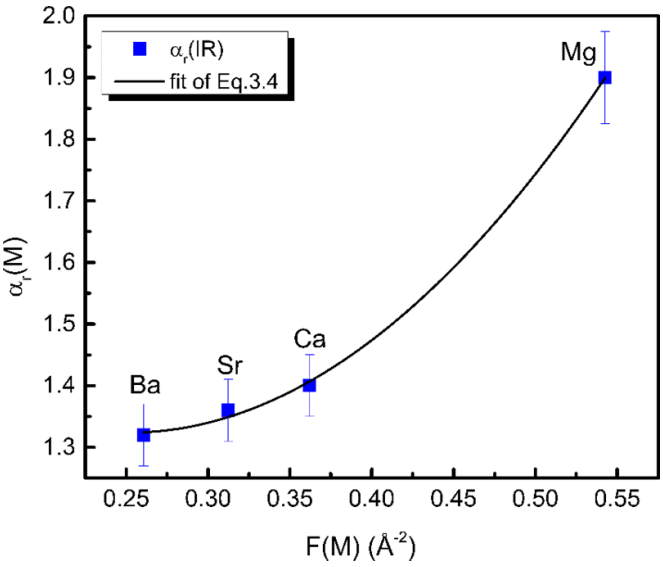

Figure 26. Relative IR absorption coefficient, $\alpha_r(M)$, as a function of cation field strength, $F(M)$, for M = Ba- Sr-, Ca- and Mg-borate glasses. The line is the fit of equation (3.4) to the data.

determine N_4. It is noted though that equation (3.4) should be applied with caution to divalent transition metal ions since the presence of d-electrons would contribute to partially covalent M–O bonding. This is in comparison to metal ions with noble gas electron configurations, like the alkaline-earths, where the M–O bonding is primarily ionic.

3.5. IR spectroscopy of borate glasses in thin film and other forms

IR spectra of thin film glasses are often used to assess their structure in relation to the corresponding bulk glasses. We

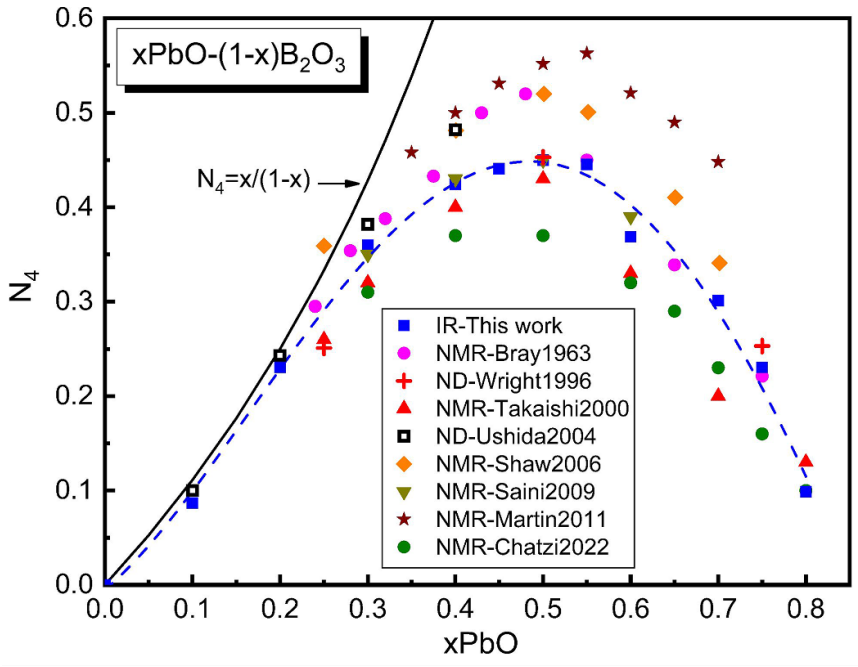

Figure 27. N_4 data obtained by IR results (A_r from [262]) using equation (3.1) and $\alpha_r(Pb^{2+}) = 1.35$, NMR spectroscopy [27, 73, 78, 80, 119, 143], and neutron diffraction [263, 264]. Dashed line between the IR data points is a guide to the eye.

show here that such comparisons and relevant conclusions should be made with caution. We use as an example the silver diborate glass doped with 20 mol% AgI, i.e. 0.2AgI-0.8[Ag_2O-$2B_2O_3$]. The specular reflectance spectrum of the bulk glass was measured and then KK-transformed to calculate the optical properties $n(\nu)$ and $k(\nu)$ shown in figure 28 [244](a).

The $n(\nu)$ and $k(\nu)$ spectra are then used as inputs to calculate the transmittance spectra, $T(\nu)$, of thin films using a formalism [244] (a) to account for multiple reflections in the films. The thin films considered here have different thickness, t, but the same chemical composition and structure as they all have exactly the same $n(\nu)$ and $k(\nu)$ properties of the bulk glass. The simulated transmittance spectra $T(\nu)$ for films of different thickness are shown in the left panel of figure 29. The absorbance spectra were calculated using $A(\nu) = -\log_{10}T(\nu)$ and are depicted in the right panel of figure 29.

It is observed that all spectra exhibit similar profiles below 1500 cm^{-1}. The strongest absorption envelopes are at ca. 970 cm^{-1} (due to borate tetrahedra, $[B\emptyset_4]^-$) and 1330 cm^{-1} (due to triangular borate units, $B\emptyset_3$ and $[B\emptyset_2O]^-$). The position of these envelopes varies from 965 to 985 cm^{-1} and from 1320 to 1340 cm^{-1}, respectively, as the film thickness increases from 0.7 to 7.0 μm. Considering the origin of the ca. 970 and 1330 cm^{-1} envelopes, it would be tempting to associate the obvious dependence of their peak frequency on film thickness with variations in the nature of the borate tetrahedral and triangular units. In addition, the relative intensity $A_r = A_4/A_3$ of these envelopes changes with film thickness as seen in figure 30, and this could be interpreted as a change in N_4. Obviously, none of these interpretations are correct since all film spectra were derived from the same $n(\nu)$ and $k(\nu)$ spectra and, thus, they should have the same bonding and structure.

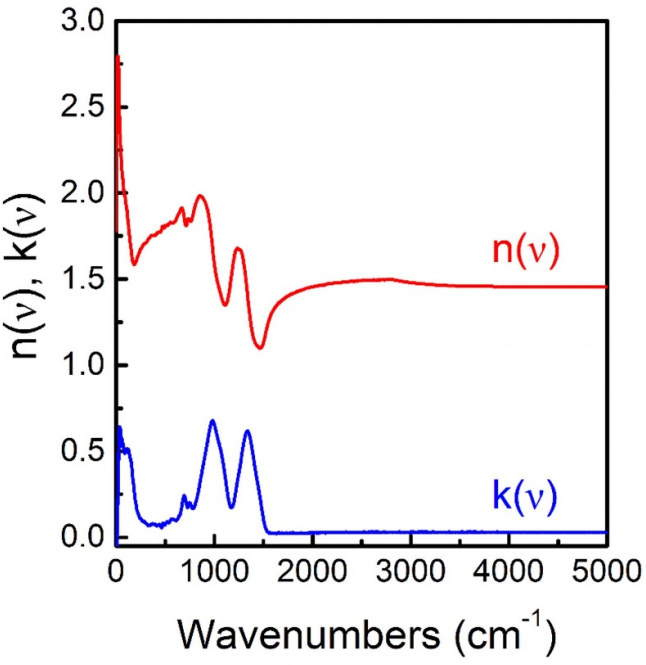

Figure 28. Refractive index, $n(\nu)$, and extinction coefficient, $k(\nu)$, spectra of the bulk glass 0.2AgI-0.8[Ag_2O-$2B_2O_3$] obtained by Kramers–Krönig transformation of the measured reflectance spectrum. Reproduced from [244](a).

The phenomena described above result directly from the influence of film thickness on the IR absorption profiles. As

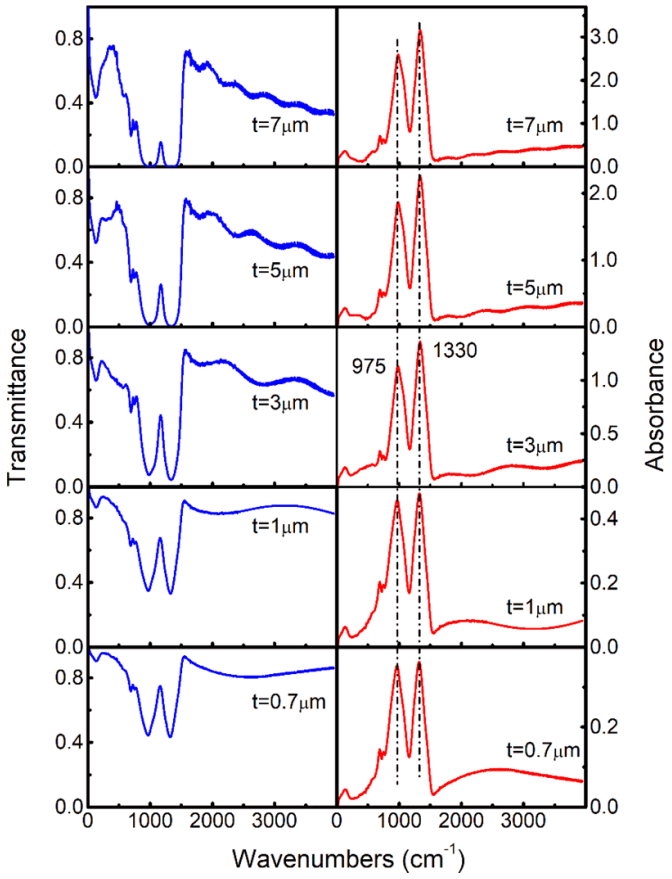

Figure 29. Effect of film thickness on the calculated transmittance (left) and absorbance (right) spectra of free-standing films, using as input the $n(\nu)$ and $k(\nu)$ spectra of figure 28 for glass films with composition 0.2AgI-0.8[Ag_2O-2B_2O_3], and variable thickness (0.7 μm $\leqslant t \leqslant$ 7 μm). Reproduced from [244](a).

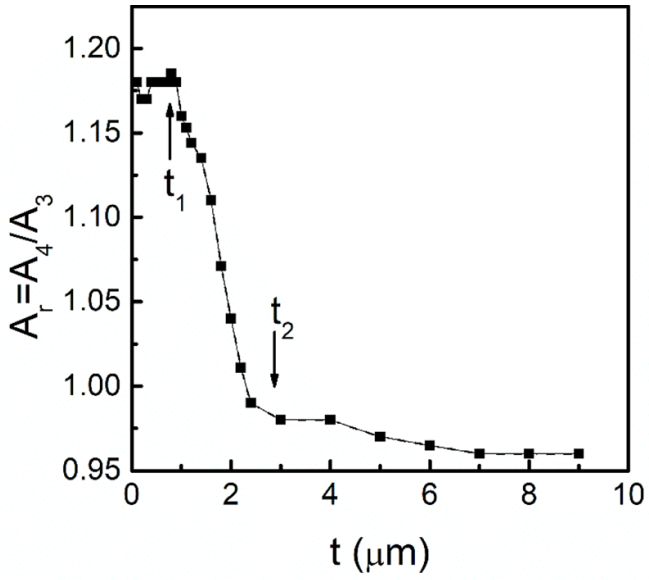

Figure 30. Dependence of the relative integrated absorption $A_r = A_4/A_3$ on film thickness (t) for glassy films with composition 0.2AgI-0.8[Ag_2O-2B_2O_3]. For $t_1 < t < t_2$ the ratio $A_r = A_4/A_3$ shows a strong dependence on the film thickness. Reproduced from [244](a).

seen in figure 29, all films exhibit interference patterns which are well visible in the region above 1500 cm^{-1} where the glass absorption is very small. The interference patterns extend over the entire IR region, and this results in absorption spectra which are superpositions of the true vibrational profile of the bulk glass and a pure optical effect, i.e. interference due to multiple reflections in the film. The period and amplitude of interference change with film thickness and, thus, these parameters influence the frequency and relative intensity of vibrational bands in a manner which depends on film thickness.

It is noted that the studied borate thin films exhibit larger values of the $A_r = A_4/A_3$ ratio than bulk glasses of the same composition, while the decrease of A_4/A_3 upon increasing film thickness was observed also for experimental thin films blown from the melt [244](a). However, the A_4/A_3 values of thin films and bulk glasses can never be the same even for thick films. A key reason for this statement is that the $A(\nu)$ spectra of thin films, derived from the $T(\nu)$ spectra, are functions of both n(ν) and $k(\nu)$ as compared to the $\alpha(\nu)$ spectra of bulk glasses which depend only on $k(\nu)$ [244](a). Besides this difference in $A(\nu)$ and $\alpha(\nu)$ spectra and the optical effects in thin films, there are usually differences in thermal histories of thin films and bulk glasses and this may introduce structural differences because of the different fictive temperatures [244].

The example presented above shows that a safe interpretation of measured IR spectra on thin films requires the comparison of measured and simulated spectra, taking into account purely optical effects as well as differences in thermal history between thin films and bulk glasses.

The use of the relative integrated intensity A_r to obtain N_4 in borate glasses has been applied also to IR transmission spectra measured on powdered glasses dispersed in KBr pellets [267–274]. In such studies, the relation $N_4 = A_4/(A_3 + A_4) = A_r/(1 + A_r)$ has been employed which implies that $\alpha_r = 1$ according to equation (3.1). However, this is not the case at least for the glasses considered here. In any case, the experimental parameter A_4/A_3 derived from IR spectroscopy by the KBr pellet technique is a useful qualitative tool to probe structural trends caused by, e.g. variations in borate glass composition; however, its quantitative conversion though to N_4 requires the knowledge of α_r for the particular borate system. Recently, proper application of equation (3.1) was made by Osipova *et al* [275] for iron-containing zinc borate glasses using $\alpha_r = 1.36$ [275], although compared to the α_r(Zn) = 1.85 value found in the present study, this would suggest a systematic offset in the N_4 values obtained.

3.6. *Bismuth borate glasses, xBi_2O_3-(1-x)B_2O_3*

The previous paragraphs presented IR-derived N_4 data for borate glasses modified by metal oxides of univalent (e.g. Li^+) and divalent (e.g. Ba^{2+}) metal ions. Here we consider the trivalent metal ion Bi^{3+} in the binary glasses $x$$Bi_2O_3$-(1-$x$)$B_2O_3$. Glasses in the bismuth-borate system can be prepared in an extended glass forming range up to ca. 88.2 mol% Bi_2O_3

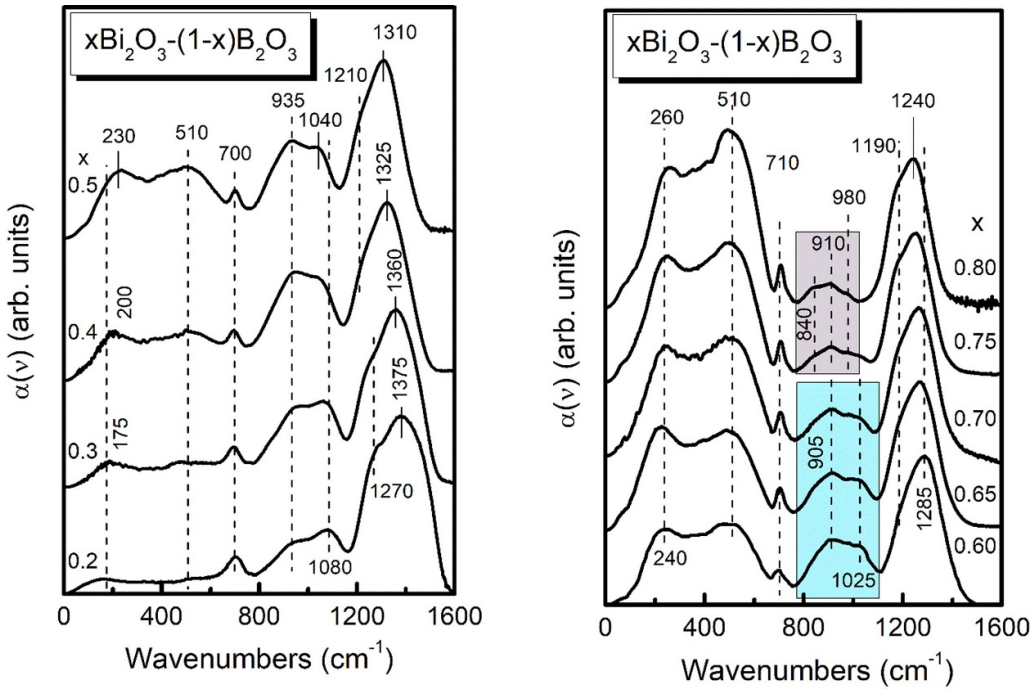

Figure 31. Calculated absorption coefficient spectra, $\alpha(\nu)$, for glasses xBi$_2$O$_3$-(1-x)B$_2$O$_3$ with $0.2 \leqslant x \leqslant 0.5$ (left) and $0.6 \leqslant x \leqslant 0.8$ (right), reproduced from [278].

by employing the twin roller quenching technique [279], and attract interest for a range of applications, e.g. in photonics [276] and radiation shielding [277].

Glasses for IR reflectance measurements were prepared by splat-quenching the melt between two polished stainless-steel blocks [279]. With this method, bulk glasses were obtained in the range $0.2 \leqslant x \leqslant 0.8$. The glass specimens have smooth and flat surfaces, suitable for specular reflectance measurements without any further treatment.

Figure 31 presents the absorption coefficient spectra, $\alpha(\nu)$, calculated from the measured specular reflectance spectra of glasses xBi$_2$O$_3$-(1-x)B$_2$O$_3$ [278]. It is observed that the 750–1150 cm^{-1} envelope originating from asymmetric boron–oxygen stretching vibration modes of tetrahedral borate units exhibits considerable activity even at very high modification levels, $x > 0.70$ (figure 31, right); in this composition range lithium borate glasses show practically no absorption of metaborate tetrahedral species, [BØ$_4$]$^-$ (figure 16(b)). This peculiarity of bismuth-borate glasses with very high modification was explained by the formation of orthoborate-type tetrahedral units, [BØ$_2$O$_2$]$^{3-}$, which coexist with their isomeric triangular orthoborate species [BO$_3$]$^{3-}$ ([BØ$_2$O$_2$]$^{3-}$ $\rightleftharpoons$ [BO$_3$]$^{3-}$).

To quantify the effect of Bi$_2$O$_3$ on the borate structure, the $\alpha(\nu)$ spectra were fitted and the integrated intensities of component bands above 800 cm^{-1} were used in combination with mass and charge balance equations to evaluate the molar fractions of the short-range borate units: X_{4m}, X_{4o}, X_3, X_2, X_1 and X_0 which correspond to borate units [BØ$_4$]$^-$, [BØ$_2$O$_2$]$^{3-}$, BØ$_3$, [BØ$_2$O]$^-$, [BØO$_2$]$^{2-}$ and [BO$_3$]$^{3-}$ (Ø and O$^-$ denote bridging and NBO atoms, respectively). Thus, this extensive IR analysis provides the molar fractions of all borate units as compared to the approach presented in previous sections, which gives only the fraction N_4 on the basis of $A_r = A_4/A_3$. The composition dependence of the total fraction of boron atoms in four-fold coordination, $N_4 = X_{4m} + X_{4o}$, is presented in figure 32(a) as derived from IR [278] and NMR spectroscopy [75], while the evolution of the fractions of units BØ$_3$, [BØ$_2$O]$^-$, [BØO$_2$]$^{2-}$ and [BO$_3$]$^{3-}$ are given elsewhere [278].

It is evident from figure 32(a) that in the composition range $0.2 \leqslant x \leqslant 0.65$, the N_4 data from IR and NMR are, generally, in good agreement. The experimental N_4 data are compared in the same figure with the theoretical value obtained if all oxygen atoms introduced by Bi$_2$O$_3$ are forming [BØ$_4$]$^-$ units, $N_{4th} = 3x/(1\text{-}x)$. Clearly, the experimental rate for [BØ$_4$]$^-$ formation is considerably lower than $3x/(1\text{-}x)$. For $x = 0.2$ the experimental rate is $1.3x/(1\text{-}x)$, indicating that only 43% of the introduced oxygen forms [BØ$_4$]$^-$ units. For $x = 0.3$ the experimental N_4 rate reduces to $x/(1\text{-}x)$, showing that 33% of the oxygen forms [BØ$_4$]$^-$ units. Therefore, the rest of the added oxygen participates in other kinds of structural groups including the NBO containing [BØ$_2$O]$^-$ and [BØO$_2$]$^{2-}$ units, without excluding the formation of a BiO$_n$ pseudophase [278].

It was also possible to separate the contributions of the [BØ$_4$]$^-$ and [BØ$_2$O$_2$]$^{3-}$ tetrahedral species to the total N_4 value from the analysis of the IR spectra. The results are shown in figure 32(b) in terms of the fractional contributions of the metaborate tetrahedral units [BØ$_4$]$^-$, X_{4m}/N_4, and of the orthoborate tetrahedral units [BØ$_2$O$_2$]$^{3-}$, X_{4o}/N_4, to the total N_4 fraction of borate tetrahedral species in the xBi$_2$O$_3$-(1-x)B$_2$O$_3$ glasses. Clearly, [BØ$_4$]$^-$ constitute the dominating tetrahedral units for $0.20 \leqslant x \leqslant 0.70$ and the [BØ$_2$O$_2$]$^{3-}$ units

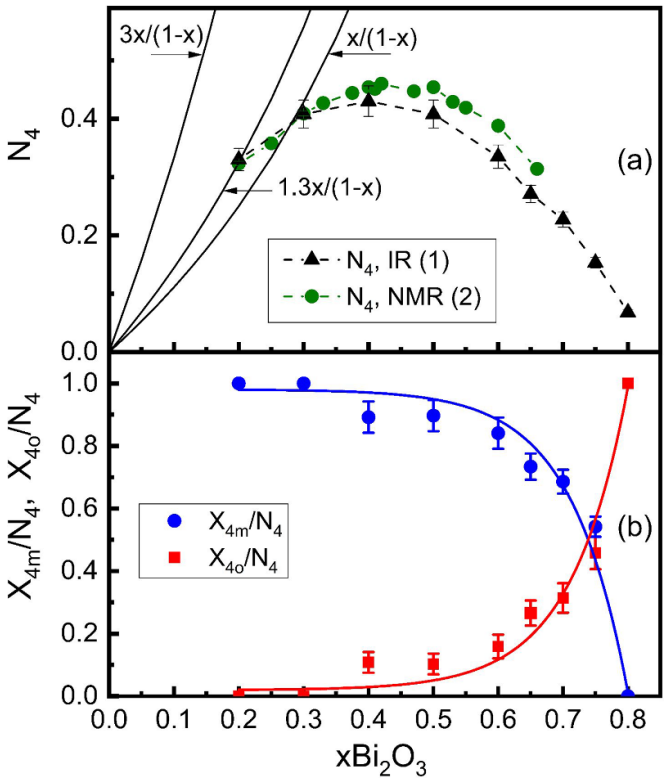

Figure 32. (a) Comparison of the molar fractions of borate tetrahedral units N_4 in glasses $x$$Bi_2O_3$-(1-$x$)$B_2O_3$ obtained by IR, (1) [278], and NMR, (2) [75], spectroscopy. The solid black lines present the theoretical value for the mole fraction of $[B\emptyset_4]^-$ units formed at rates 3x/(1-x), 1.3x/(1-x) and x/(1-x). (b) Fractional contributions of the metaborate tetrahedral units $[B\emptyset_4]^-$, X_{4m}/N_4, and of the orthoborate tetrahedral units $[B\emptyset_2O_2]^{3-}$, X_{4o}/N_4, to the total fraction N_4 of borate tetrahedra in these bismuth borate glasses [278]. Dashed lines in (a) and solid lines in (b) are drawn as guides to the eye.

prevail at higher Bi_2O_3 levels ($x > 0.7$), where they coexist with their isomeric triangular orthoborate species $[BO_3]^{3-}$.

The formation of $[B\emptyset_2O_2]^{3-}$ tetrahedral species could be at the origin of the very broad glass-forming region of glasses $x$$Bi_2O_3$-(1-$x$)$B_2O_3$. While the nominal orthoborate composition (O/B = 3/1) corresponds to $x = 0.5$ in this system, the glass-forming region extends well-above this limit and reaches $x = 0.80$ by splat-quenching and even $x = 0.88$ by twin roller quenching [279]. This is in contrast to lithium-borate glasses $x$$Li_2O$-(1-$x$)$B_2O_3$ for which glass formation by splat-quenching was possible up to $x = 0.73$, i.e. the pure orthoborate glass ($x = 0.75$) could not be prepared due to crystallization [235]. This can be rationalized in terms of the main structural difference between the two glass systems: while $[BO_3]^{3-}$ triangles are the only borate species present in Li-orthoborate, they coexist, with their isomeric tetrahedral orthoborate units $[B\emptyset_2O_2]^{3-}$ in highly-modified Bi-borate glasses, in addition to the parallel glass-forming role of Bi_2O_3 at high x values i.e. formation of BiO_n polyhedral species [278]; both these factors prevent crystallization and extend the glass-forming region of the Bi-borate system. Recently, the preparation of the $x = 0.75$ Li-borate glass was achieved by intentionally leaving some carbonate species $[CO_3]^{2-}$ in the melt, from the starting Li_2CO_3 material, to avoid crystallization upon quenching [280].

The glass-forming role of Bi_2O_3 in bismuthate glasses above the orthoborate composition ($x > 0.5$) is probably related to the involvement of the d-electrons of Bi in primarily covalent Bi-O bonds in BiO_n polyhedral species [278]. The fact that part of the added oxygen is involved in covalent bonding with Bi allows the borate component to maintain its orthoborate composition by the coexisting $[BO_3]^{3-}$ and $[B\emptyset_2O_2]^{3-}$ isomeric units, with the latter forming at increasing rates for $x > 0.5$ (see figure 32(b)). This trend is consistent with the composition dependence of the glass transition temperature which decreases from $T_g = 407$ °C at $x = 0.50$ to $T_g = 312$ °C at $x = 0.80$ [75]. Assuming that the fictive temperature shows a behavior similar to T_g, then the structure of the supercooled liquid for $x = 0.80$ would be arrested into the glassy state at lower temperature than that for $x = 0.50$ and, naturally, this would drive the structure to the more condensed orthoborate units. As reported by Lower *et al* [281], the $[B\emptyset_4]^-$ tetrahedral unit has smaller effective volume than its isomeric $[B\emptyset_2O]^-$ triangular species. Assuming that the same trend is exhibited by the orthoborate isomers, then the $[B\emptyset_2O_2]^{3-}$ tetrahedra would have smaller effective volume than their $[BO_3]^{3-}$ isomers and, thus, the decreasing fictive temperature would favor the formation of the tetrahedral orthoborate isomers.

3.7. Raman spectroscopy of borate glasses

Compared to IR, the number of Raman studies devoted to the quantification of the borate structure are limited. This is due to the lack of knowledge about the Raman scattering cross section of vibrations related to borate species. Instead, Raman spectroscopy can provide a semi quantitative description of the structure in terms of relative band intensities of borate species. Such an approach was employed in the Raman study of glasses $x$$Na_2O$-(1-$x$)$B_2O_3$ with $0 \leqslant x \leqslant 0.75$ [282], noting that glass-formation for $x = 0.45$, 0.50 and 0.55 was achieved by replacing 0.05, 0.07 and 0.05 moles B_2O_3 by equal number of moles Al_2O_3, respectively. Assignment of the complex Raman profiles supported the use of the following characteristic bands: 805 cm^{-1} for boroxol rings; 545, 765, 780, and 1120 cm^{-1} for $[B\emptyset_4]^-$ tetrahedral units; 1490 cm^{-1} for triangular metaborate units $[B\emptyset_2O]^-$; 820 cm^{-1} for pyroborate units $[B_2O_5]^{4-}$ and 890 cm^{-1} for orthoborate triangular units $[BO_3]^{3-}$. Assuming that the bandwidths of the Raman bands do not change with composition, the band intensity of a specific borate unit was approximated by the peak height of its Raman band, or by the sum of peak heights of the four bands related to $[B\emptyset_4]^-$ units.

The composition dependence of the relative Raman intensity of the previously mentioned borate units has been estimated and the results are given in figure 33. As depicted in

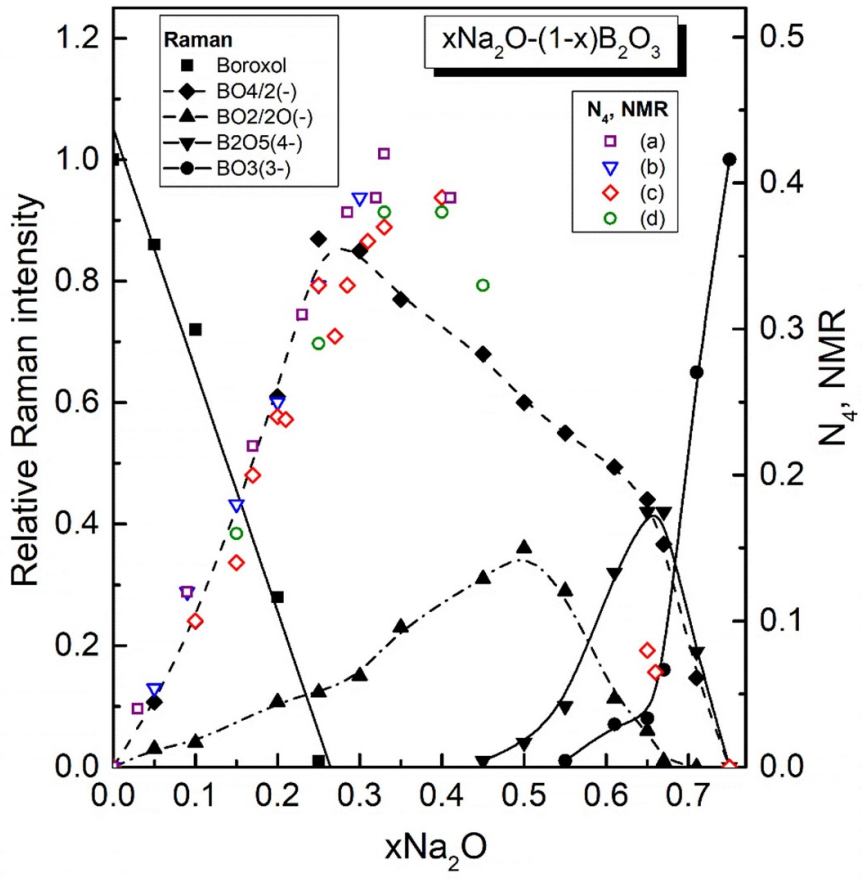

Figure 33. Composition dependence of the relative Raman intensity of borate units in sodium borate glasses xNa$_2$O-(1-x)B$_2$O$_3$ spanning the composition range $0 \leqslant x \leqslant 0.75$ (reproduced from [282]). The Raman results for BØ$_4^-$ tetrahedral units are compared with N_4 data from NMR spectroscopy, (a) [36], (b) [9], (c) [161] and (d) [35]. Lines connecting the Raman data points are guides to the eye.

this figure, the analysis of the Raman spectra gives a semi quantitative mapping of the borate structure in the entire glass forming range; it starts with boroxol rings of neutral BØ$_3$ triangles at $x = 0$ and progresses, through [BØ$_4$]$^-$, [BØ$_2$O]$^-$, and [B$_2$O$_5$]$^{4-}$ formation and destruction, to a completely depolymerized borate structure of highly charged orthoborate units [BO$_3$]$^{3-}$. Figure 33 also shows corresponding N_4 data from NMR spectroscopy [9, 35, 36, 161, 283]. Considering the approximations made to analyze the Raman spectra, the agreement in the composition dependence of [BØ$_4$]$^-$ species from Raman and N_4 from NMR is satisfactory especially for glasses with $x < 0.33$.

Despite the semi quantitative nature of the trends exhibited by the Raman data in figure 33, it is observed that NBOs appear to form on [BØ$_2$O]$^-$ units well below the ca. $x = 0.25$ composition, which signals the formation of NBOs according to NMR spectroscopy on the same glasses (figure 14(a)). The high sensitivity of Raman spectroscopy to NBOs may be related to the strong Raman cross-section of B–O$^-$ stretching in comparison to B-Ø stretching. It is noted that NBO formation starts at about $x = 0.30$ in Li-borate glasses (see figures 7(a), 20 and [235]), while increasing alkali cation size was found to favor the early formation of NBOs for compositions $x < 0.50$ [285]. This was associated with the decreasing polarizing power, i.e. increasing softness of the alkali cations (Lewis acids).

In a later study of xNa$_2$O-(1-x)B$_2$O$_3$ glasses and melts with $0 \leqslant x \leqslant 0.33$ [284], the Raman spectra were fitted in the entire frequency range with Gaussian-type bands which were attributed to different borate species. The scaling of Raman data with corresponding NMR data allowed the evaluation from Raman spectroscopy of N_{3a}/N_{3s} and N_4, where N_{3a} and N_{3s} stand for the relative population of [BØ$_2$O]$^-$ and BØ$_3$ species. The composition and temperature dependence of N_4 as derived from Raman spectroscopy is shown in figure 34 [284]. It is clear that at each Na$_2$O content there is a decreasing trend of N_4 with temperature, indicating the conversion of [BØ$_4$]$^-$ to [BØ$_2$O]$^-$ species at high temperatures. This is an example of the effectiveness of Raman spectroscopy to characterize melt structures, using instrumentation and experimental setups more accessible than those of some other techniques.

The temperature-induced conversion [BØ$_4$]$^- \rightarrow$[BØ$_2$O]$^-$ in alkali borate glasses has been supported by a range of studies including statistical mechanical calculations [286], high-temperature NMR [40, 287], high temperature Raman [284, 288, 289], molecular dynamics simulations [290, 291], neutron diffraction [292, 293], and high-energy x-ray diffraction [294, 295].

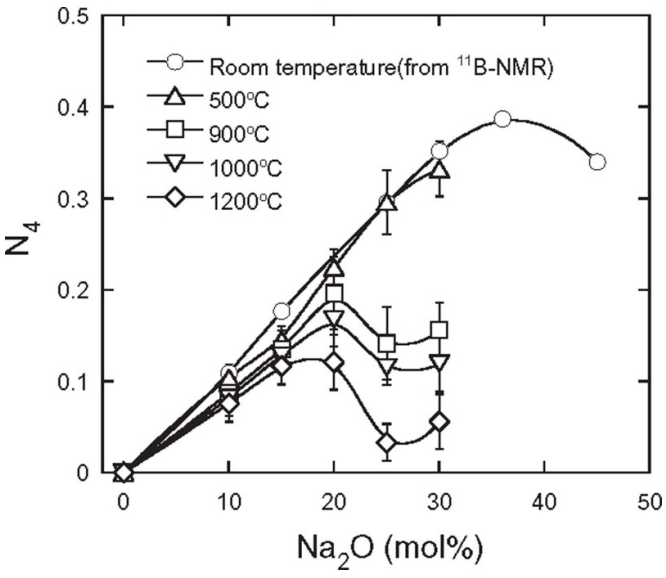

Figure 34. Plot of N_4 at various temperatures as a function of Na_2O content for glasses $x$$Na_2O$-(1-$x$)$B_2O_3$. ^{11}B-NMR data are employed to scale the room temperature Raman data [35]. Lines between the data points are guides to the eye. (a) Reprinted from [284] (a) Yano, T.; Kunimine, N.; Shibata, S.; Yamane, M. Structural Investigation of Sodium Borate Glasses and Melts by Raman Spectroscopy.: I. Quantitative Evaluation of Structural Units. J. Non-Cryst. Solids 2003, 321 (3), 137–146. https://doi.org/10.1016/S0022-3093(03)00158-3. Copyright 2003 with permission from Elsevier. (b) Reprinted from [284] (b) Yano, T.; Kunimine, N.; Shibata, S.; Yamane, M. Structural Investigation of Sodium Borate Glasses and Melts by Raman Spectroscopy. II. Conversion between BO_4 and BO_2O^- Units at High Temperature. J. Non-Cryst. Solids 2003, 321 (3), 147–156. Copyright 2003 with permission from Elsevier.

4. Neutron and x-ray methods

4.1. Introduction

The application of x-ray diffraction methods to study the structure of glasses was developed by Warren and coworkers in the 1930s [296, 297], applied to sodium borate glasses to determine N_4 for the very first time in 1938 [5], and subsequently to calcium [298] and potassium [299] borate glasses in the early 1940s. In the late 1940s, neutron diffraction methods at reactor sources became available, and subsequently, in the early 1970s, the pulsed neutron scattering technique was developed for particle accelerator based sources of neutrons. Importantly, this latter method enabled the exploitation of more energetic, epithermal, neutrons and to collect diffraction patterns to high momentum transfers. This is important for studying glass structure since the maximum momentum transfer is reciprocally related to the real-space resolution in the resulting pair distribution functions, which are the weighted histograms of all of the interatomic separations occurring in the scattering material. At a similar time, Mozzi and Warren [300, 301] demonstrated the collection of higher quality x-ray diffraction data from glasses, in part by use of higher energy x-rays derived from a heavier metal source (Rh Kα as opposed to Mo Kα). A step change came in the mid-1990s with the use of much higher-energy x-rays, produced at intense synchrotron sources, being applied to study glass structure by diffraction [302, 303]. As for pulsed neutron sources, these 'hard' x-rays allowed for measurements of high real-space resolution pair distribution functions. In addition, the use of pulsed neutrons or high-energy synchrotron x-rays have several other advantages that allow the collection of high quality diffraction patterns from glasses, including reduced neutron capture and photoelectric absorption cross-sections respectively. As such, the study of glass structure by diffraction methods has come to be dominated by pulsed neutrons and hard synchrotron x-rays, although reactor neutrons also play a strong part. What these sources have in common is that they are too large and costly for a typical laboratory to house, and tend to be run as national or international facilities. This has meant that, whilst such large-scale facilities provide diffraction data of much higher quality than can be obtained with small-scale laboratory sources of x-rays (or even neutrons or electrons), there is, at least a perception of, lower accessibility. The result is that, as can be seen from this review, the number of studies of N_4 in borate glasses by diffraction methods is much lower than by NMR or vibrational spectroscopy, techniques which are more widely available. The opportunity to reduce this gap is already ripe for the picking, given the increases in brightness and throughput of both synchrotron and neutron sources over recent decades, along with the development of improved analysis techniques, as discussed below.

Historically, the first reports of the measurement of binary borate glass structure by neutron diffraction appeared in the late 1980s, with pulsed neutron diffraction studies of heavy metal borate glasses by Yasui *et al* [304, 305]. However, it was not until the early 1990s that neutron diffraction measurements were used to derive N_4 values, by Wright and Vedishcheva *et al* in lead borate glasses [263, 306, 307], and by Kita *et al* in sodium borate melts [308]. The first use of high-energy synchrotron x-ray diffraction to study binary borate glasses (and melts) came in the late 1990s with a study including $15Li_2O$-$85B_2O_3$ by Herms *et al* [309], with the first reports of N_4 coming from Herms and Sakowski in 2000, on more highly modified alkali borate glasses and melts [310]. As such, the vast majority of diffraction studies reviewed below are those originating in the 1990s and the decades since, representing 30 years of research, because these studies are the ones in which reasonably accurate quantitative determinations of N_4 in binary borate glasses and melts have been made. In total we review about 315 diffraction measurements where N_4 has been reported, with half of those being from the borate melt studies of Alderman *et al* [258, 294, 295, 311, 312]. This covers about 32 studies and 17 different modifiers.

4.2. Outline of diffraction theory

As is evident from the introduction above, diffraction based determinations of N_4 in binary borate glasses and melts have historically been made using either x-rays or neutrons. The theoretical background and equations used to interpret such measurements are introduced below, using a superscript R to denote a dependence on radiation type, and $R = N$ or X to

denote neutrons or x-rays respectively. Other types of radiation used for diffraction measurements, such as electrons, have thus far played a minor role and are therefore considered beyond the scope of the present article, although many of the concepts are identical. In a total scattering diffraction experiment, the measured quantity is the differential scattering cross section:

$$\frac{\mathrm{d}\sigma^N}{\mathrm{d}\Omega}(Q) = I^N(Q) = S^N(Q) + \sum_{\alpha=1}^{n} c_\alpha \overline{b_\alpha^2}, \tag{4.1}$$

$$\frac{\mathrm{d}\sigma^X}{\mathrm{d}\Omega}(Q) = I^X(Q) = S^{X'}(Q) + \sum_{\alpha=1}^{n} c_\alpha f_\alpha^2(Q) + \sum_{\alpha=1}^{n} c_\alpha C_\alpha(Q). \tag{4.2}$$

Here $Q = (4\pi/\lambda)\sin\theta$ is the scattering vector magnitude for elastic scattering, between radiation quanta with incident and scattered wavelength λ and 2θ is the scattering angle between their wavevectors $\boldsymbol{k_i}$ and $\boldsymbol{k_f}$, with $|\boldsymbol{k_f}| = |\boldsymbol{k_i}| = k = 2\pi/\lambda$. For isotropic media, including most glasses, the cross section depends only on the magnitude of $\boldsymbol{Q} = \boldsymbol{k_i}$–$\boldsymbol{k_f}$, that is $|\boldsymbol{Q}| = Q$. σ^R is the scattering cross section and Ω the solid angle. $S^R(Q)$ is the distinct scattering which contains all of the structural information relating to distances between pairs of atoms within the scattering volume. The meaning of the prime in the x-ray distinct scattering is explained below. The remaining terms on the right hand side of equations (4.1) and (4.2) are self-scattering terms which do not contain structural information and contribute only an incoherent background signal which must be subtracted from the measured differential cross sections to obtain the distinct scattering. The summations represent compositional averaging over the n unique elements present, with c_α the fractions of atoms of identity α within the scattering volume. The $\bar{b}_\alpha$ are the neutron scattering lengths averaged over all isotopes and spin states of the nucleus-neutron system for a given element α. The $f_\alpha(Q)$ and $C_\alpha(Q)$ are respectively the x-ray form factors and Compton scattering for element α. The distinct scattering term can be represented as a summation over pair terms:

$$S^N(Q) = \sum_{\alpha\geqslant\beta}^{n}\sum_{\beta=1}^{n}(2-\delta_{\alpha\beta})\,c_\alpha c_\beta\,\overline{b_\alpha}\,\overline{b_\beta}\,(S_{\alpha\beta}(Q)-1) \tag{4.3}$$

$$S^X(Q) = \frac{S^{X'}(Q)}{\left(\sum_{\alpha=1}^{n} c_\alpha f_\alpha\ (Q)\right)^2} = \sum_{\alpha\geqslant\beta}^{n}\sum_{\beta=1}^{n}\frac{(2-\delta_{\alpha\beta})\,c_\alpha c_\beta f_\alpha(Q) f_\beta(Q)\,(S_{\alpha\beta}(Q)-1)}{\left(\sum_{\alpha=1}^{n} c_\alpha f_\alpha\ (Q)\right)^2} \tag{4.4}$$

where $\delta_{\alpha\beta}$ is the Kronecker delta with α and β the chemical elements within the scattering volume. The $S_{\alpha\beta}(Q)$ are known as the partial structure factors, encoding the information on distances between atoms of type α and β, there being $(n^2 + n)/2$ unique pair terms. The x-ray distinct scattering $S^{X'}(Q)$ is divided by a sharpening function $(\sum_{\alpha=1}^{n} c_\alpha f_\alpha\ (Q))^2$ in order to approximately remove its form-factor related Q-dependence, this approximation becomes exact only for monatomic scatterers.

Note that the $S_{\alpha\beta}(Q)$ partial structure factors depend only on the structure of the material, and not on the radiation type. The influence of the radiation type is encapsulated in the pair weighting factors which we define as:

$$W_{\alpha\beta}^N = (2-\delta_{\alpha\beta})\,c_\alpha c_\beta\ \overline{b_\alpha}\,\overline{b_\beta}, \tag{4.5}$$

$$W_{\alpha\beta}^X(Q) = \frac{(2-\delta_{\alpha\beta})\,c_\alpha c_\beta f_\alpha(Q) f_\beta(Q)}{\left(\sum_{\alpha=1}^{n} c_\alpha f_\alpha(Q)\right)^2}. \tag{4.6}$$

Such that

$$S^R(Q) = \sum_{\alpha\geqslant\beta}^{n}\sum_{\beta=1}^{n} W_{\alpha\beta}^R(Q)\,(S_{\alpha\beta}(Q)-1). \tag{4.7}$$

An example of both $QS^N(Q)$ and $QS^X(Q)$ are shown in figure 35 for the case of a barium diborate glass [258]. In this example there is considerable contrast due to the relatively high weighting of the Ba–β pair terms in the x-ray scattering. Nonetheless, many similar features can be observed in the two interference functions, including the positions of the first two peaks at $Q_1 \simeq 1.25$ Å^{-1} and $Q_2 \simeq 1.91$ Å^{-1}, as well as the oscillations at high-Q which are dominated by the B-O pair term. These similarities stem from the fact that both functions are based on the same set of $S_{\alpha\beta}(Q)$, only with different pair weightings.

Defining the partial radial distribution function $\rho_{\alpha\beta}(r)$ as the average number of β atoms within a spherical shell at separations between r and $r + \mathrm{d}r$ of an α atom, the site-site partial pair distribution function is defined by:

$$g_{\alpha\beta}(r) \equiv \frac{\rho_{\alpha\beta}(r)}{4\pi r^2 \rho_0} \tag{4.8}$$

where ρ_0 is the number of atoms per unit volume. Likewise, the partial differential distribution function is defined by:

$$d_{\alpha\beta}(r) = 4\pi r\rho_0\,[g_{\alpha\beta}(r) - 1] \tag{4.9}$$

and relates by sine Fourier transform to the partial structure factor:

$$d_{\alpha\beta}(r) = \frac{2}{\pi}\int_0^\infty Q\,[S_{\alpha\beta}(Q)-1]\sin Qr\,\mathrm{d}Q\,. \tag{4.10}$$

Average CNs can be determined by integration as:

$$n_{\alpha\beta}(r_1, r_2) = c_\beta\int_{r_1}^{r_2}\rho_{\alpha\beta}(r)\,\mathrm{d}r = c_\beta\int_{r_1}^{r_2} r t_{\alpha\beta}(r)\,\mathrm{d}r = 4\pi\rho_0 c_\beta\int_{r_1}^{r_2} r^2 g_{\alpha\beta}(r)\,\mathrm{d}r \tag{4.11}$$

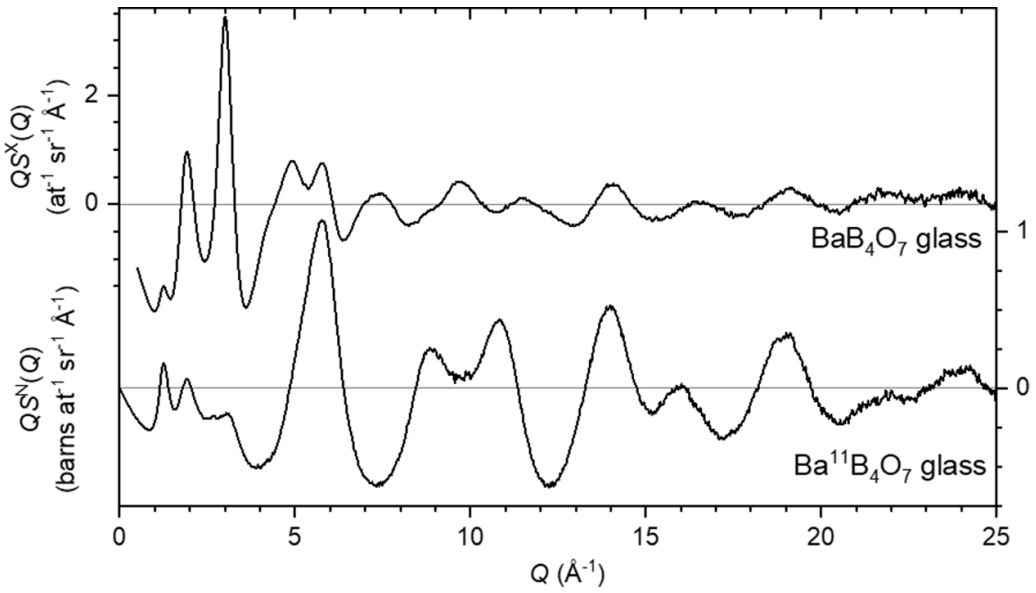

Figure 35. Interference functions for $Ba^{11}B_4O_7$ glass as measured with neutrons on the GEM instrument at the ISIS Neutron and Muon Source (lower) [258] and for BaB_4O_7 glass as measured with x-rays at sector 6-ID-D of the Advanced Photon Source (upper) [258].

where

$$t_{\alpha\beta}(r) = d_{\alpha\beta}(r) + 4\pi r\rho_0 \,. \tag{4.12}$$

This is key to the subject of our review, because within the assumption that boron in borate glasses coordinates either to 3 or 4 oxygen atoms:

$$N_4 = n_{BO} - 3 \tag{4.13}$$

where it is implicit that the integration limits encompass only the first coordination shell.

Since in practice it is rare that all of the partial $S_{\alpha\beta}(Q)$ and $d_{\alpha\beta}(r)$ can be determined experimentally, it is usual to define x-ray or neutron differential distribution functions:

$$D^R(r) = \frac{2}{\pi}\int_0^{Q_{\max}} QS^R(Q)M(Q)\sin Qr\,\mathrm{d}Q \tag{4.14}$$

wherein it is explicitly acknowledged that measurements can only attain a certain finite maximum $Q = Q_{\max}$, and a modification function, $M(Q)$, is used to describe the truncation at $Q_{\max}$. This truncation can be performed sharply with a step function:

$$M_{\text{step}}(Q) = 1 \text{ for } Q \leqslant Q_{\max} \text{ or } 0 \text{ for } Q > Q_{\max} \tag{4.15}$$

or more smoothly with, for example, a Lorch function:

$$M_{Lorch}(Q) = \frac{Q_{\max}}{\pi Q}\sin\left(\frac{\pi Q}{Q_{\max}}\right) \text{ for } Q \leqslant Q_{\max} \text{ or } 0 \text{ for } Q > Q_{\max}. \tag{4.16}$$

The total correlation functions are given by:

$$T^R(r) = D^R(r) + 4\pi r\rho_0 \sum_{\alpha\geqslant\beta}^{n}\sum_{\beta=1}^{n} W^R_{\alpha\beta}(Q=0) \tag{4.17}$$

where it should be noted that within our formalism the summation over pair weighting factors is unity for x-rays and equal to the compositionally averaged neutron scattering length squared, $\langle\bar{b}\rangle^2$, for neutrons:

$$T^N(r) = D^N(r) + 4\pi r\rho_0\langle\bar{b}\rangle^2 \tag{4.18}$$

$$T^X(r) = D^X(r) + 4\pi r\rho_0. \tag{4.19}$$

An example of $T^N(r)$ is shown in figure 36 for the case of a barium diborate glass [258].

In terms of partial pair correlations:

$$T^R(r) = \sum_{\alpha\geqslant\beta}^{n}\sum_{\beta=1}^{n} P^R_{\alpha\beta}(r)\otimes t_{\alpha\beta}(r) \tag{4.20}$$

where $\otimes$ denotes a convolution and the peak shape functions are given by

$$P^R_{\alpha\beta}(r) = \frac{1}{\pi}\int_0^{\infty} W^R_{\alpha\beta}(Q)M(Q)\cos Qr\,\mathrm{d}Q. \tag{4.21}$$

From the above, it is clear that care must be taken when determining CNs from $T^R(r)$. This is because even when, e.g. the B–O bond length distribution *circa* 1.4 Å, is apparently fully resolved from other partial pair contributions, its peak shape function will mean that its total area is spread out. Thus, strictly speaking a broad integration range is needed which may not be possible due to correlations at higher r. Furthermore, there may still be subtle influences from other partial pair contributions, especially in the case of x-rays where the weighting factors are Q-dependent, as well as in the case of relatively low $Q_{\max}$. For this reason, peak fitting methods are often applied, as described in the following sections.

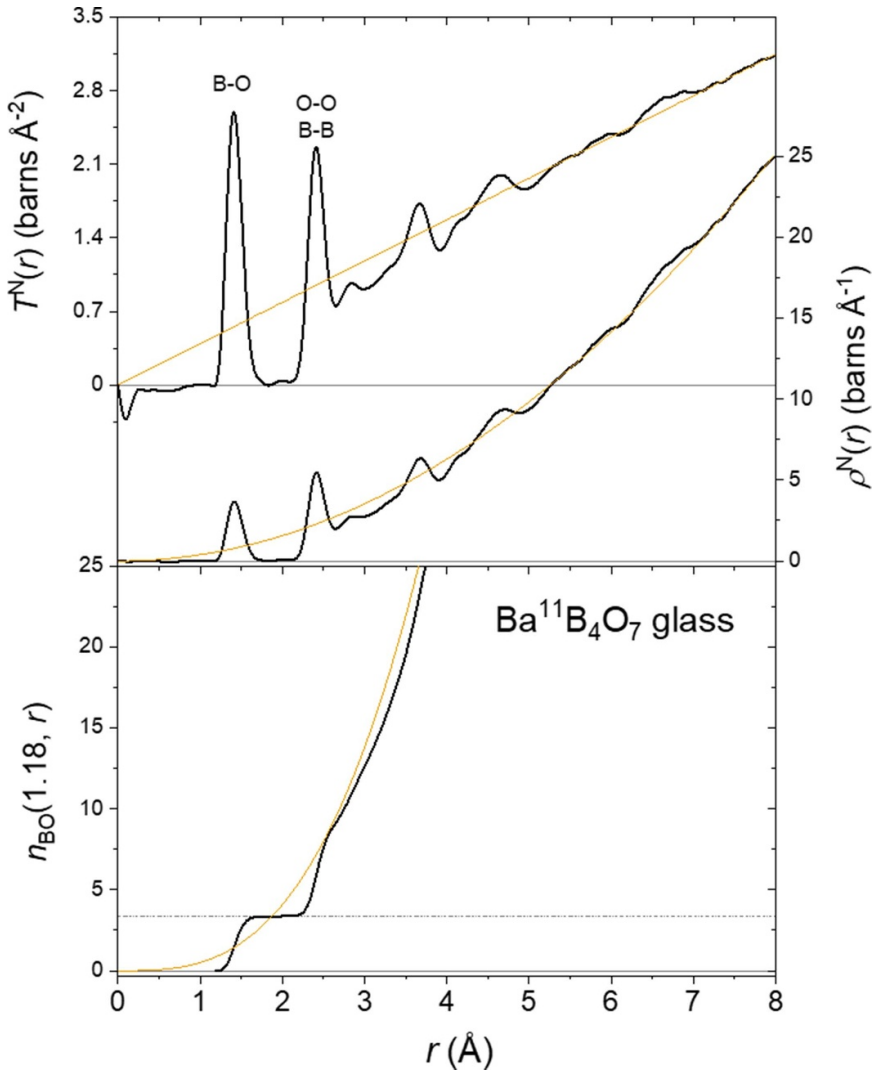

Figure 36. Neutron (a) total correlation function; (b) radial distribution function; (c) running B–O coordination number for $Ba^{11}B_4O_7$ glass as measured on the GEM instrument at the ISIS Neutron and Muon Source. The yellow curves represent the average density contributions which are (a) $4\pi r\rho_0\langle\bar{b}\rangle^2$; (b) $4\pi r^2\rho_0\langle\bar{b}\rangle^2$; (c) $\frac{4}{3}\pi r^3\rho_0\langle\bar{b}\rangle^2\frac{c_O}{W^N_{BO}}$. Since $n_{\mathrm{BO}}(1.18, r)$ is calculated from the total $\rho^N(r)$, it corresponds only to $n_{\mathrm{BO}}(r)$ below about 2 Å. The plateau prior to this indicates $n_{\mathrm{BO}} = 3.35(10)$, as indicated by the chained horizontal line, and $N_4 = 0.35(10)$ [258]. The data were obtained by Fourier transform of the interference function in figure 35, using a Lorch modification function and $Q_{\max} = 40$ Å^{-1}.

4.3. Methods for extracting N_4 from diffraction data

Note that all methods for calculation of N_4 from diffraction data are based on measurement of the mean CN, n_{BO}, and predicated on the assumption that only 3- and 4-coordinated boron atoms are present, such that $N_4 = n_{\mathrm{BO}} - 3$.

4.3.1. Direct integration of the pair distribution function. In order to determine the B–O CN by direct integration, one needs access to the partial radial distribution function $\rho_{\mathrm{BO}}(r)$. For determination of N_4, it is only the local CN that is of interest, and so only $\rho_{\mathrm{BO}}(1.0 \lesssim r \lesssim 1.8$ Å) is actually required. Thus, even though it is $T^N(r)$ or $T^X(r)$ that are determined from a single neutron or x-ray diffraction measurement, rather than $\rho_{\mathrm{BO}}(r) = rt_{\mathrm{BO}}(r)$, in the cases where there is no real-space overlap with other pair terms, then n_{BO} and N_4 can be determined by suitable integration of the total correlation function. For the case of neutrons, the pair weighting factors are independent of Q, and therefore the W^N_{BO} can be divided out in real-space. Thus, the integral of equation (4.11) becomes:

$$n_{BO}(r_1, r_2) = c_O\int_{r_1}^{r_2} rt_{BO}(r)\,\mathrm{d}r = \frac{c_O}{W^N_{BO}}\int_{r_1}^{r_2} rT^N(r)\,\mathrm{d}r \quad (4.22)$$

where the second equality holds only for integration limits chosen to encompass the B–O bond length distribution, without overlap with any other non-zero partial pair distribution. An example of this is shown in figure 36 for the case of a barium diborate glass [258].

For the x-ray case, the Q-dependence of the weighting factors necessitates the division by $W^X_{BO}(Q)$ in reciprocal space:

$$S^X_{BO}(Q) = \frac{S^X(Q)}{W^X_{BO}(Q)}. \tag{4.23}$$

Fourier transform of this modified structure factor using equation (4.14) leads to a real-space function $D^X_{BO}(r)$ and

$$T^X_{BO}(r) = D^X_{BO}(r) + 4\pi r\rho_0 \sum_{\alpha\geqslant\beta}^{n}\sum_{\beta=1}^{n} \frac{W^R_{\alpha\beta}(Q=0)}{W^X_{BO}(Q=0)}. \tag{4.24}$$

Then finally,

$$n_{BO}(r_1, r_2) = c_O \int_{r_1}^{r_2} r T^X_{BO}(r)\,\mathrm{d}r. \tag{4.25}$$

As for equation (4.22), equation (4.25) holds only for integration limits chosen to encompass the B–O bond length distribution, without overlap with any other non-zero partial pair distributions. In practice a small amount of overlap with other partial pair terms can be difficult to avoid, especially due to the complex peak function for the pair terms other than B–O for the x-ray case.

If there is overlap of the B–O nearest-neighbor peak with peaks arising from other pair terms, then integration of the total $T^N(r)$ or $T^X_{BO}(r)$ will not yield the desired result. It may be possible to remove the overlap by defining a suitable difference function taken between differently weighted measurements. This could be either a difference between a neutron and x-ray measurement, or between neutron measurements made on suitable isotopically distinct samples. Since this method is not commonly practiced for boron or oxygen isotopes in borates, we do not discuss it any further herein. Alternatively, more commonly practiced methods for removal of overlap are to use some kind of model for the overlapping peaks, or to rely on peak fitting methods.

4.3.2. Peak fitting. Peak fitting is often performed to real-space diffraction data at short interatomic separations typical of the bonded (B–O, *M*–O) and nearest neighbor non-bonded (O–O, *M*–*M*, B–B, *M*–B) pair distances. Whilst any underlying distribution of interatomic distances can in principle be used, normal Gaussian distributions are the most commonly applied, being the expected peak shapes for bonded interactions within the harmonic approximation. Such peaks have the following form:

$$\tilde{t}_{\alpha\beta}(r) = \frac{n_{\alpha\beta}}{c_\beta r_{\alpha\beta}\sqrt{2\pi\left\langle u^2_{\alpha\beta}\right\rangle}} \exp\left(-\frac{(r-r_{\alpha\beta})^2}{2\left\langle u^2_{\alpha\beta}\right\rangle}\right) \otimes P^R_{\alpha\beta}(r) \tag{4.26}$$

where again $\otimes$ denotes a convolution by the peak shape function. The mean bond length between the α–β pair is denoted $r_{\alpha\beta}$, with $\left\langle u^2_{\alpha\beta}\right\rangle$ its mean-square deviation due to static and thermal disordering and $n_{\alpha\beta}$ the CN. In reciprocal space this takes the form:

$$s_{\alpha\beta}(Q) = \frac{n_{\alpha\beta} W^R_{\alpha\beta}(Q)}{c_\beta} \frac{\sin Q r_{\alpha\beta}}{Q r_{\alpha\beta}} \exp\left(-\frac{\langle u^2_{\alpha\beta}\rangle Q^2}{2}\right) \tag{4.27}$$

where it is implicit that to transform this to real-space, the same $Q_{\max}$ and modification function must be used in the Fourier transform as for the experimental data, such that the peak function is identical.

Clearly, in the case of borates, there can be both trigonal and tetrahedral species present which will have different r_{BO}, $\left\langle u^2_{BO}\right\rangle$ and abundances. It is important to note that the trigonal and tetrahedral B–O bond lengths are about $r_{\mathrm{BO3}} = 1.37$ Å and $r_{\mathrm{BO4}} = 1.48$ Å, respectively, and, to date, these have never been resolved from one another in a measured pair distribution function. Using pulsed neutrons to obtain high $Q_{\max} = 50$ Å^{-1} Hoppe *et al* [313] resolved the bridging P–O and terminal P=O bonds in P_2O_5 glass. These occur respectively at $r_{\mathrm{P\text{-}Ob}} = 1.58$ Å and $r_{\mathrm{P{=}Ot}} = 1.43$ Å, which is a larger separation than for r_{BO3} and r_{BO4}. Furthermore, the terminal double bond leads to a rather small $\left\langle u^2_{P=Ot}\right\rangle^{1/2} = 0.028$ Å, both factors make resolving the two P–O distances more accessible than the two B–O bond length distributions. Indeed, even for arbitrarily high $Q_{\max}$, it may never be possible to resolve the two B–O bond length distributions, which would require that their widths were both, on average, $\left\langle u^2_{BO}\right\rangle^{1/2} < 0.05$ Å, which may not be the case. Nonetheless, the existence of the two boron coordination species needs to be considered when peak fitting. When $Q_{\max}$ is relatively low, and real-space resolution $\Delta r \sim 1/Q_{\max}$ relatively poor, it can be sufficient to fit a single B–O bond length distribution. This is typical in the case of both x-ray diffraction [258, 294, 295, 311, 312] and reactor source neutron diffraction, where often $Q_{\max} \lesssim 25$ Å^{-1} and B–O peaks appear relatively symmetric. Clearly a single peak is also likely sufficient in the limiting cases of $N_4 = 0$ or 1. Using pulsed neutrons, larger $Q_{\max}$ are routinely obtained, typically in the range $30 \lesssim Q_{\max} \lesssim 50$ Å^{-1}, and asymmetry in the B–O peak becomes apparent when $0 < N_4 < 1$ [258].

When fitting a single Gaussian B–O bond length distribution to the real-space diffraction data, the N_4 follows directly from the n_{BO} in equation (4.26) using $N_4 = n_{\mathrm{BO}} - 3$. If two peaks have been fitted, then their individual CNs can be summed and $N_4 = n_{\mathrm{BO}} - 3 = n_{\mathrm{BO(1)}} + n_{\mathrm{BO(2)}} - 3$. In this manner, the two peak fit can be considered as an arbitrary characterisation of an asymmetric peak using two symmetric ones, where only their averaged or summed properties are considered. On the other hand, if one considers the fitting capable of distinguishing the bonds within trigonal and tetrahedral species, then the two peak fit can be considered to yield:

$$n_{BO} = n_{BO_4} + n_{BO_3} = 4N_4 + 3(1 - N_4) = N_4 + 3 \tag{4.28}$$

such that N_4 follows not only from the total CN, but also from the CNs obtained from either of the two individual peaks. I.e.:

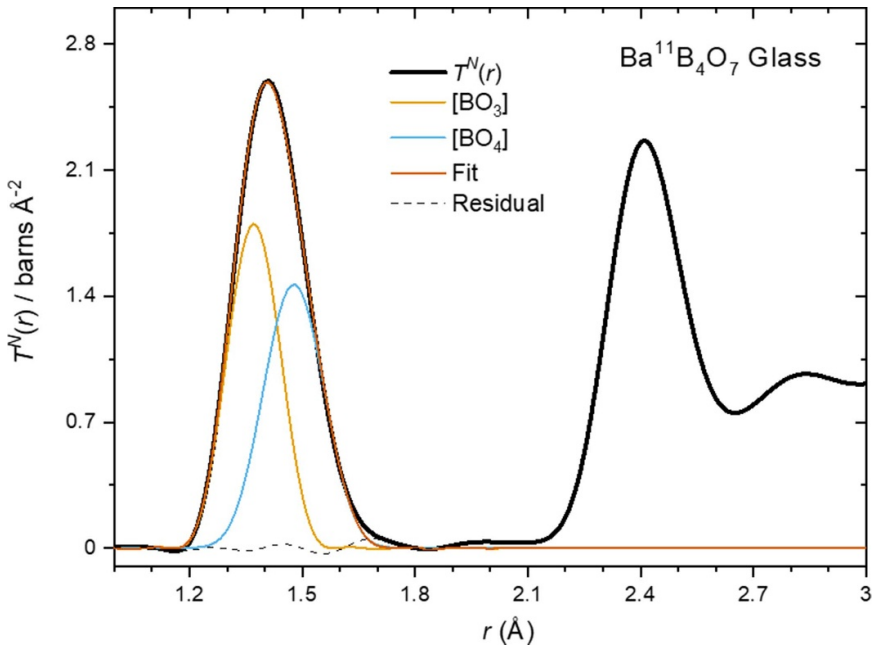

Figure 37. Two peak fit to the neutron total correlation function for $Ba^{11}B_4O_7$ glass, as measured on the GEM instrument at the ISIS Neutron and Muon Source (figure 36) [258]. The two individual peaks are shown, along with their sum, and the residual between this and the data fitted to.

Table 3. Parameters derived from the peak fit shown in figure 37 for $Ba^{11}B_4O_7$ glass. *The individual BO_3 and BO_4 bond lengths were kept fixed at their ideal bond-valence expectation values. N_4 can be calculated from the individual peak areas (equations (4.29) and (4.30)) as well as the total area (equation (4.28), see table 4 for additional methods). $n_{OB} = c_B n_{BO}/c_O$ are also shown, along with the fraction of non-bridging oxygen, $f_{nbr} = 2 - n_{OB}$, which is non-zero at this composition if $N_4 < 0.5$ (assuming oxygen are either bridging or non-bridging and coordinate to either 2 or 1 boron atoms respectively).

Peak	r_{BO} (Å)	$\langle u^2_{BO}\rangle^{1/2}$ (Å)	n_{BO}	N_4	n_{OB}	f_{nbr}
BO_3	1.371*	0.047(2)	1.65(15)	0.45(5)	0.94(5)	0.03(3)
BO_4	1.4774*	0.062(3)	1.67(15)	0.42(4)	0.95(5)	0.05(2)
Total	1.4225	n.a.	3.32(10)	0.32(10)	1.90(7)	0.10(7)

$$N_4 = n_{BO_4}/4 \tag{4.29}$$

$$N_4 = 1 - n_{BO_3}/3. \tag{4.30}$$

Furthermore, N_4 may also be obtained by ratio, a method which is independent of the absolute normalization (scaling) of the dataset:

$$N_4 = n_{BO_4}/\left(n_{BO_4} + n_{BO_3}\right). \tag{4.31}$$

In the author's (OLGA) experience, sensible two-peak fitting results are only reliably obtained with the use of some kind of fitting constraint. For example, the positions of the two peaks can be fixed at the expected positions for ideal trigonal and tetrahedral species from empirical bond-valence theory (1.371 Å and 1.477 Å). An example using this constraint is shown in figure 37, for the neutron diffraction measurement of $Ba^{11}B_4O_7$ glass [258]. Final fitting parameters are given in table 3. Interestingly, the $\langle u^2_{BO}\rangle^{1/2}$ obtained indicate that the peaks are unlikely to be resolvable, even with arbitrarily high real-space resolution, since their sum is very similar to the peak separation. The total area of the two peaks together yields a similar $N_4 = 0.32(10)$ to direct integration ($N_4 = 0.35(10)$, see table 4). This is to be expected, whilst the slighter smaller value appears to arise from the inability of the fit to account for the small shoulder *circa* 1.7 Å, figure 37. This might indicate either distortion (static disorder) or anharmonicity in the thermal vibrations of the BO_4 units, indicating that the harmonic approximation made in the use of Gaussian bond length distributions is beginning to break down. Notably, using the areas of the individual peaks yields higher N_4 values, of 0.45(5) and 0.42(4) for the BO_3 and BO_4 peaks respectively (tables 3 and 4). At first it might seem counterintuitive that the individual peaks could yield higher N_4 than that derived from their total summed area. However, it can be seen from equation (4.28) that the two instances of N_4 partially cancel out (since one is preceded by a minus sign), and will only give agreement with the N_4 from their area if they are equal. Such a condition could be used as an additional fitting constraint. Note that inclusion of the 'missing area' *circa* 1.7 Å into the BO_4 peak area improves agreement slightly, to $N_4 = 0.43(4)$. Another method for extracting N_4 from the two-peak fit is to use their CN ratio, as in equation (4.31). For our example, this method yields a slightly larger $N_4 = 0.50(10)$. Notably this method is often applied in the literature, but to the ratio

Table 4. N_4 derived for a single neutron diffraction dataset for $Ba^{11}B_4O_7$ glass, in seven different ways. These can be grouped into four methods (i) from total area of the B–O bond length distribution; (ii) from the areas of the BO_3 or BO_4 bond length distributions; (iii) from the ratio of the coordination numbers of the two bond length distributions; (iv) from the mean bond length using bond-valence methods.

Method	N_4	Equation
Integration	0.35(10) [26]	(4.22)
Fitted BO_3 peak	0.45(5)	(4.29)
Fitted BO_4 peak	0.42(4)	(4.30)
Fitted total area	0.32(10)	(4.28)
Fitted peaks ratio	0.50(10)	(4.31)
Bond valence, mean $r_{BO} = 1.4225$ Å from fit	0.45(1)	(4.36)
Bond valence, mean $r_{BO} = 1.4251$ Å from integration	0.47(1) [26]	(4.36)

of the peak *areas*. If the peak areas are determined from the $\rho_{BO}(r)$, then this is equivalent to the CN ratio. However, if the peak areas are determined from $t_{BO}(r) = \rho_{BO}(r)/r$, then N_4 will be underestimated, with $N_4 = 0.48(10)$ in our example. The underestimation will be more extreme if peak areas are determined for $g_{BO}(r) = \rho_{BO}(r)/4\pi\rho_0 r^2$.

Another example of peak fitting, this time taken from the literature [312], is shown in figure 38. In this case, x-rays were used to measure the structure factor for supercooled liquid lithium pyroborate. In contrast to the previous example of barium diborate glass measured with neutrons, here the Q_{max} is lower, at 22.8 $Å^{-1}$, and hence only a single B–O bond length distribution has been fitted. The example highlights the effects of overlap with the B–O peak, which occur here due to the presence of short modifier-oxygen (Li-O) bonds, lower real-space resolution and the complex peak shape functions arising from the electron density distributions from which the x-rays scatter. As such, it is often instructive to fit and/or model peaks to higher r, in order to extract the most accurate B–O peak parameters and hence N_4.

In summary there are three main ways that peak fitting is used to obtain N_4 from the:

(i) total area of the B–O bond length distribution, akin to the direct integration method
(ii) individual (unresolved) BO_3 and BO_4 peak areas
(iii) ratio of the (unresolved) BO_3 and BO_4 peak areas.

Note that method (i) is largely insensitive to the details of the fitting model, as long as it gives a good fit. Methods (ii) and (iii) are highly sensitive to the partitioning of the B–O bond length distribution into those from BO_3 and BO_4 units, and this cannot in general be done uniquely due to the unresolved nature of the two features. This sensitivity notwithstanding, methods (ii) and (iii) have the advantage that they are independent of the absolute scaling or normalization of the dataset being fitted.

Another means to determine N_4 from fitting parameters also exists, which is to exploit the high sensitivity of diffraction methods to length-scales and to use the bond-valence

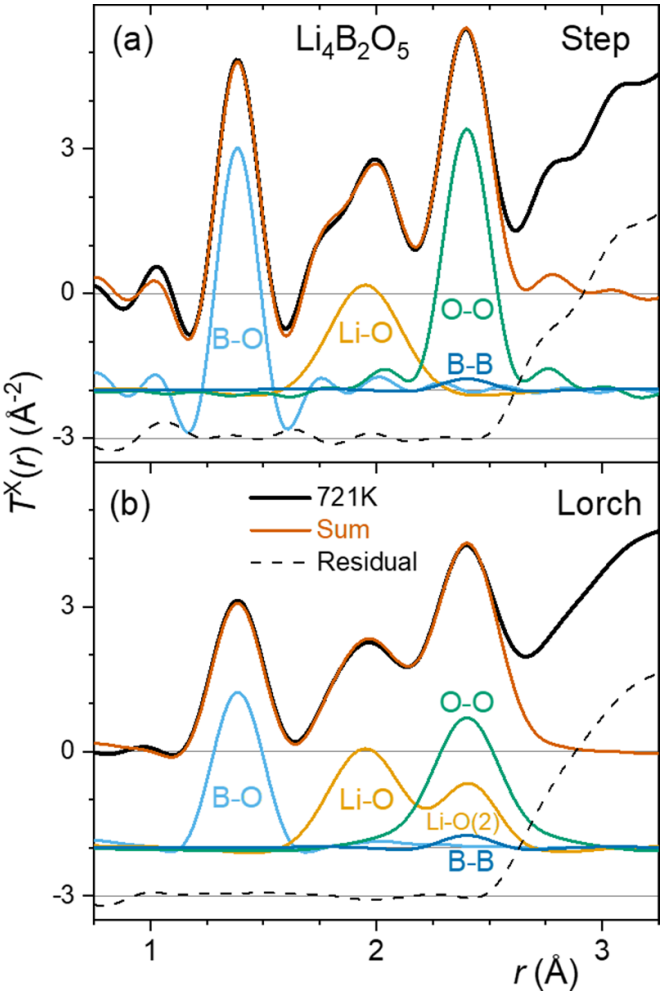

Figure 38. Peak fits to the x-ray total correlation function for supercooled liquid $Li_4B_2O_5$ at $T = 721$ K [312], obtained using $Q_{max} = 22.8$ $Å^{-1}$ and (a) step modification; (b) Lorch modification function. (a) Shows results from a four-peak simultaneous fit, with the small B–B peak estimate held fixed. This method leads to overestimation of the O–O coordination number, at the expense of longer Li–O bonds. (b) Shows results from a five-peak sequential fit, including a second distribution of longer Li–O bonds, with the O–O peak modeled at the expected coordination number. Individual peaks are offset vertically by -2 $Å^{-2}$ and the residual by -3 $Å^{-2}$ for clarity.

method for mapping mean B–O bond lengths to mean CNs, and this is discussed in the following section.

4.3.3. Mapping mean B–O bond length to N_4 using the bond valence method. The structural information contained within a diffraction measurement arises from the path length differences between radiation quanta scattered from different scattering centers. As such, diffraction is an interference technique which is highly sensitive to length scales and distances within the scattering material. This means that mean bond lengths, $r_{\alpha\beta}$, are typically determined with much higher precision than are CNs, $n_{\alpha\beta}$, because the latter depend on the absolute normalization of the scattering data, as well as on a host of corrections that are necessary in real experiments due to effects including attenuation, multiple and inelastic scattering in the sample under study, as well as in any container and sample environment apparatus. Meanwhile, the length (or Q) scaling is calibrated by measurement of a crystalline powder standard of precisely known cell parameter. Therefore, if a means exists to quantitatively relate $r_{\alpha\beta}$ to $n_{\alpha\beta}$, this could serve, at the very least, as a consistency check on the $n_{\alpha\beta}$ determined by direct integration or peak fitting, or, in cases where these lack the desired precision, to determine $n_{\alpha\beta}$ more precisely. The bond-valence (BV) methodology provides such a means and is introduced and discussed below.

The bond-valence method splits the formal valence of a central ion, V_α, between its bonds, depending upon the length of those bonds:

$$V_\alpha = \sum_\beta v_{\alpha\beta} \tag{4.32}$$

where the summation is over the bonds, and with the bond valences (strengths), $v_{\alpha\beta}$, related exponentially to the bond lengths $r_{\alpha\beta}$:

$$v_{\alpha\beta} = \exp\left(\frac{R_{\alpha\beta} - r_{\alpha\beta}}{b}\right). \tag{4.33}$$

In equation (4.33) the $R_{\alpha\beta}$ are the bond-valence parameters for the α–β pair and b is often treated as a universal constant. Using a large database of crystal structures, Brown and Altermatt [314] derived an empirical value of $b = 0.37$ Å and $R_{\mathrm{BO}} = 1.371(1)$ Å. A useful simplification can be made by assuming that all bond lengths within a coordination polyhedron are equivalent, such that

$$V_\alpha = n_{\alpha\beta}\exp\left(\frac{R_{\alpha\beta} - r_{\alpha\beta}}{b}\right) \tag{4.34}$$

and the $r_{\alpha\beta}$ can be directly related to the $n_{\alpha\beta}$ by

$$n_{\alpha\beta} = V_\alpha\exp\left(\frac{r_{\alpha\beta} - R_{\alpha\beta}}{b}\right). \tag{4.35}$$

This simplification has been shown to be a useful approximation, [258, 294, 295, 311, 312], despite the fact that certain (if not all) borate polyhedra are expected *not* to have equivalent bonds, such as the asymmetrical metraborate $[B\text{Ø}_2O]^-$ and pyroborate $[B\text{ØO}_2]^{2-}$ triangles. In these cases the distortion theorem states that the mean bond will be elongated due to the non-equivalence of the three individual bonds, an effect arising from the exponential nature of the bond-valence relationship. As such, use of equation (4.36) below could lead to overestimation of N_4 in highly modified borates. This effect is nonetheless small when compared to the changes in mean bond length induced by boron coordination change from 3 to 4, and neglecting it therefore has only a small impact on the precision of N_4 determination via the mean bond length. Note that when $n_{\alpha\beta} = V_\alpha$, then it follows that $r_{\alpha\beta} = R_{\alpha\beta}$. For boron, $V_\alpha = V_B = 3$ and

$$N_4 = 3\left\{\exp\left(\frac{r_{BO} - R_{BO}}{b}\right) - 1\right\}. \tag{4.36}$$

So in pure B_2O_3, where $n_{\mathrm{BO}} = 3$, indeed the mean bond length r_{BO} is very close to $R_{\mathrm{BO}} = 1.371(1)$ Å, as can be seen in table 5 which lists total scattering diffraction measurements of r_{BO} in pure B_2O_3 glass. Equation (4.36), plotted in figure 39, can therefore be used to map measured mean r_{BO} to N_4, providing a means of interpolation between the integer values of $N_4 = 0$ and 1 ($n_{\mathrm{BO}} = 3$ and 4). To fully exploit the sensitivity of this method, a BV parameter can be derived from a measurement of r_{BO} in pure B_2O_3 glass using the same experimental setup and calibration as applied to the binary borate glasses under investigation, and for which precise N_4 are sought. This has been exploited for a range of binary borate glasses and melts [258, 294, 295, 311, 312], including a correction for the observed temperature dependence (thermal expansion) of the B–O bond [315] in B_2O_3, used to derive $R_{\mathrm{BO}}(T) = 1.375 + (5.14 \times 10^{-6})T$ in K and Å units, using 100 keV synchrotron x-rays. Some examples are shown in figure 40. The N_4 derived using the BV method have typical uncertainties as low as 0.01, approaching the sensitivity of high-field solid-state ^{11}B MAS NMR, but with the advantage that diffraction methods are equally applicable in the high-temperature molten state. Notably, if a BV parameter is not calibrated under the same conditions as the diffraction experiment, then an uncertainty in N_4 of 0.05 can be inferred from the range of r_{BO} measured for pure B_2O_3 glass in table 5, and represented by the blue shaded area in figure 39. The N_4 values for $Ba^{11}B_4O_7$ glass derived using equation (4.36) and the standard $R_{\mathrm{BO}} = 1.371(1)$ Å are given at the bottom of table 4. Systematic uncertainties which could arise using this method include the violation of the bond length equivalence within individual polyhedra discussed above, as well as variability of the thermal expansion coefficient for different borate polyhedra. Despite these challenges, the method appears, to date, to be the most precise and accurate means for extracting N_4 from diffraction data.

4.3.4. Holistic bulk structural modeling using diffraction data. Popular methods for diffraction data analysis include those which refine space-filling three dimensional models of atomic configurations to the measured structure factors. These include

Table 5. Summary of total scattering diffraction measurements of the mean B–O bond length in B_2O_3 glass ($^{11}B_2O_3$ for neutrons). Unweighted mean values are also given for x-rays (excluding the earliest measurement at 1.39(2) Å, and the high temperature measurement at 1.38(1) Å, denoted by *), neutrons, and both together, along with the standard deviations in parentheses. The r_{BO} obtained as part of high-pressure studies are systematically lower, with larger uncertainties, and have also been excluded (denoted by †). The r_{BO} from Suzuya *et al* [316] was determined by our own Fourier transform and peak fitting to their data (denoted by ‡). In the final row is the mean B–O bond length in crystalline B_2O_3-I, calculated from the crystallographic unit cell by averaging over the six unique bonds present. Notably the value thus obtained is slightly different from the 1.372 Å quoted by Gurr *et al* [317]. Furthermore it should be noted that crystallographic bond lengths are determined from the long-range average structure, as opposed to the local structure probed by total scattering diffraction, and can in cases with local disorder differ appreciably.

r_{BO} (Å)	R	Q_{max} (Å^{-1})	Mod. function	Year	Authors	References
1.39(2)*	X Cu & Mo Kα	11.3	Step	1936	Warren *et al*	[318]
1.37	X Cu & Rh Kα	20	Gaussian	1970	Mozzi and Warren	[301]
1.38(1)*	X Mo Kα @ 973 K	15	Step	1995	Sugiyama *et al*	[319]
1.3656(5)‡	X 40.9 keV sync.	24.47	Lorch	2000	Suzuya *et al*	[316]
1.3600	X 61.5 keV sync.	25	?	2003	Kajinami *et al*	[320]
1.351(10)†	X E dispersive	10	?	2008	Brazhkin *et al*	[321]
1.3765(5)	X 100 keV sync.	24.47	Lorch	2015	Alderman *et al*	[315]
1.3680(70)	Mean X					
1.366	N pulsed	40	Lorch	1982	Johnson *et al*	[322]
1.375	N pulsed	36	?	1990	Misawa	[323]
1.365(1)	N pulsed	44.56	Lorch	1994	Hannon *et al*	[12]
1.3655(2)	N pulsed	40	Lorch	2009	Hannon *et al*	[324]
1.347(10)†	N pulsed	19.5	step	2014	Zeidler *et al*	[325]
1.353(10)†	N reactor	21.7	step	2014	Zeidler *et al*	[325]
1.3741(2)	N pulsed, V cell	38.8	Lorch	2025	Alderman	[326]
1.3732(5)	N pulsed, Pt cell	38.8	Lorch	2025	Alderman	[326]
1.3698(48)	Mean N					
1.3691(54)	Mean					
1.371(20)	X crystallography	n.a.	n.a.	1970	Gurr *et al*	[317]

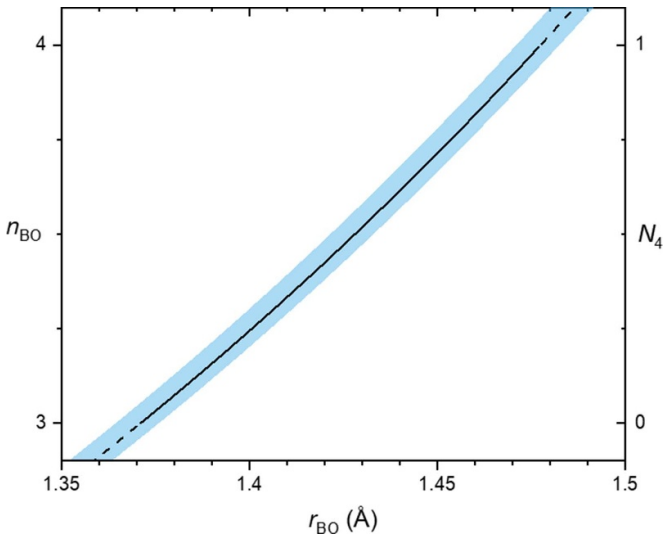

Figure 39. Exponential relationship between $n_{BO} = N_4 + 3$ and mean bond length r_{BO}, using the bond-valence methodology for equivalent bonds, equation (4.36). The black curve uses the standard BV parameters from Brown and Altermatt [314] ($b = 0.37$ Å and $R_{BO} = 1.371(1)$ Å). The blue shaded area represents the uncertainty bounds inferred from the range of measured r_{BO} in pure B_2O_3 glass, table 5. Specifically, based on $R_{BO} = 1.365(1)$ Å [12] and $R_{BO} = 1.3765(5)$ Å [315].

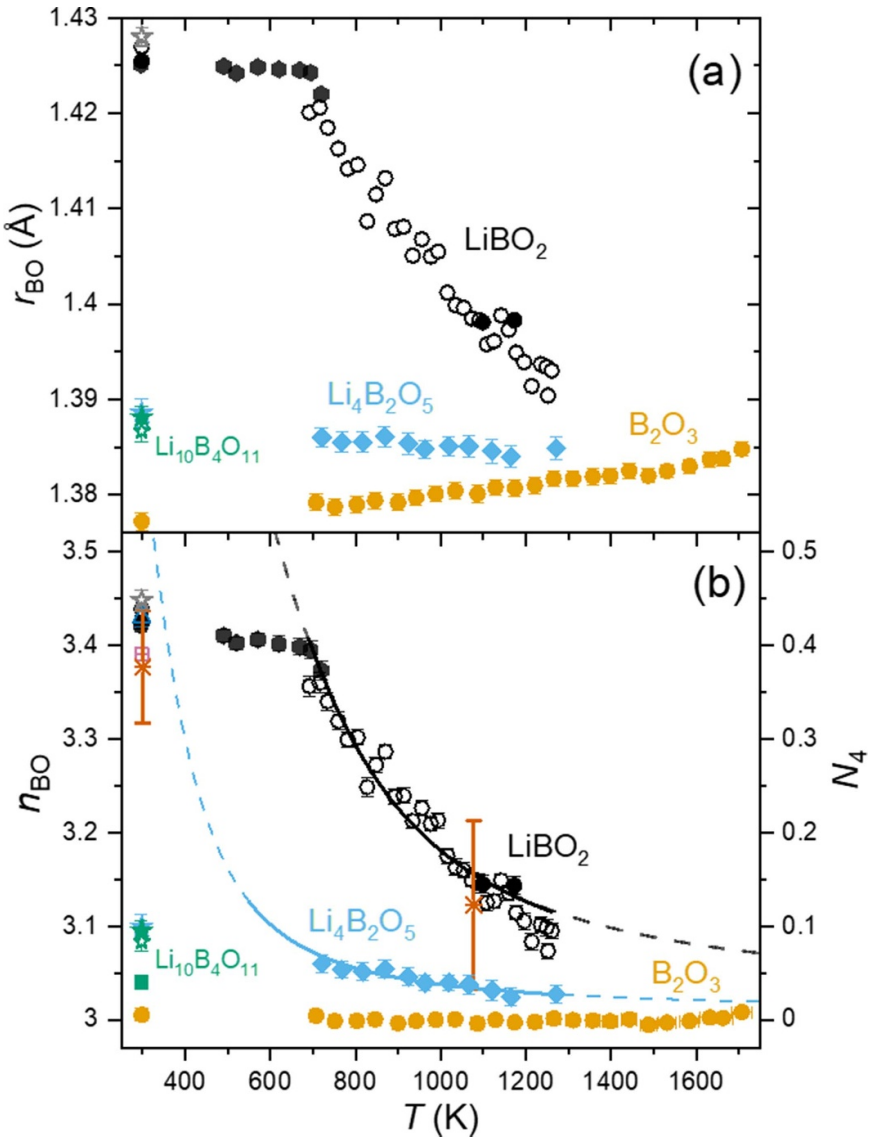

Figure 40. High-energy x-ray diffraction results for the (a) Mean B–O bond lengths, $r_{BO}(T)$ and (b) Mean B–O coordination numbers, $n_{BO}(T)$, as derived from $r_{BO}(T)$ using the temperature dependent bond-valence method [294, 311], for $Li_4B_2O_5$ [312], $LiBO_2$ [295] and B_2O_3 [315] melts and glasses, as well as $Li_{10}B_4O_{11}$ glasses [312]. The curves are the results of van't Hoff analysis based on the $[B\emptyset_4]^- \rightleftharpoons [B\emptyset_2O]^-$(and related) coordination changing isomerization reaction(s), with dashed extrapolations. Exemplary N_4 values from ^{11}B NMR are shown for comparison in (b) for $LiBO_2$ (blue triangle [42], pink crossed square [162]) and $Li_{10}B_4O_{11}$ (green square [178]), and from non-resonant inelastic x-ray scattering for $LiBO_2$ (orange double crosses [327]).

reverse Monte Carlo (RMC), empirical potential structure refinement (EPSR) and its successor Dissolve. As far as determining N_4 values is concerned, this might be considered analogous to the peak fitting methods discussed above, but with a more holistic consideration of the longer r contributions, and with the constraint(s) that the model be consistent with a chemically and physically plausible arrangement of atoms at the measured bulk density.

4.4. Diffraction studies of binary borate glasses

4.4.1. Monovalent alkali and group 11 modifiers. N_4 data compiled from diffraction experiments on alkali and silver borate glasses are plotted in figure 41. The diffraction data are shown as filled colored symbols such that they stand out against the representative N_4 data from NMR shown as open grey symbols. Taking an overview in this way, it becomes immediately apparent that the majority of the diffraction data are limited to modifier contents $R < 0.5$ where, largely, both diffraction and NMR measurements indicate that $N_4 = R$. The only examples of diffraction measurements of N_4 in highly modified (alkali or silver) binary borate glasses are those of Wright *et al* [328] for an $R = 2.13$ rubidium borate, and those of Alderman *et al* [295, 312] for $R = 1$, 2 and 2.5 lithium borate glasses. Interestingly, at such high modification levels ($R \geqslant 2$), the observed $N_4 > 0$ imply the presence of either NBO associated with tetrahedral boron units (e.g. $[BO\emptyset_3]^{2-}$) or a disproportionation into large borate

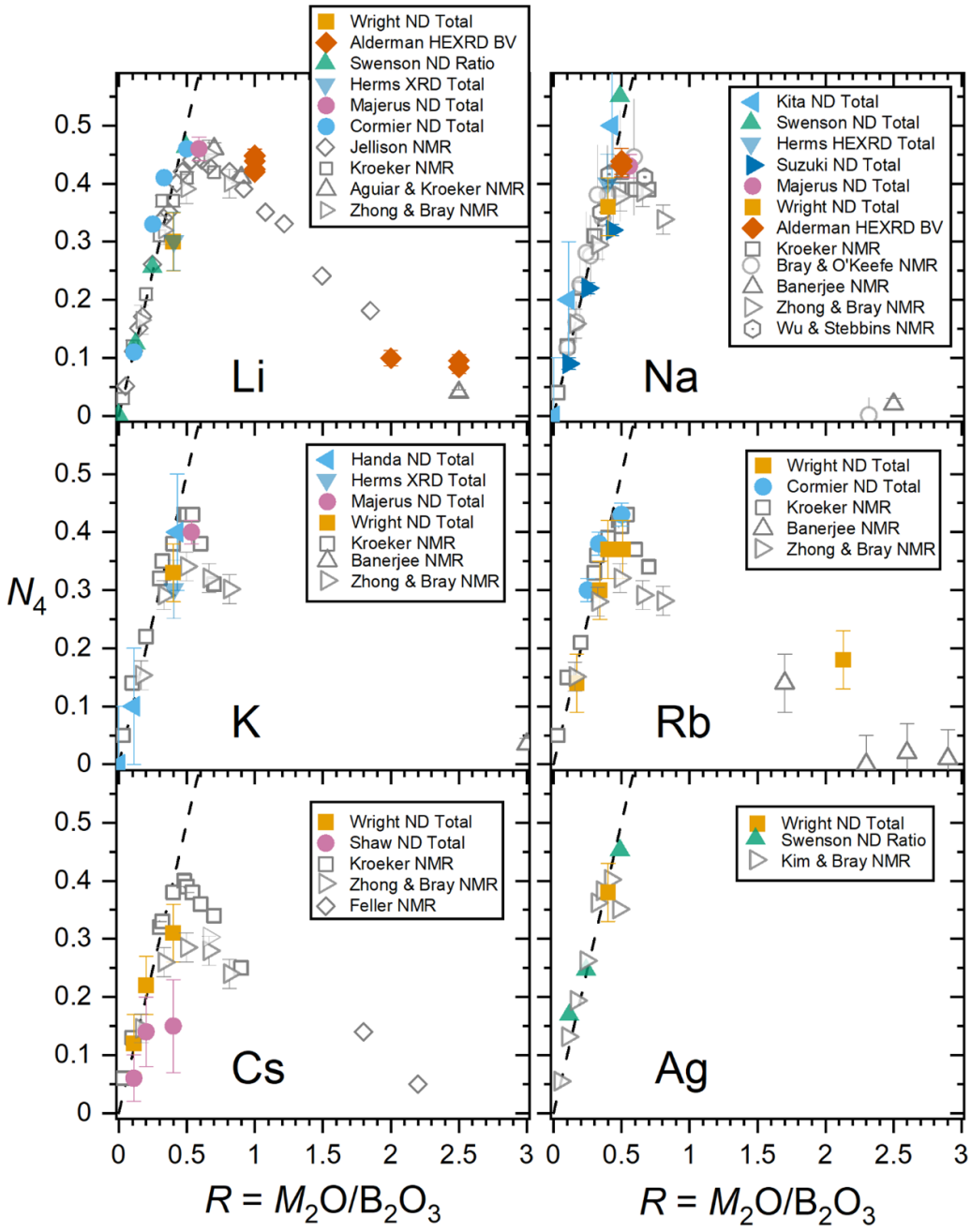

Figure 41. $N_4 = n_{BO} - 3$ values for M_2O–B_2O_3 borate glasses with monovalent modifier cations. For Li, using pulsed ND [329], reactor ND [254, 292, 330], HEXRD [295, 310, 312] and NMR [30, 35, 36, 178]. For Na using pulsed ND [329, 331] (including 1073 K melts by Kita *et al* [308]), reactor ND [254, 292], HEXRD [310, 311] and NMR [27, 35, 36, 71, 90]. For K using pulsed ND [332], reactor ND [254, 292], HEXRD [22] and NMR [35, 36, 71]. For Rb using reactor ND [254, 328, 333] and NMR [35, 36, 71]. For Cs using pulsed ND [334], reactor ND [254, 328] and NMR [35, 36, 72, 178]. For Ag using pulsed ND [329], reactor ND [254] and NMR [51].

polyanions centered around e.g. $[B\emptyset_4]^-$metaborate units (e.g. $[B\emptyset_4 \cdot 4(BO_2\emptyset)]^{9-}$), along with orthoborate $[BO_3]^{3-}$. Given that NMR studies indicate a decrease in N_4 with increasing alkali mass [35, 36, 178], at least in the $0.5 < R < 1$ composition range, it would be instructive to confirm this result using neutron diffraction on a glass series in this range, as a function of alkali, to complement the study of Wright *et al* [254] at $R = 0.4$.

4.4.2. Divalent alkaline earth and group 12 modifiers. For the divalent alkaline earth and group 12 transition metals, figure 42, there are far fewer diffraction data available, with no measurements at all for Mg or Cd. The largest number of diffraction studies in this category focus on Ba borate glasses, showing good agreement with NMR and IR studies. Kajinami *et al* [335] used a laboratory source of Mo Kα x-rays to study zinc borate glasses, and reported fitting parameters for a BO_3

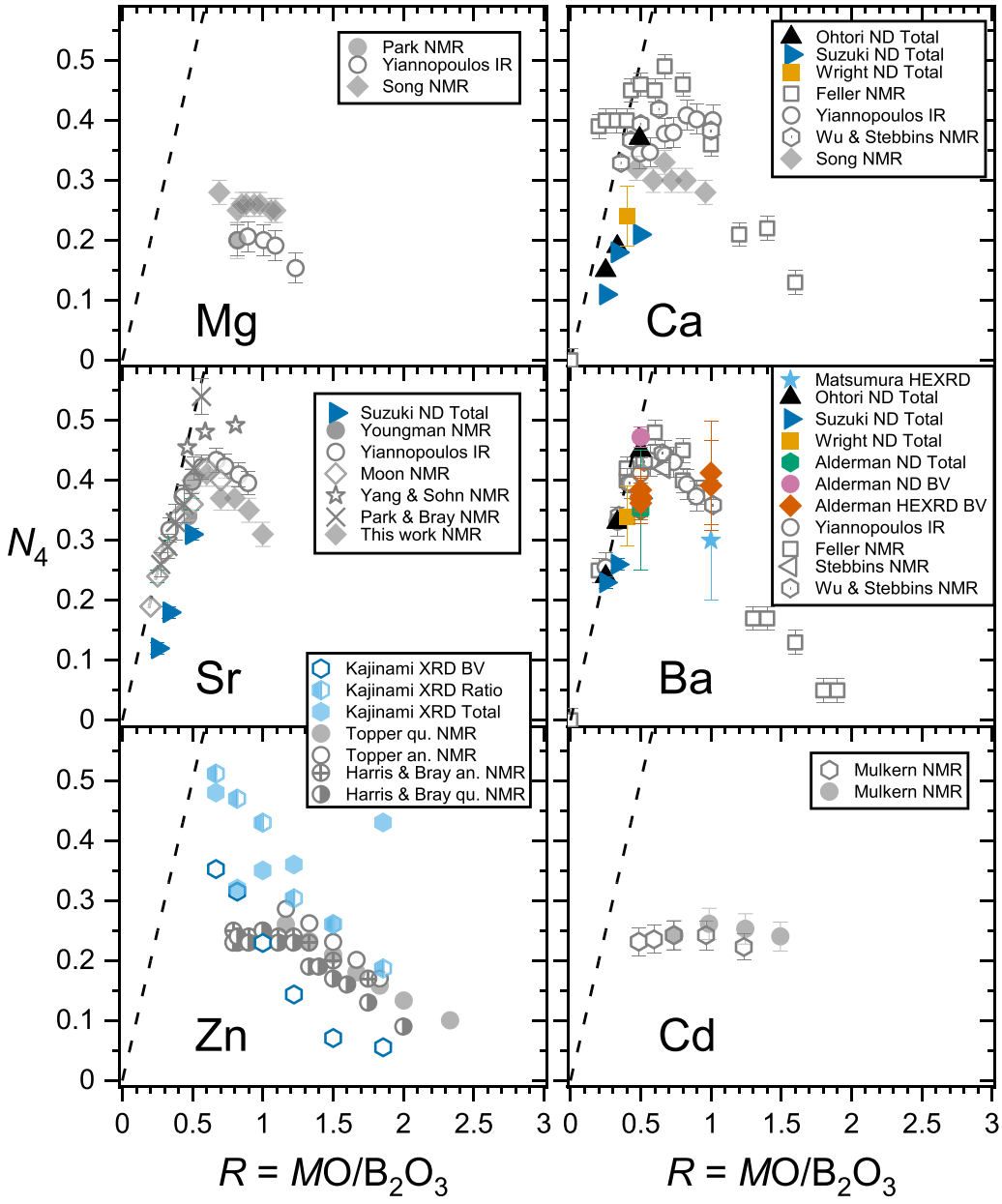

Figure 42. $N_4 = n_{BO} - 3$ values for MO-B_2O_3 borate glasses with divalent modifier cations. For Mg using NMR [53] and IR [256]. For Ca using pulsed ND [257, 331], reactor ND [254], NMR [90, 179] (data from Song *et al* [127] have been corrected for spinning sideband intensities) and IR [256]. For Sr using pulsed ND [331], NMR [50, 61, 122, 336] including the NMR data from the present work (figure 15), and IR [256]. For Ba using pulsed ND [257, 258, 331], reactor ND [254], HEXRD [258, 337], NMR [39, 90, 179] and IR [256]. For Zn using Mo Kα XRD [335] and NMR [125, 175] (for both quenched and annealed glasses). For Cd using NMR [57].

and BO_4 2-peak fit. In addition to the total n_{BO} (N_4) reported, these allow us to calculate N_4 using the ratio and BV methods, both of which give improved agreement with the trend of decreasing N_4 with increasing R observed by NMR. The data are less accurate than those obtained with NMR due to the Zn ions dominating the x-ray scattering, and the relatively small $Q_{max} = 12$ Å^{-1}. Nonetheless, this points towards the importance of reporting all fitting parameters, as well as calculating N_4 by multiple methods. As for the alkali borate glasses, it would be instructive to perform neutron diffraction on a glass series in the $0.5 < R < 1$ composition range, as a function of divalent modifier, given that IR spectroscopic data indicate the opposite trend to the alkali case, that is, an increase in N_4 with increasing alkaline earth mass [256]. There is quite a large spread in datasets for Ca borate glasses, and this is discussed further in section 5.

4.4.3. Tl^+ borate glasses. The thallium borate glasses are an unusual case where $N_4 > R$ were originally observed by Baugher and Bray using NMR methods [47], figure 43. Since that time, both ^{11}B NMR and pulsed neutron diffraction were applied to the Tl_2O-B_2O_3 glasses as part of the PhD thesis research of Nattapol Laorodphan [84]. Lower N_4

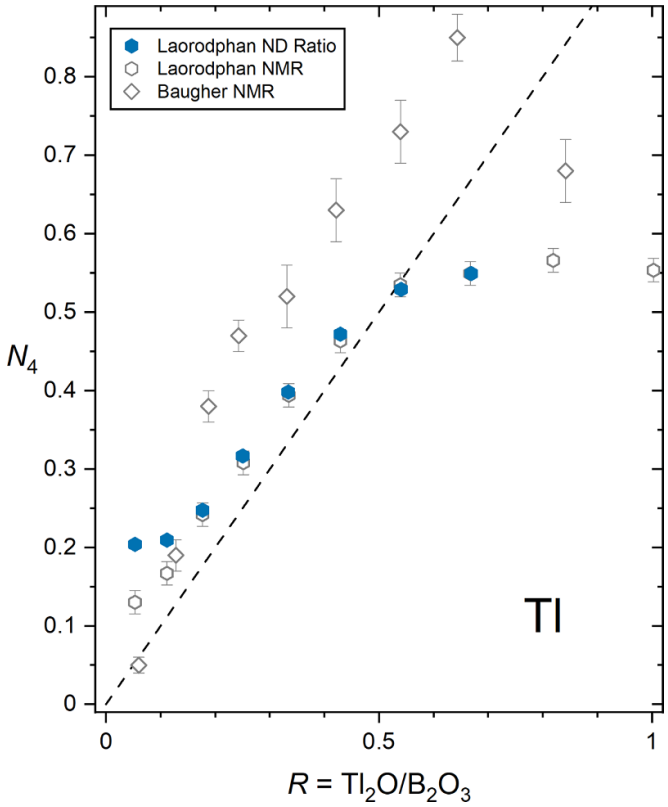

Figure 43. $N_4 = n_{BO} - 3$ values for Tl_2O–B_2O_3 glasses from the pulsed neutron diffraction study of Laorodphan *et al* [84] along with the ^{11}B NMR data from the same study and from Baugher and Bray [47].

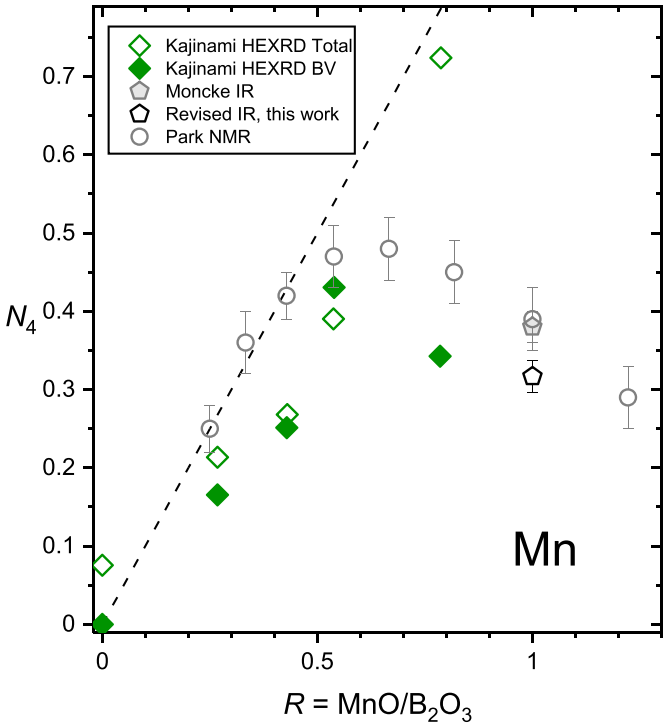

Figure 44. $N_4 = n_{BO} - 3$ values for MnO-B_2O_3 glasses from the high-energy x-ray diffraction study of Kajinami *et al* [320], digitized from their figure 3. The mean B–O bond lengths digitized from the same figure were also used to calculate N_4 using the bond valence method, and using $R_{BO} = 1.360$ Å from their r_{BO} measured for pure B_2O_3. Also shown is the IR reflectance spectroscopic determination of N_4 for manganese metaborate from Möncke *et al* [266], a revised value based on the $\alpha_r \approx 1.74$ estimated herein for Mn^{2+}, table 2, and the wide-line NMR derived data of Park and Bray [174].

than those reported by Baugher and Bray [47] were found using both techniques, but nonetheless, the glasses from 5 to 30 mol% Tl_2O were all found to have excess tetrahedral boron, with $N_4 > R$, figure 43. The neutron diffraction results were obtained by constrained fitting of two peaks to the B–O bond length distribution, fixed at the positions expected from BV. However, it is not clear if the ratio method, or the absolute areas of the peaks were used to derive the N_4 values. Unfortunately, the mean B–O bond lengths were not reported, which would provide a highly instructive check on the N_4 using the BV method. This is especially so given both the considerably atypical $N_4 > R$, as well as the large values of $N_4 > 0.5$, for $R > 0.5$, which is something rarely seen for any binary borate glasses, as is evident from this review. Laorodphan discusses possible reasons for the $N_4 > R$ observations, including the possibility of water attack, for which there was some evidence for in Raman spectra (at low Tl_2O content), and which could be exacerbated in the ^{11}B NMR measurements due to the pulverization of the samples prior to measurement. It was also noted that for two crystalline compounds known to have $N_4 = R$ from their crystal structures, $N_4 > R$ was observed by NMR, which at least raises the possibility that the same systematic effect could be at play for the glasses. The neutron diffraction data would be relatively sensitive to water content, but do not appear to show evidence for this, consistent with the fact that larger glass fragments were used in those measurements. Nonetheless, confidence in the neutron diffraction derived N_4 would be enhanced considerably if error bars could be calculated, and if agreement was found using the mean bond lengths and BV based methodology. Such confirmation should be sought before concluding that unusual structural units, such as oxygen triclusters (oxygen bonded to three boron atoms), are present to charge balance excess tetrahedral boron, such as in the high-pressure B_2O_3-II phase, or other $N_4 = 1$ structures, including SrB_4O_7 and PbB_4O_7.

4.4.4. Mn^{2+} borate glasses. Kajinami *et al* [320] studied MnO-B_2O_3 glasses using 61.5 keV synchrotron x-rays. The authors used alumina crucibles, which can lead to contamination of the melts [324]. They state that compositions were checked by inductively coupled plasma atomic emission spectroscopy, but do not present the results. They do not discuss taking any precautions to prevent the formation of Mn^{3+}, the melting temperature being 1423 K. Nonetheless, the reported CNs yield N_4 in reasonable agreement with the wide-line NMR study of Park and Bray [174], figure 44, other than the outlier at $R = 0.79$ with unusually high $N_4 = 0.72$. We have used the mean B–O bond lengths reported in the same study to calculate N_4 by the BV method, using their self-consistent

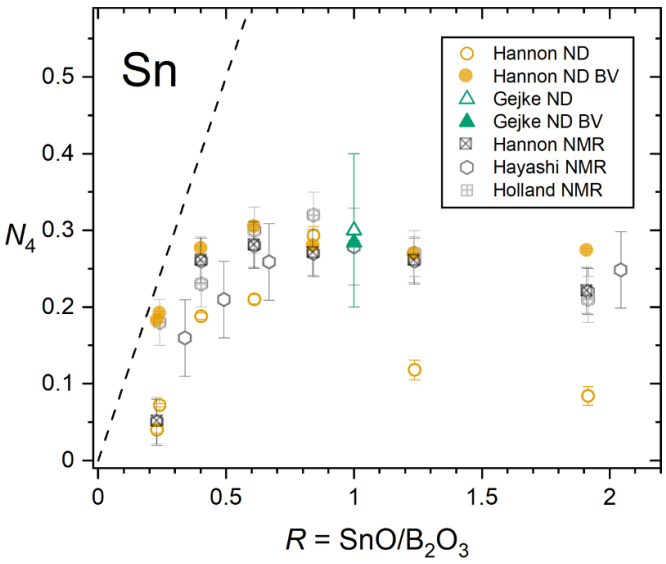

Figure 45. $N_4 = n_{BO} - 3$ values for SnO-B_2O_3 glasses from the pulsed neutron diffraction study of Hannon, Barney and Holland [324] (containing 3–9 mol% Al_2O_3), and the reactor based neutron diffraction study of Gejke *et al* [338]. Data from three ^{11}B NMR studies are shown for comparison [324, 339, 340].

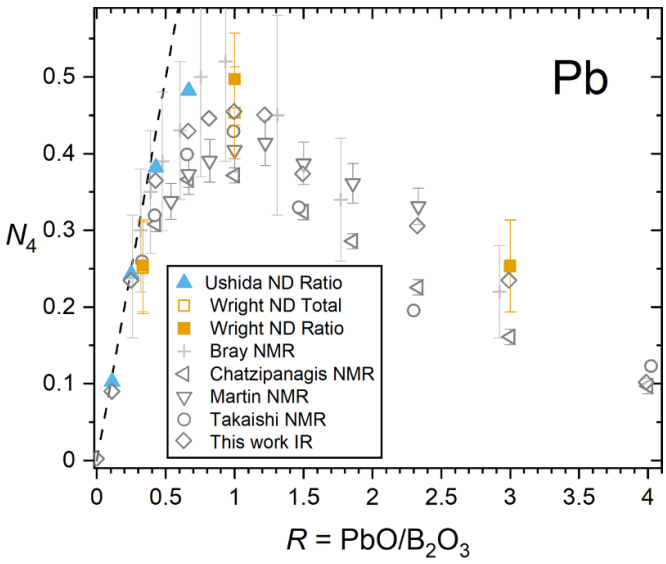

Figure 46. $N_4 = n_{BO} - 3$ values for PbO–B_2O_3 glasses from the pulsed neutron diffraction studies of Wright *et al* [263, 306, 307, 341] and Ushida *et al* [264]. Data from several ^{11}B NMR studies [44, 80, 119, 214] are also shown for comparison, along with the IR values determined in the present work.

r_{BO} reported for B_2O_3 glass as the bond-valence parameter R_{BO}, see figure 44. Not only is good agreement observed with the reported $N_4 = n_{BO} - 3$ in the $0.27 \leqslant R \leqslant 0.54$ range, but remarkably, at $R = 0.79$ we find $N_4 = 0.34$, in much closer alignment with the NMR of Park and Bray [174], and the IR study of Möncke *et al* [266] at $R = 1$. Overall, the behavior of Mn^{2+} borate glasses, in terms of N_4, appears to be rather similar to barium borate glasses, as opposed to the higher field strength Zn^{2+} and Mg^{2+} borate glasses which tend to have lower N_4 for a given composition. This is despite the fact that Mn^{2+} has a field strength intermediate between Mg^{2+} (and Zn^{2+}) and Ca^{2+}, which could imply an important effect of the 3d electrons on the bonding and resultant N_4. We should caveat this with cautionary statements regarding all of the studies represented in figure 44, including the aforementioned possibility of contamination and multivalent Mn in the x-ray diffraction work, the inherent challenges in collecting and quantifying NMR spectra from strongly paramagnetic glasses, and the uncertainty in relative IR absorption coefficient, α_r. Indeed, using the $\alpha_r \approx 1.74$ estimated herein for Mn^{2+}, table 2, yields a revised value of $N_4 = 0.32(2)$ at $R = 1$, based on the IR data of Möncke *et al* [266], and as shown in figure 44.

4.4.5. Sn^{2+} and Pb^{2+} borate glasses. There are relatively few diffraction studies of binary tin borate glasses, figure 45. We are aware only of the reactor neutron diffraction measurement by Gejke *et al* [338] on tin metaborate, up to the rather limited $Q_{max} = 10$ Å^{-1}, where they report a range of N_4 between 0.0 and 0.5 that is consistent with their observed structure factor, with a most probable value of $N_4 = 0.3$. Hannon, Barney and Holland report on a detailed neutron diffraction study of tin borate based glasses [324], melted in alumina crucibles. This led to contamination by between 3 and 9 mol% Al_2O_3, as was well characterized and discussed by the authors, such that the glasses were in fact ternary tin aluminoborates, nominally beyond the scope of the present review. Nonetheless, it is worth mentioning that with the corrected compositions, the authors found N_4 values in reasonable accord, if somewhat lower, than NMR on glasses made in both alumina [324, 339] and carbon [340] crucibles. Again, we have used the mean B–O bond lengths reported in the same study to calculate N_4 by the BV method, using their self-consistent r_{BO} reported for B_2O_3 glass as the bond-valence parameter R_{BO}, see figure 45. Remarkably, agreement with the NMR results is improved for all compositions, with a possible exception at the lowest tin content glass, where the same authors report a rather low N_4 from ^{11}B NMR, which is not in accord with earlier NMR studies, unlike their results for all other compositions.

Compared to tin borate glasses, lead borate glasses tend to have higher values of N_4, see figure 46. This implies that the higher-field-strength lone-pair cation Sn^{2+} tends to bond somewhat more covalently, and demonstrates more network former character than does Pb^{2+}. The two pulsed neutron diffraction studies of PbO–B_2O_3 glasses [263, 264, 306, 307, 341] show good agreement with both NMR and IR determinations of N_4 (figure 46), including demonstrating the presence of tetrahedral boron at very high modifier contents.

4.4.6. Sb^{3+} and Bi^{3+} borate glasses. A single neutron diffraction study of antimony borate glasses has been reported in the PhD thesis of Orman [342]. The N_4 derived from the reported n_{BO} are plotted in figure 47. Whilst Sb^{3+} is the primary modifying cation present, the Sb^{5+} content was reported to increase gradually with the total antimony content, up to about 14% of the total Sb at the highest nominal,

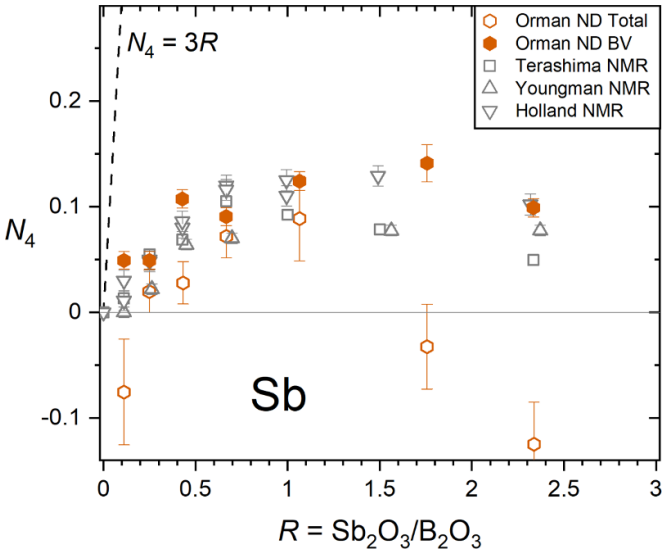

Figure 47. $N_4 = n_{BO} - 3$ values for Sb_2O_3-B_2O_3 glasses from the pulsed neutron diffraction study of Orman [342]. N_4 derived from the total area of the B–O bond length distribution are plotted (open hexagons), as reported in the doctoral thesis of Orman. In addition, the mean bond lengths reported in the thesis, obtained from single peak fits to the B–O bond length distribution, have been used herein to derive N_4 via the bond valence method (filled hexagons), using $R_{BO} = 1.365(1)$ Å from the pulsed neutron diffraction determination of r_{BO} by Hannon *et al* [12] in pure B_2O_3. Note that the antimony borate glasses were reported to contain between 1 and 14% (increasing with R) of the antimony in the Sb^{5+} oxidation state [68]. Data from several ^{11}B NMR studies [67, 68, 163] are shown for comparison.

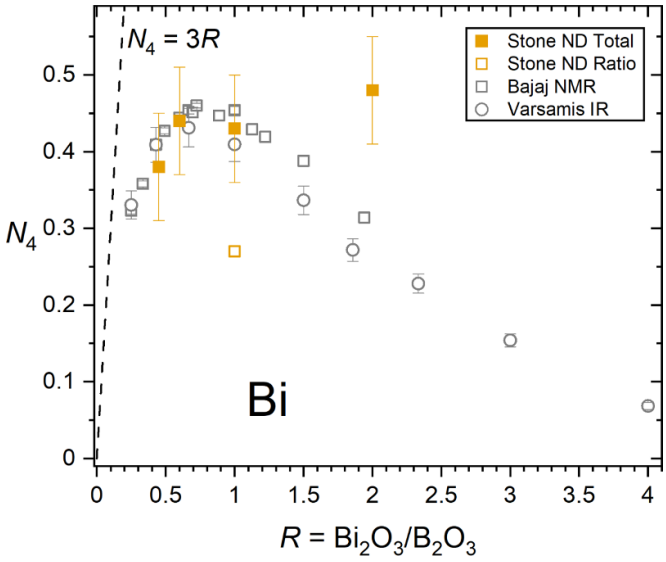

Figure 48. $N_4 = n_{BO} - 3$ values for Bi_2O_3-B_2O_3 glasses from the pulsed neutron diffraction study of Stone *et al* [341, 343]. Data from the ^{11}B NMR study of Bajaj *et al* [75] and the infrared reflectance spectroscopy study of Varsamis *et al* [278] are shown for comparison.

70 mol%, Sb_2O_3 composition [68]. As can be seen, the N_4 in these glasses are remarkably low, in stark contrast to Bi borate glasses (figure 48), an observation which is analogous to the differences between the Sn and Pb borate glasses, but of greater magnitude. In other words, the Sb is apparently bonding largely covalently, with a strongly network forming character. Notably, using the $N_4 = n_{BO} - 3$ from the total B–O peak areas [342] leads to several unphysical negative results (figure 47). This indicates systematic errors in the normalization of the diffraction data, rather than e.g. two-coordinated boron species, as can be concluded using the BV method to map the reported mean B–O bond lengths onto N_4 values. As can be seen in figure 47, this leads to $N_4 \geqslant 0$, as expected, and much better agreement with the available ^{11}B NMR data [67, 68, 163], in all cases.

For bismuth borate glasses, again, only a single neutron diffraction study has been made [341, 343] and the N_4 derived from the reported n_{BO} are plotted in figure 48. There is largely good agreement with available ^{11}B NMR [75] and IR spectroscopic [278] data, with the exception of the $R = 2$ diffraction measurement, and the $R = 1$ measurement derived using the peak ratio method, which is expected to be less reliable owing to the non-uniqueness of such fits.

4.4.7. Te^{4+} borate glasses. Tellurium borate glasses have been obtained at rather low boron contents, between R of 2 and 198 [58]. As such, one can consider tellurium as the primary network former (pure TeO_2 glass can also be obtained [344], with difficulty). Remarkably, these binary borotellurite glasses have the highest N_4 values of any of the binary borate glasses reviewed herein, as measured by both neutron diffraction [76] and NMR [58], and ranging from 0.39 to 0.91, figure 49. In this case, the N_4 derived from the n_{BO} reported by neutron diffraction are in excellent agreement with those derived from the mean B–O bond lengths and the BV method.

4.4.8. Water borate glasses. Early x-ray diffraction studies of water borate glasses (H_2O-B_2O_3) by Milberg and Meller in 1959 [345] ($R = 0$ and 0.33) and 1960 [346] ($R = 0$, 0.42, 0.50 and 0.63) indicated that the majority of boron were contained within trigonal planar units, but the 'possibility that a small fraction of the boron atoms [were] coordinated by four oxygen atoms [was] not completely excluded'. Unfortunately, the uncertainties on the CNs reported do not permit any quantitative assessment of N_4 values. Nonetheless, the authors' conclusions were consistent with contemporary NMR measurements by Silver in 1960 [43] who estimated an $N_4 = 0.05$ for an $R = 0.5$ water borate glass, with the spectrum for an $R = 0.6$ glass indicating a slightly lower, but non-zero, N_4 fraction. Meanwhile, for an $R = 0.4$ glass, obtained at higher temperatures, no resonance arising from tetrahedral boron was detected. Notably the three crystalline polymorphs of metaboric acid (HBO_2) provide precedent for tetrahedral boron in water borate structures, having N_4 values of 0, 0.33 and 1.0 for the orthorhombic, monoclinic and cubic forms respectively. Brüning & Patterson [347] studied a large number of water borate glasses, from $R = 0$–1, and Brüning *et al* [348] a large number of more water-rich liquids, by x-ray diffraction. They only measured to $Q_{max} = 7$ Å^{-1}, and do not calculate Fourier

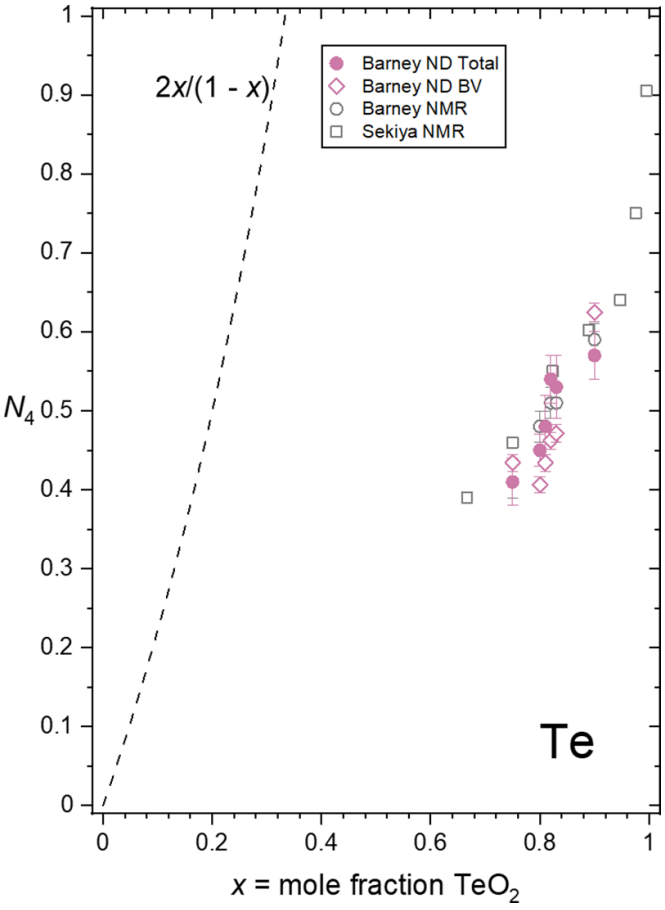

Figure 49. $N_4 = n_{BO} - 3$ values for TeO_2-B_2O_3 glasses from the pulsed neutron diffraction study of Barney *et al* [76] along with the ^{11}B NMR data from the same study and from Sekiya *et al* [58]. Note that the abscissa is the mole fraction of TeO_2, rather than a molar ratio as in the previous figures, because the $R = TeO_2/B_2O_3$ values are very large (3–9 for the ND study, 2–198 for the NMR study).

transforms or report CNs or N_4 values. Wright [349] gives an excellent discussion of water borate glasses and crystals in the context of the chemistry of B_2O_3.

Overall, it is clear that knowledge regarding H_2O-B_2O_3 glasses and liquids could be improved upon using modern quantitative methods of structure and N_4 determination.

4.5. Diffraction studies of binary borate melts

One advantage of diffraction methods is that they view both glasses and melts in the same way, which is distinct to NMR methods where the timescales for nuclear spin relaxation play a key role. In particular, in high-temperature melts the exchange of boron between 3- and 4-coordinated environments becomes more rapid than the NMR timescale set by the relaxation time, and so only a single, site-averaged, resonance is observed [287, 350]. This means that N_4 cannot be quantified in melts by ^{11}B NMR in the same manner as proves so effective in the solid state. As such, diffraction methods have played a greater role in the elucidation of N_4 in borate melts, whilst ^{11}B NMR has been applied effectively for studies of glasses as a function of their *fictive* temperatures. Alderman [351] reviewed structural studies of borate melts up to about the year 2017. All studies reviewed, including those by diffraction, show that N_4 tends to decline with increasing temperature, but the extent to which this happens is highly composition dependent. For example, the temperature dependence of N_4 is small at low Na_2O contents [294], but is clearly significant at 33 mol% Na_2O, figure 50 [311]. Since the time of the review, a few further high-energy x-ray diffraction studies have shown a dramatic decline in N_4 with temperature for lithium metaborate [295], figure 40, a gradual decline for lithium pyroborate [312], which has only a small N_4 fraction (figure 40), and for barium metaborate and diborate [258] similar $N_4(T)$ to sodium diborate were found, figure 51. The complex temperature and composition dependence of $N_4(R, T)$ has been described within a simple boron coordination change isomerization model [258, 295, 312], and related to the configurational heat capacity and entropy contributions, as well as qualitatively to the fragility indices. It is likely that, in general, the enthalpies and entropies of isomerization will depend not only on composition parameter R, as has been demonstrated, but also on the modifier identity. This could be verified by measurements on borate melts with other modifiers, as well as by calculating model $N_4(R, T)$ at the fictive temperature, T_f, (or glass transition temperature, T_g, as a proxy), for comparison to the N_4 measured for glasses, as reviewed herein.

4.6. X-ray spectroscopic and high-pressure studies of binary borate glasses and melts

Although this section of the review is focused on x-ray and neutron diffraction, x-ray spectroscopy has also been used to derive N_4 values in binary borate glasses and melts. In 1995 Li *et al* [352] used soft x-rays and the total electron yield (TEY) method to observe B K-edge x-ray absorption near-edge structure (XANES) spectra in several potassium borophosphosilicate glasses, demonstrating that N_4 could be estimated by this method. Later, in 1999, Fleet and Muthupari [353] applied the same method to borosilicate glasses, as well as a sodium diborate glass. In this work fluorescence yield (FY) spectra were collected simultaneously, which the authors point out is a more bulk-sensitive method (about 110 nm penetration depth) compared to TEY, the latter probing only about 6 nm into the surface. In 2001 a study from Yamamoto *et al* [354] built on the earlier work to study a series of binary sodium borate glasses with TEY B K-edge XANES spectroscopy. These authors showed that N_4 could be estimated from the spectra, mostly in good agreement with ^{11}B NMR.

Of particular note is the development of the non-resonant inelastic x-ray scattering method, also referred to as x-ray Raman scattering. This method is capable of providing spectra analogous to x-ray absorption spectroscopy, but uses high-energy x-rays, achieving greater bulk sensitivity, and obviating the need for the soft x-rays and ultra-high vacuum otherwise required for observing the boron K-edge. This method has been applied to the study of levitated liquid and glassy lithium borates [327] (figure 40(b)) as well as to cold-compressed borate glasses at up to 30 GPa [355, 356]. The high-pressure work indicates a dramatic increase in N_4 for pure B_2O_3 and

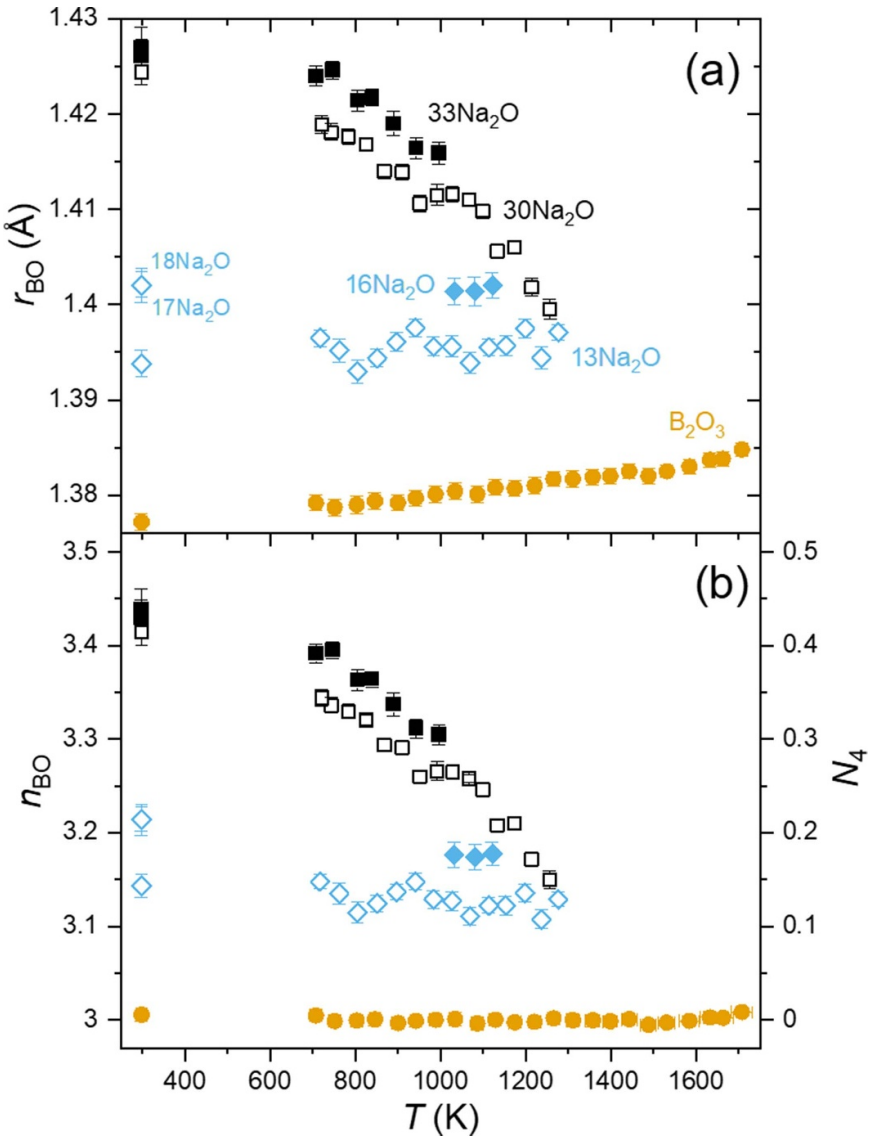

Figure 50. High-energy x-ray diffraction results for the (a) Mean B–O bond lengths, $r_{BO}(T)$ and (b) Mean B–O coordination numbers, $n_{BO}(T)$, as derived from $r_{BO}(T)$ using the temperature dependent bond-valence method [294, 311], for B_2O_3 [315] and sodium borate melts and glasses [294, 311]. Molar percentages soda are indicated in part (a).

$Li_2B_4O_7$ glasses above 4 GPa, approaching $N_4 = 1$ for the highest pressures studied [356]. Meanwhile the increase in N_4 for $Na_2B_4O_7$ glass was shown to be more gradual with pressure [355].

Pure B_2O_3 has been studied at high pressures by both x-ray [321, 357] and neutron [325] diffraction methods. High-pressure neutron diffraction of a $30(^{11}B_2O_3).70GeO_2$ glass has been reported in the PhD thesis of Buscemi [358].

4.7. Future prospects

It is clear from this review that despite decades of research into binary borate glasses using diffraction methods, there are still many gaps in knowledge to be filled. This is the case even if considering only the fundamental structural parameter N_4. These gaps include:

1. There are still very few diffraction measurements of highly modified binary alkali or alkaline earth borate glasses, above the diborate composition ($R > 0.5$). This is despite this being a structurally rich region in which NBOs begin to dominate over tetrahedral boron as charge-balancing species.
2. There are no diffraction measurements at all for Mg borate glasses, or for most of the transition metal and rare-earth borate glasses. X-ray diffraction measurements of some rare-earth borates have been made [359] but since the heavy rare-earth ions dominate the x-ray scattering, N_4 were not determined. Neutron diffraction would be highly applicable here, at least for the rare-earth elements that do not have strong neutron absorption resonances. Diffraction methods have an advantage over standard ^{11}B NMR methods when it comes to paramagnetic glasses, due to paramagnetic

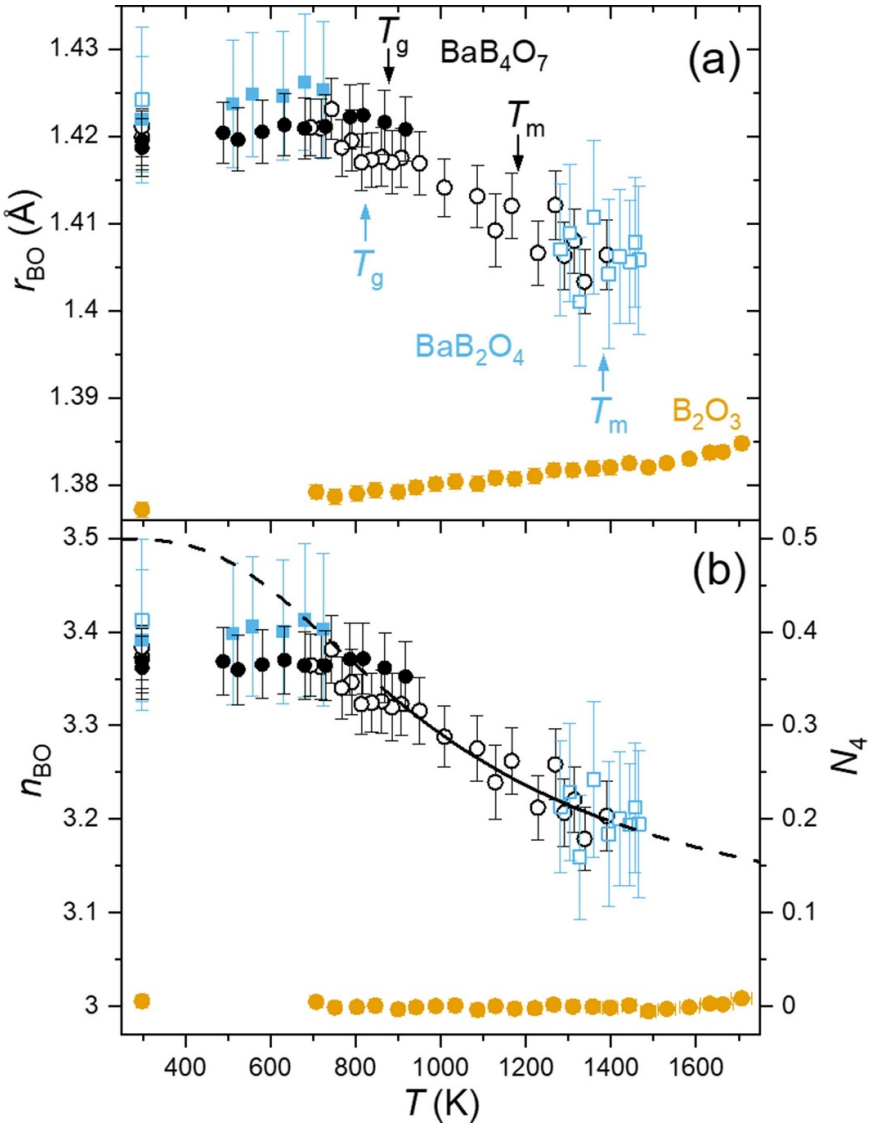

Figure 51. High-energy x-ray diffraction results for the (a) Mean B–O bond lengths, $r_{BO}(T)$ and (b) Mean B–O coordination numbers, $n_{BO}(T)$, as derived from $r_{BO}(T)$ using the temperature dependent bond-valence method [294, 311], for B_2O_3 [315] and barium borate melts and glasses [258]. The curve in (b) is the result of van't Hoff analysis for BaB_4O_7, based on the $[B\emptyset_4]^- \rightleftharpoons [B\emptyset_2O]^-$ coordination changing isomerization reaction, with dashed extrapolations. Note the larger error bars compared to the measurements on Li (figure 40) or Na (figure 50) borates, reflecting the dominance of the modifier (Ba) in the x-ray scattering signal.

relaxation enhancement induced broadening of the NMR spectra. Thus, diffraction methods should be taken advantage of for studying the structure of the paramagnetic rare-earth and transition metal borate glasses.

In terms of high-temperature and high-pressure measurements, the field is almost completely wide open, since only a handful of alkali and alkaline earth borate melt compositions have been studied at high temperature, and there are no *published* high-pressure diffraction studies of binary borate glasses known to the authors.

The success of the bond-valence based approach to precise and accurate determination of B–O CNs, using the mean B–O bond length as proxy, is evident from this review, especially in figures 44, 45 and 47, as well as in the temperature dependent studies of Alderman *et al* (e.g. figures 40, 50 and 51). Therefore, we call on all future authors reporting on diffraction measurements of borate glasses to report the mean B–O bond length if at all possible. Furthermore, to use this as a check on the directly determined CN, and if necessary, to provide a more precise and accurate estimate of n_{BO} and N_4 via the bond-valence method.

5. Conclusions

It is clear from this review that in the almost nine decades since the first measurements of N_4 in binary borate glasses by x-ray diffraction, the ability to study this aspect of borate glass structure has been transformed by the advent of new technologies and methodologies. In particular the application of nuclear magnetic resonance spectroscopies to the

boron isotopes, especially ^{11}B, has become the most commonly applied technique, and gold standard for N_4 quantification, nowadays most commonly by high-field MAS, with requisite correction for the intensity in the spinning sidebands.

IR *reflectance* spectroscopy has also been shown capable of N_4 quantification, so long as suitable care is taken to address the relative absorption of borate triangles and tetrahedra. This is typically achieved by scaling IR reflectance data for a compositional series to an accurate ^{11}B NMR measurement at one or more composition, or else to $N_4 = x/(1–x)$ if this relationship has been established at the given composition by NMR or diffraction. Importantly, it has been shown that the relative absorption is modifier cation dependent, but that it scales e.g. quadratically with the divalent modifier field strength (figure 26, allowing for interpolations to be made where necessary (table 2). While scaling with NMR measurement(s) is the direct way to convert IR reflectance data into N_4, a more detailed IR analysis combining spectral deconvolution with mass and charge balance equations is capable of providing the molar fractions of all short-range borate units and not just of BO_4 (i.e. N_4). This has been demonstrated for bismuth borate glasses and opens the way for application to other borate glasses (see section 3.6 and Varsamis *et al* [278]).

Total scattering diffraction methods have also come along a great deal, with the advent of both reactor and particle accelerator based neutron sources, and intense synchrotron sources of high-energy x-rays. Although inherently quantitative, the uncertainties in the direct determination of B–O CN, and thereby N_4, have traditionally been larger than those associated with ^{11}B NMR. However, it has recently been established [258, 294, 295, 311, 312] that N_4 values rivaling the accuracy and precision of ^{11}B NMR can be determined from diffraction data. This is achieved by exploiting the inherent sensitivity of total scattering diffraction, as an interference based method, to length scales, and mapping accurate and precise determinations of the mean B–O bond length onto N_4 values using bond-valence methodology.

Certain general observations about binary borate glasses can be made considering the entire corpus of studies reporting N_4:

Firstly, ambient pressure binary borate glass structures typically tend to have $N_4 < 0.5$, such that trigonal borate species predominate. There are notable exceptions to this rule, such as the unusual TeO_2–B_2O_3 glasses, where B_2O_3 contents are exceptionally low, and it is quite well established by NMR and neutron diffraction that $N_4 > 0.5$ when TeO_2 content exceeds about 82 mol% [76]. On the other hand, the high $N_4 > 0.5$ reported by Park and Bray [50] for SrO–B_2O_3 glasses have been identified as outliers and should be discarded, as discussed above. The single $N_4 > 0.5$ reported by Kajinami *et al* [320] for MnO–B_2O_3 glasses by x-ray diffraction has also been ruled out by us as an outlier. This is because it is not consistent with the reported B–O bond length, and our bond-valence based determination of $N_4 < 0.5$, nor with the remarkable NMR study of Park and Bray [174] on this paramagnetic glass system. Other cases are less clear cut. A few NMR studies have reported $N_4 > 0.5$ for lead borate glasses with PbO content close to, or exceeding, 50 mol% (figure 27). However, these data are not supported by existing neutron diffraction or IR reflectance data, or indeed by several other NMR studies (figures 27 and 46). Very large $N_4 > 0.5$ were reported early on for Tl_2O–B_2O_3 glasses by Baugher and Bray [47] using NMR, including many values of $N_4 > x/(1–x)$. The thesis work of Laorodphan [84] using both NMR and neutron diffraction has since revised these values downwards, but not to the extent that the two anomalies, $N_4 > x/(1–x)$ for $x < 50$ mol% Tl_2O and $N_4 > 0.5$ for $x > 50$ mol% Tl_2O, disappear altogether. Overall, the general predominance of binary borate glasses having $N_4 < 0.5$ is in stark contrast to the well-established fact that many modified borosilicate glasses, especially at high SiO_2 contents, tend to have $N_4 > 0.5$. Historically this has led to development of models for borate glass structure which invoke Lowenstein type avoidance rules for the negatively charged borate tetrahedra [15]. However, the foundations of such models have been strongly questioned by Möncke *et al* [237] who present evidence for corner-sharing pairs of $[BØ_4]^-$, as well as $[BØ_2O_2]^{3-}$, tetrahedra in glasses. Such moieties are of course also well known in borate and borosilicate crystal structures. An alternative explanation for the $N_4 < 0.5$ in binary borate glasses *could* involve the temperature dependence of $N_4(T)$ observed in the molten and supercooled liquid states. $N_4(T)$ is typically observed to progressively increase as the liquid is (super)cooled towards the glass transition at T_g. Since this boron coordination change mechanism contributes to the super-Arrhenian temperature dependence of the liquid viscosity (liquid fragility), it has a self-limiting effect, in that the rapid rise in viscosity results in glass transition at T_g, arresting the increase in $N_4(T)$ as it falls out of equilibrium, and before it can exceed 0.5, in most cases. This idea that the equilibrium N_4 fractions in highly modified glasses could in fact be much higher than the non-equilibrium values observed to date remains to be explored.

Secondly, as discussed by Holland *et al* [68] there is an interesting linear correlation between the composition, n^{max}, at which N_4 reaches its maximum value, expressed as molar fraction modifier oxide $M_{2/Z}O$, and the modifier cation potential $\varphi = Z/r_M$. This makes sense if one considers that as φ increases, modifier charge becomes progressively localized, and the space available around it to pack charge balancing borate tetrahedra diminishes. In figure 52 we have updated this correlation plot between n^{max} and φ using our large database of N_4 values, and included points for additional modifier cations Tl^+, Ag^+, Ba^{2+}, Cd^{2+}, Mn^{2+}, Mg^{2+}, La^{3+}, and Te^{4+}, see also table 6.

To generate the data shown in table 6 and figure 52, n^{max} were determined from spline fits to the NMR derived N_4 in our database, except in the case of Mg^{2+} where the IR data were used. In the cases of Cd^{2+} and Sn^{2+}, the N_4 maxima are rather broad and poorly determined. In the cases of Ag^+ and Tl^+, there are very few points at modifier contents beyond the maxima. For Ca^{2+}, the spread in the various datasets is very large, again leading to significant uncertainty in n^{max}. In order to derive $\varphi = Z/r_M$ values, total scattering diffraction measurements of the modal M–O bond lengths were used in most cases, and the oxygen radius of $r_O = 1.35$ Å subtracted to yield r_M. Note that modal bond lengths are often

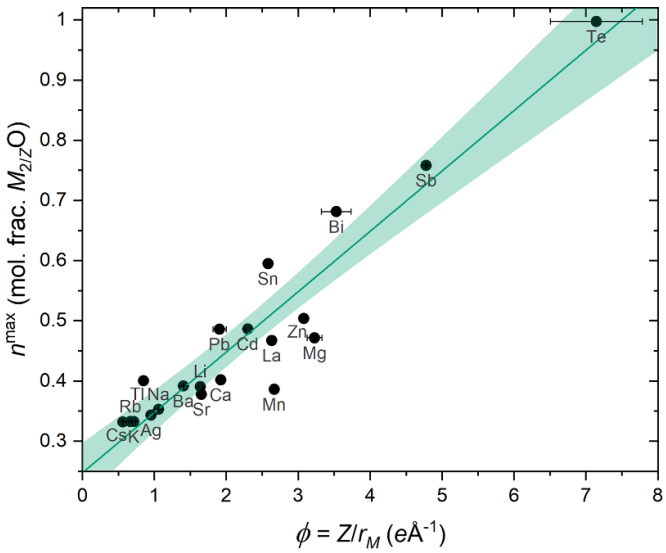

Figure 52. Correlation plot between composition, n^{max}, at which N_4 reaches its maximum value, expressed as molar fraction modifier oxide $M_{2/Z}O$, and the modifier cation potential $\varphi = Z/r_M$. Here Z is the formal cation charge and r_M the modifier cation radius. The unweighted linear fit is given by $n^{max} = 0.25(2) + 0.100(8)\,\varphi$, in the units shown on the axes, with 95% confidence bounds shaded.

Table 6. Modal cation-oxygen bond lengths, r_{MO}, as derived from diffraction studies, together with the corresponding cation potentials φ, and observed compositions of maximum N_4, n^{max} (in mole fraction $M_{2/Z}O$). Cation radii are simply obtained using $r_M = r_{MO} - r_O$, with $r_O = 1.35$ Å, the Shannon–Prewitt radius for two-fold oxygen (other values could be chosen, yielding qualitatively identical results). The penultimate column gives the reference used for obtaining r_{MO}, and the final column indicates the glass system used for r_{MO}, or else the cation-oxygen coordination number used to obtain the Shannon–Prewitt radius, in lieu of suitable diffraction data.

Cation	Z (e)	Modifier oxide	r_{MO} (Å)	r_M (Å)	$\varphi = Z/r_{MO}$ (eÅ^{-1})	n^{max} (mol. frac. $M_{2/Z}O$)	References	Glass system or n_{MO}
Cs	1	Cs_2O	3.13(1)	1.78	0.562(3)	0.3320	[360–362]	9
Rb	1	Rb_2O	2.85(5)	1.5	0.67(2)	0.3326	[254]	borate
K	1	K_2O	2.75(5)	1.4	0.71(3)	0.3325	[254]	borate
Tl	1	Tl_2O	2.527(1)	1.177	0.8496(7)	0.4003	[363]	germanate
Ag	1	Ag_2O	2.40(5)	1.05	0.95(5)	0.3433	[329]	borate
Na	1	Na_2O	2.295(2)	0.945	1.058(2)	0.3529	[364]	silicate
Ba	2	BaO	2.775(5)	1.425	1.403(5)	0.3917	[258]	borate
Li	1	Li_2O	1.96(1)	0.61	1.64(3)	0.3906	[312]	borate
Sr	2	SrO	2.56(1)	1.21	1.65(1)	0.3777	[360–362]	7
Pb	2	PbO	2.40(5)	1.05	1.90(9)	0.4861	[143]	borate
Ca	2	CaO	2.39(1)	1.04	1.92(2)	0.4018	[21]	germanate
Cd	2	CdO	2.22(1)	0.87	2.30(3)	0.4865	[360–362]	5
Sn	2	SnO	2.125(1)	0.775	2.581(3)	0.5950	[324]	borate
La	3	$La_{2/3}O$	2.490(1)	1.14	2.632(2)	0.4674	[359]	borate
Mn	2	MnO	2.10(1)	0.75	2.67(4)	0.3862	[360–362]	5 (high spin)
Zn	2	ZnO	2.00(1)	0.65	3.08(5)	0.5038	[335]	borate
Mg	2	MgO	1.97(2)	0.62	3.23(10)	0.4716	[365]	phosphate
Bi	3	$Bi_{2/3}O$	2.20(5)	0.85	3.53(21)	0.6815	[343]	borate
Sb	3	$Sb_{2/3}O$	1.978(1)	0.628	4.777(8)	0.7583	[342]	borate
Te	4	$Te_{1/2}O$	1.91(5)	0.56	7.14(64)	0.9974	[76]	borate

shorter than mean bond lengths, but easier to determine, and likely more pertinent. In most cases, diffraction data on borate glasses themselves were used [76, 143, 254, 258, 312, 324, 329, 335, 342, 343, 359]. In other cases data from other glass systems were used, including silicates (Na^+) [364], germanates (Ca^{2+} and Tl^+) [21, 363] and phosphates (Mg^{2+}) [365]. In the remaining cases Shannon-Prewitt ionic radii [360–362] were used for five-fold Mn^{2+} (high spin) and Cd^{2+}, 7-fold Sr^{2+} and 9-fold Cs^+.

Ultimately the linear relationship displayed in figure 52 terminates at $\varphi \simeq 7.5$ eÅ^{-1}, where n^{max} reaches its limiting value of 1. Notably this is before the tetravalent (Si^{4+}, Ge^{4+}) and pentavalent (P^{5+}) glass formers which all have larger $\varphi \gtrsim 10$. In the case of Si^{4+} and Ge^{4+}, $N_4 = 0$ for the compositions measured [37, 366]. P_2O_5-B_2O_3 glasses are rather curious in that they only form at rather low P_2O_5 contents, where $N_4 \gtrsim 0$ has been found [52]. This limited glass forming region has been attributed to the need for perfect topological

ordering between $[B\emptyset_4]^-$ and $[P\emptyset_4]^+$ units, which tends to lead to crystallization of BPO_4. Indeed, extrapolations from ternary borophosphate glasses indicate high N_4 fractions in the hypothetical P_2O_5-rich binary borate glasses [52]. Te^{4+} appears to be right on the limit of the linear relationship, with high $\varphi \simeq 7.1\ e\text{Å}^{-1}$ and $n^{\max}$ approaching 1. Indeed, it should be noted that the $n^{\max} \simeq 1$ is not a true maximum in the sense that it is not clear from the available data if the derivative $\partial N_4/\partial n$ goes to zero. Interestingly, trivalent Al^{3+} has a similar $\varphi \simeq 7.5\ e\text{Å}^{-1}$ but is not known to generate tetrahedral boron in pure aluminoborate glasses [182]. This is likely due to the propensity for tetrahedral aluminum $[Al\emptyset_4]^-$ units which are not suitable for charge balancing $[B\emptyset_4]^-$, whereas in the tellurborate glasses, the Te^{4+} lone pair causes a small number of short bonds to form to oxygen, and $[Te\emptyset_3]^+$ units are well suited to charge balancing $[B\emptyset_4]^-$. Overall, it is clear that the linear relationship breaks down at high φ, where the specific mechanisms of charge balance become quite different, and very much cation dependent. It is also worth mentioning that the linear relationship fitted to the data in figure 52 has no theoretical justification, it is merely the simplest functional form available that approximately describes the data. Furthermore, there are several outliers which are not described by the linear relationship, particularly Mn^{2+}, but for which the true uncertainties in $n^{\max}$ are unclear.

Finally, it is apparent that in some cases, particularly that of $CaO–B_2O_3$ glasses, that the consensus on $N_4(x)$ is quite poor, figure 53. Does this point toward a particularly large sensitivity of $N_4(x)$ to thermal history in this case? Or is it simply down to the various systematic uncertainties of the individual studies, which by chance plague this system more than others? These questions can be readily answered with suitably designed studies. In the first instance, through studies of the temperature, and fictive temperature, dependencies of N_4. In the second instance, through multi-technique approaches, whereby, for example, ^{11}B MAS NMR, IR reflectance spectroscopy and diffraction methods are all applied to a single set of glasses, with the expectation that a consensus would be obtained, at least for that set of glasses with their given thermal histories. Notably, the study by Lepry and Nazhat [115] involved sol-gel derived amorphous calcium borate solids, with a calcination temperature of 673 K, which is well below the glass transition temperatures of 870–930 K [281]. The low-temperature synthesis route explains the very high CaO contents achieved. It is also tempting to speculate that the relatively high N_4 values obtained by both NMR and IR methods [115], figure 53, at high $R > 1$, are a result of the general expectation for higher $N_4(T_f)$ at lower fictive temperature T_f. This would however require a special mechanism enabling the metastable equilibrium for N_4 to be approached, one possibly provided by the very high surface areas of the amorphous powders, which imbues higher mobility and additional relaxation routes. However, another explanation might be the presence of organic and hydroxyl impurities which might be expected, especially considering that the glass powders were all discolored off-white, or even black in the case of the lowest CaO content.

It is worth noting that the neutron diffraction studies by Ohtori *et al* [257] and Suzuki *et al* [331] were seemingly based on the same experimental data, but report different N_4 values, especially for calcium diborate glass. In this latter case, the result from Ohtori *et al* [257] appears to be in better agreement with a wider range of other studies.

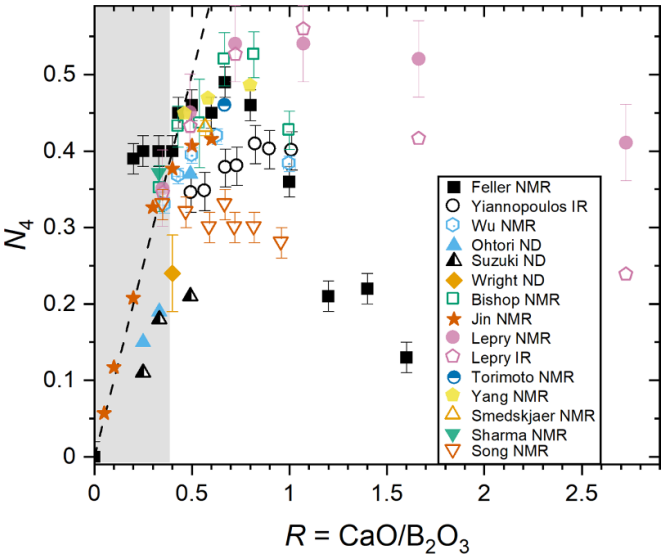

Figure 53. Compilation of N_4 measurements on $CaO–B_2O_3$ glasses and amorphous solids. The shaded region indicates that of stable liquid-liquid immiscibility in the equilibrium phase diagram, and therefore data in this region may refer to inhomogeneous phase separated glasses. The dashed line is $N_4 = R$. References for ND [254, 257, 331], NMR [45, 79, 90, 107, 110, 115, 122, 126, 127, 179] (data from Song *et al* [127] have been corrected for spinning sideband intensities) and IR [115, 256]. The study by Lepry and Nazhat [115] involved sol-gel derived amorphous calcium borate solids.

6. Future prospects and recommendations

The use of ^{11}B MAS NMR will likely remain the go-to method for N_4 measurement in borate glasses. It should be reiterated here that this method typically requires corrections to be made to account for spinning sideband intensities in order to avoid systematic inaccuracies. Nonetheless, despite the tremendous numbers of N_4 measurements made to date using ^{11}B NMR, looking at figure 13 it is quite clear that there are gaps in our knowledge. Most glaring are the lack of N_4 measurements in paramagnetic borate glasses. This is for good reason, and largely due to the severe broadening effects arising due to interactions with unpaired electrons and paramagnetic relaxation enhancement of the nuclear spins, which has led to a general tendency of practitioners to avoid measuring spectra from glasses containing paramagnetic ions as major components (above dopant levels). The pioneering early work by Park and Bray [174] on $MnO–B_2O_3$ glasses, as well as Bucholtz and Bray [56] on $Fe_2O_3–PbO-B_2O_3$ glasses used low frequency field-sweep methods to enable collection of the incredibly broad ^{11}B NMR spectral signals. It would be a tremendous development to see a revival of such capability, particularly in light of the plethora of wideline NMR methodologies now available [367], including those developed

specifically for tackling paramagnetic systems [368, 369], and taking advantage of modern capabilities including rapid MAS and pulsed Fourier transform methodologies. Indeed, progress has already been made in this direction in the case of Si ^{29}Si NMR spectroscopy of paramagnetic minerals and glasses [370].

In terms of vibrational spectroscopies, IR *reflectance* has been shown to be preeminent in terms of quantifying N_4, and this is the method which should be applied when seeking accurate N_4 values and trends. Of course, it still relies to some extent on other methods in order to pin down the relative absorption of borate triangles and tetrahedra. However, the dependence of the relative absorption on cation field strength developed herein is now ripe for exploitation and extension to other modifier cations, and to mixed-modifier glasses.

As demonstrated by this review, it is clear that a reasonable number of diffraction studies of binary borate glasses have been made, and used to quantify N_4. Nonetheless, diffraction methods appear underutilized when compared to both NMR and IR spectroscopies. This is understandable given the reliance on large-scale facilities: x-ray synchrotrons, nuclear reactors and proton accelerator driven spallation neutron sources. However, this needn't be the case. The issue here is perhaps largely one of a perception of difficulty in accessing these facilities, and this barrier requires breaking down. For one thing, advancements in radiation sources, detectors and instrumentation have led to a steady increase in throughput, and it is perfectly feasible nowadays to measure the neutron or x-ray structure factors for large numbers (several 10 s) of glasses in a single experiment, with each measurement *typically* on the order of a few hours with neutrons, and minutes with synchrotron x-rays. Furthermore, light modifier containing borate glasses can be measured routinely with specialized laboratory-based x-ray sources (typically based on Ag-source x-rays) on hour to day timescales. An additional barrier to the application of neutron diffraction to borate glasses is the need to isotopically enrich in ^{11}B, in order to avoid significant levels of the strongly neutron absorbing ^{10}B isotope (20% natural abundance). However, ^{11}B is relatively cheap as isotopes go, partly due its status as a by-product of ^{10}B enrichment utilized by the nuclear industry.

Diffraction methods present an excellent opportunity for addressing the paucity of information available on the structure of paramagnetic borate glasses, and with far fewer challenges than those posed by the application of NMR to such materials. Diffraction methods are also relatively well suited to quantitative *in-situ* measurements under extreme conditions of high-temperature and/or high-pressure, with clear opportunities in this direction.

We call on future authors of diffraction studies to report on the mean B–O bond length in borate glasses wherever possible, and at the very least to use this as a check on the directly determined B–O CNs, if not to also provide a more precise and accurate estimate of N_4 using bond-valence based methodology.

Water borate glasses deserve the attention of both modern NMR methods and high-Q diffraction studies, in order to build on the early work done by Silver [43], Meller and Milberg [345, 346], and later studies by Brüning *et al* [347, 348]. This could include neutron diffraction, where isotopic substitution of hydrogen by deuterium can be exploited to provide contrast and more detailed structural information than is available from a single measurement or isotopologue. An example includes recent work on aqueous potassium borate solutions [371].

The two apparent anomalies of the thallium borate glasses also deserve further attention, with the caveat that thallium is incredibly toxic and requires great care when working with it. Specifically, the observations that $N_4 > R$ for $R < 1$ and $N_4 > 0.5$ for $R > 1$ (figure 43) require confirmation and explanation. Given sufficient safety precautions, other binary borate systems containing toxic modifiers would also be of interest, but they can pose additional challenges, including phase separation with a very wide immiscibility gap for beryllium, and likely mixed oxidation states for low melting arsenic (As^{3+}/As^{5+}) borates. As is apparent from figure 13, there are many other binary borate systems for which no N_4 measurements have been reported, and many of which likely do form glasses. One example are vanadium borate glasses, which have been prepared containing largely only pentavalent V^{5+} [372]. These would be excellent candidates for combined x-ray and neutron diffraction studies, and should be amenable to standard ^{11}B NMR methods given the absence of lower valence, paramagnetic, vanadium species.

Overall, whilst the field has been progressed a long way, we cannot claim to have a quantitative means for predicting N_4 in any arbitrary binary borate glass composition, much beyond the limited applicability of the $N_4 = x/(1–x)$ relationship which holds for low levels ($x \lesssim 30$ mol% M_2O or MO) of monovalent (excluding hydrogen) and some divalent modifiers. In this spirit, the application of machine learning to the N_4 database presented herein could be incredibly fruitful, and should be tested for predicting $N_4(x, T)$, including for the cases of modifiers for which no measurements exist. This could be achieved by characterizing modifiers by their field strengths, cation potentials, electronegativities and polarizabilities, for example. Such endeavors will not be without their challenges, but should be well worth the effort.

It is worth noting here that we have not reviewed models which do exist for predicting N_4 over extended ranges of composition and/or temperature. These include the simple axiomatic models for $N_4(x)$ proposed by Abe, Beekenkamp, Gupta, Krogh-Moe and Griscom, which have been previously reviewed and compared by Wright [15]. These models have the advantage of simplicity, ease of calculation and lack of empirical adjustable parameters. On the other hand, since they do not include temperature dependence, and tend to maximize N_4 under the constraints of their assumptions, they can be considered only as low temperature limiting cases [15]. Furthermore, since these models contain no explicit dependence on modifier identity, no single model can capture the plethora of different $N_4(x)$ curves observed for binary borate glasses across the periodic table of 'modifier' oxides (figure 13). At the other end of the scale is the model of

ideal associated solutions (IAS), which considers the molten state as comprised of chemical groupings found in the crystalline phases, with abundances based on their relative free energies of formation. This model has the advantage of including temperature (and in principle pressure) dependence, as well as composition dependence, but requires knowledge of not only the stable crystal structures found within a given system, but so too their temperature dependent free energies of formation. The IAS model has been applied reasonably successfully to Li and Na borates [373]. Intermediate between the two aforementioned approaches is the boron coordination change isomerization (BCCI) model [258, 295, 312], which has been fitted to experimental $N_4(x, T)$ data. The BCCI model is a relatively simple phenomenological model which allows for interpolation, and perhaps limited extrapolation of, $N_4(x, T)$, but which requires empirically estimated enthalpies and entropies of the boron coordination change reaction. These parameters have been shown to depend somewhat on x [258, 312], and are also expected to depend on modifier identity, requiring further measurements to constrain the model over a wider compositional space. Finally, there are now numerous classical interaction potential parameterizations, as well as first principles approaches for modeling borate melts and glasses using molecular dynamics. It is unlikely any of these can capture the temperature and composition dependence of $N_4(x, T)$, owing to the unrealistically high quenching rates necessitated by available computational resources. Or in other words, molecular dynamics might allow for reasonable prediction of $N_4(x, T)$ in the equilibrium and mildly supercooled liquid state, but will then tend to underestimate it in the glassy state owing to the overly rapid quenching timescale. Or, if the potentials are tuned to yield agreement with experimental $N_4(x)$ for glasses, they will then likely fail to capture $N_4(x, T)$ in the liquid state.

In limiting the scope of this review to just a single important structural parameter (N_4), and to *binary* borate glasses, containing only a single cation in addition to boron, and with only a single anion (O^{2-}), we have been able to be reasonably comprehensive with our review. To obtain an analogous review and database for more complex, multicomponent, borate-bearing glasses will likely require a large degree of automated data mining, in addition to the necessary human input, given the daunting vastness of the glass-forming composition space and the correspondingly larger number of studies involving such materials to date.

Data availability statement

All data that support the findings of this study are included within the article (and any supplementary files) or upon reasonable request from the authors. A database of all of the N_4 values presented, along with associated metadata, is included as a supplementary file to support future efforts. We note that during the proof stages of this manuscript, it was noticed that an NMR study of GeO_2-B_2O_3 glasses had been omitted [374]. This study effectively demonstrates that $N_4 = 0$ for all glass compoistions in this binary system, at least from 16 to 92 mol% GeO_2.

Acknowledgment

EIK and NST acknowledge support by the project 'National Infrastructure in Nanotechnology, Advanced Materials and Micro-/Nanoelectronics' (MIS 5002772), co-financed by Greece and the European Union (European Regional Development Fund). This material is based upon work supported by the National Science Foundation Graduate Research Fellowship under Grant Nos. DGE-2039655 (IS). Any opinions, findings, and conclusions or recommendations expressed in this material are those of the authors and do not necessarily reflect the views of the National Science Foundation. Steve A Feller, Rebecca M Gabrielsson, Harry Hawbaker, Piper Boggs, Sophia John, Leilani Rocha, and Robert M Wilson acknowledge NSF Grant DMR-2203142.

Professor Scott Kroeker is gratefully acknowledged for providing his perspective on the NMR spectroscopy of paramagnetic materials. We wish to thank an anonymous reviewer for their careful reading and extensive constructive comments that led to the improvement of our original manuscript.

ORCID iDs

Oliver L G Alderman https://orcid.org/0000-0002-2342-811X
Nagia S Tagiara https://orcid.org/0000-0002-1347-8287
Ian Slagle https://orcid.org/0000-0001-7221-0988
Rebecca M Gabrielsson https://orcid.org/0009-0005-7818-1870
Alex C Hannon https://orcid.org/0000-0001-5914-1295
Efstratios I Kamitsos https://orcid.org/0000-0003-4667-2374
Steve A Feller https://orcid.org/0000-0002-5133-6132

Reference

[1] Burianek M, Birkenstock J, Mair P, Kahlenberg V, Medenbach O, Shannon R D and Fischer R X 2016 High-pressure synthesis, long-term stability of single crystals of diboron trioxide, B_2O_3, and an empirical electronic polarizability of $^{[3]}B^{3+}$ *Phys. Chem. Mineral.* **43** 527–34
[2] Sinclair R, Stone C, Wright A, Polyakova I, Vedishcheva N, Shakhmatkin B, Feller S, Johanson B, Venhuizen P and Williams R 2000 Inelastic neutron scattering studies of superstructural units in borate glasses and crystalline phases *Phys. Chem. Glasses* **41** 286–9
[3] Shelby J E 2005 *Introduction to Glass Science and Technology* (Royal Society of Chemistry)
[4] Gooding E J and Turner W E S 1934 A study of the series of glasses containing sodium oxide, boric oxide and silica *J. Soc. Glass Technol.* **18** T032–T66
[5] Biscoe J and Warren B E 1938 X-ray diffraction study of soda-boric oxide glass *J. Am. Ceram. Soc.* **21** 287–93
[6] Prewitt C T and Shannon R D 1968 Crystal structure of a high-pressure form of B_2O_3 *Acta Cryst.* **24** 869–74
[7] Huang C, Mutailipu M, Zhang F, Griffith K J, Hu C, Yang Z, Griffin J M, Poeppelmeier K R and Pan S 2021 Expanding the chemistry of borates with functional $[BO_2]^-$ anions *Nat. Commun.* **12** 2597

[8] Jellison G Jr, Panek L, Bray P and Rouse G Jr 1977 Determinations of structure and bonding in vitreous B_2O_3 by means of B^{10}, B^{11}, and O^{17} NMR *J. Chem. Phys.* **66** 802–12

[9] Jellison G Jr and Bray P 1978 Structural determinations for sodium borate glasses using B^{10} and B^{11} NMR *Borate Glasses: Structure, Properties, Applications* (Springer) pp 353–67

[10] Gravina S J, Bray P J and Petersen G L 1990 Pure nuclear quadrupole resonance spectroscopy studies of the structure of glasses *J. Non-Cryst. Solids* **123** 165–9

[11] Bray P, Emerson J, Lee D, Feller S, Bain D and Feil D 1991 NMR and NQR studies of glass structure *J. Non-Cryst. Solids* **129** 240–8

[12] Hannon A, Grimley D, Hulme R and Sinclair R 1994 Boroxol groups in vitreous boron oxide: new evidence from neutron diffraction and inelastic neutron scattering studies *J. Non-Cryst. Solids* **177** 299–316

[13] Kroeker S and Stebbins J F 2001 Three-coordinated boron-11 chemical shifts in borates *Inorg. Chem.* **40** 6239–46

[14] Hung I, Howes A, Parkinson B, Anupõld T, Samoson A, Brown S P, Harrison P, Holland D and Dupree R 2009 Determination of the bond-angle distribution in vitreous B_2O_3 by ^{11}B double rotation (DOR) NMR spectroscopy *J. Solid State Chem.* **182** 2402–8

[15] Wright A C 2010 Borate structures: crystalline and vitreous *Phys. Chem. Glasses* **51** 1–39

[16] Galeener F L 1982 Planar rings in glasses *Solid State Commun.* **44** 1037–40

[17] Meera B N and Ramakrishna J 1993 Raman spectral studies of borate glasses *J. Non-Cryst. Solids* **159** 1–21

[18] Huppertz H and von der Eltz B 2002 Multianvil high-pressure synthesis of $Dy_4B_6O_{15}$: the first oxoborate with edge-sharing BO_4 tetrahedra *J. Am. Chem. Soc.* **124** 9376–7

[19] Jin S, Cai G, Wang W, He M, Wang S and Chen X 2010 Stable oxoborate with edge-sharing BO_4 tetrahedra synthesized under ambient pressure *Angew. Chem., Int. Ed.* **49** 4967–70

[20] Mutailipu M, Zhang M, Li H, Fan X, Yang Z, Jin S, Wang G and Pan S 2019 $Li_4Na_2CsB_7O_{14}$: a new edge-sharing $[BO_4]^{5-}$ tetrahedra containing borate with high anisotropic thermal expansion *Chem. Commun.* **55** 1295–8

[21] Alderman O L G, Hannon A C, Feller S, Beanland R and Holland D 2017 The germanate anomaly in alkaline earth germanate glasses *J. Phys. Chem. C* **121** 9462–79

[22] Barney E R, Hannon A C, Holland D, Umesaki N, Tatsumisago M, Orman R G and Feller S 2013 Terminal Oxygens in Amorphous TeO_2 *J. Phys. Chem. Lett.* **4** 2312–6

[23] Howes A P, Vedishcheva N M, Samoson A, Hanna J V, Smith M E, Holland D and Dupree R 2011 Boron environments in Pyrex® glass—a high resolution, double-rotation NMR and thermodynamic modelling study *Phys. Chem. Chem. Phys.* **13** 11919–28

[24] Kroeker S 2015 Nuclear magnetic resonance spectroscopy of glasses *Modern Glass Characterization* ed M Affatigato (The American Ceramic Society and John Wiley & Sons, Inc) pp 1–30

[25] Massiot D, Bessada C, Coutures J and Taulelle F 1990 A quantitative study of ^{27}Al MAS NMR in crystalline YAG *J. Magn. Reson.* **90** 231–42

[26] Silver A and Bray P 1958 Nuclear magnetic resonance absorption in glass. I. Nuclear quadrupole effects in boron oxide, soda-boric oxide, and borosilicate glasses *J. Chem. Phys.* **29** 984–90

[27] Bray P J and O'Keefe J G 1963 Nuclear magnetic resonance investigations of the structure of alkali borate glasses *Phys. Chem. Glasses* **4** 37–46

[28] Alderman O L, Iuga D, Howes A P, Pike K J, Holland D and Dupree R 2013 Spectral assignments and NMR parameter–structure relationships in borates using high-resolution ^{11}B NMR and density functional theory *Phys. Chem. Chem. Phys.* **15** 8208–21

[29] Soldate A M 1938 *J. Am. Chem. Soc.* **21** 287

[30] Jellison G E Jr., Feller S A and Bray P J 1978 A re-examination of the fraction of 4-coordinated boron atoms in the lithium borate glass system *Phys. Chem. Glasses* **19** 52–53

[31] Taylor P C and Bray P J 1969 Lineshape program manual

[32] Taylor P and Bray P 1970 Computer simulations of magnetic resonance spectra observed in polycrystalline and glassy samples *J. Magn. Reson.* **2** 305–31

[33] Müller-Warmuth W, Poch W and Sieleff O 1970 Bestimmung Der Mittleren Koordinationgrade Der Bor in KF–B2O3 Gläsern Aus Dem B-Kernresonance Spectrum *Glastech. Ber.* **43** 5–7

[34] Kim K, Bray P and Merrin S 1976 Nuclear magnetic resonance studies of the glasses in the system $PbO–B_2O_3–SiO_2$ *J. Chem. Phys.* **64** 4459–65

[35] Zhong J and Bray P J 1989 Change in boron Co2.5, and mixed alkali effects, as elucidated by NMR *J. Non-Cryst. Solids* **111** 67–76

[36] Kroeker S, Aguiar P, Cerquiera A, Okoro J, Clarida W, Doerr J, Olesiak M, Ongie G, Affatigato M and Feller S A 2006 Alkali dependence of tetrahedral boron in alkali borate glasses *Phys. Chem. Glasses* **47** 393–6

[37] Bunker B 1990 Multinuclear nuclear magnetic resonance and raman investigation of sodium borosilicate glass structure *Phys. Chem. Glasses* **31** 30

[38] Prabakar S, Rao K and Rao C N R 1990 ^{11}B NMR spectra and structure of boric oxide and alkali borate glasses *Proc. R. Soc.* **429** 1–15

[39] Stebbins J F, Zhao P and Kroeker S 2000 Non-bridging oxygens in borate glasses: characterization by ^{11}B and ^{17}O MAS and 3QMAS NMR *Solid State Nucl. Magn. Reson.* **16** 9–19

[40] Sen S, Xu Z and Stebbins J 1998 Temperature dependent structural changes in borate, borosilicate and boroaluminate liquids: high-resolution ^{11}B, ^{29}Si and ^{27}Al NMR studies *J. Non-Cryst. Solids* **226** 29–40

[41] Dorn R W, Paterson A L, Hung I, Gor'kov P L, Thompson A J, Sadow A D, Gan Z and Rossini A J 2022 Dipolar heteronuclear correlation solid-state NMR experiments between half-integer quadrupolar nuclei: the case of $^{11}B–^{17}O$ *J. Phys. Chem. C* **126** 11652–66

[42] Montouillout V, Fan H, Del Campo L, Ory S, Rakhmatullin A, Fayon F and Malki M 2018 Ionic conductivity of lithium borate glasses and local structure probed by high resolution solid-sate NMR *J. Non-Cryst. Solids* **484** 57–64

[43] Silver A 1960 Nuclear magnetic resonance in $B_2O_3–H_2O$ glasses and boric acids *J. Chem. Phys.* **32** 959–62

[44] Bray P, Leventhal M and Hooper H 1963 Nuclear magnetic resonance investigations of the structure of lead borate glasses *Phys. Chem. Glasses* **4** 47–66

[45] Bishop S and Bray P 1966 Nuclear magnetic resonance studies of calcium boroaluminate glasses *Phys. Chem. Glasses* **7** 73

[46] Kline D and Bray P 1966 Nuclear magnetic resonance investigations of structure of glasses in system $NaF-Na_2O-B_2O_3$ *Phys. Chem. Glasses* **7** 41

[47] Baugher J and Bray P 1969 Magnetic resonance studies of thallium borate glasses *Phys. Chem. Glasses* **10** 77–88

[48] Kriz H and Bray P 1971 A study of the distribution of boron sites in glassy B_2O_3 using ^{11}B NMR *J. Non-Cryst. Solids* **6** 27–36

[49] Rhee C and Bray P J 1971 Nuclear magnetic resonance studies of the structure of caesium borate glasses and crystalline compounds *Phys. Chem. Glasses* **12** 165–74

[50] Park M and Bray P 1972 ^{11}B NMR studies of strontium borate glasses and compounds *Phys. Chem. Glasses* **13** 50–62

[51] Kim K and Bray P 1974 B^{11} nuclear magnetic resonance studies of the system Ag_2O-B_2O_3 *J. Non-Metals* **2** 95–101

[52] Yun Y and Bray P 1978 Nuclear magnetic resonance studies of the glasses in the system K_2O-B_2O_3-P_2O_5 *J. Non-Cryst. Solids* **30** 45–60

[53] Park M J and Pj B 1979 The determination of the structures of compounds and glasses in the system MgO-B_2O_3 using B^{11} NMR *Phys. Chem. Glasses* **20** 31

[54] Göring R, Schnabel B, Buerger H and Nass H 1981 ^{11}B NMR study on glasses of the system TeO_2-B_2O_3 *Phys. Status Solidi* **68** K29–K32

[55] Geissberger A, Bucholtz F and Bray P J 1982 ^{7}Li, ^{11}B and ^{19}F NMR in amorphous alkali halogen borate solid ionic conductors *J. Non-Cryst. Solids* **49** 117–27

[56] Bucholtz F and Bray P 1983 ^{11}B and ^{207}Pb NMR studies of glasses in the system $xFe_2O_3 \cdot yPbO \cdot zB_2O_3$ ($0 \leqslant x \leqslant 15.3$ Mol%, z/Y≅3) *J. Non-Cryst. Solids* **54** 43–80

[57] Mulkern R, Chung S, Bray P, Chryssikos G, Turcotte D and Risen W 1986 An NMR study of the photoconducting glass systems CdO-B_2O_3-GeO_2 and CdO-B_2O_3-SiO_2 *J. Non-Cryst. Solids* **85** 69–78

[58] Sekiya T, Mochida N, Ohtsuka A, Soejima A, Yasumori A and Yamane M 1993 ^{11}B MAS NMR spectra of $BO_{3/2}$-TeO_2 glasses *Glastech. Ber.* **66** 15–20

[59] Youngman R and Zwanziger J 1994 Multiple boron sites in borate glass detected with dynamic angle spinning nuclear magnetic resonance *J. Non-Cryst. Solids* **168** 293–7

[60] Zhang X-Q 1994 *NMR Computer Simulation of Glassy and Powdered Samples: Application to Studies of Sodium Borovanadate Glasses* (New Jersey Institute of Technology) (available at: https://digitalcommons.njit.edu/theses/1708)

[61] Moon S-J, Kim M-S, Chung S-J and Kim H-T 1996 Studies on the structure in strontium borate glasses *J. Korean Phys. Soc.* **29** 213

[62] Berryman J R, Feller S A, Affatigato M, Kodama M, Meyer B M, Martin S W, Borsa F and Kroeker S 2001 Thermal, acoustic, and nuclear magnetic resonance studies of cesium borate glasses *J. Non-Cryst. Solids* **293** 483–9

[63] Hayashi A, Nakai M, Tatsumisago M, Minami T, Himei Y, Miura Y and Katada M 2002 Structural investigation of SnO–B_2O_3 glasses by solid-state NMR and x-ray photoelectron spectroscopy *J. Non-Cryst. Solids* **306** 227–37

[64] Clarida W, Berryman J, Affatigato M, Feller S, Kroeker S, Zwanziger J, Meyer B, Borsa F and Martin S 2003 Dependence of N_4 upon alkali modifier in binary borate glasses *Phys. Chem. Glasses* **44** 215–7

[65] Kroeker S, Feller S, Affatigato M, O'Brien C, Clarida W and Kodama M 2003 Multiple four coordinated boron sites in caesium borate glasses and their relation to medium range order *Phys. Chem. Glasses* **44** 54–58

[66] Metwalli E 2003 Copper redox behavior, structure and properties of copper lead borate glasses *J. Non-Cryst. Solids* **317** 221–30

[67] Youngman R, Sen S, Cornelius L and Ellison A 2003 Novel structural aspects of Sb_2O_3-B_2O_3 glasses *Phys. Chem. Glasses* **44** 69–74

[68] Holland D, Hannon A, Smith M, Johnson C, Thomas M and Beesley A 2004 The role of Sb^{5+} in the structure of Sb_2O_3-B_2O_3 Binary glasses—an NMR and Mössbauer spectroscopy study *Solid State Nucl. Magn. Reson.* **26** 172–9

[69] Epping J D, Eckert H, Imre Á W and Mehrer H 2005 Structural Manifestations of the mixed-alkali effect: NMR studies of sodium rubidium borate glasses *J. Non-Cryst. Solids* **351** 3521–9

[70] Epping J D, Strojek W and Eckert H 2005 Cation environments and spatial distribution in Na_2O–B_2O_3 glasses: new results from solid state NMR *Phys. Chem. Chem. Phys.* **7** 2384–9

[71] Banerjee J, Ongie G, Harder J, Edwards T, Larson C, Sutton S, Moeller A, Basu A, Affatigato M and Feller S 2006 Structural studies of solution-made high alkali content borate glasses *J. Non-Cryst. Solids* **352** 674–8

[72] Feller S, Nijhawan S, Royle M, MacKenzie J, Taylor J, Sharma M, Kamitsos E I, Chryssikos G D, Patsis A and Bray P 1994 Physical properties and spectroscopy of rubidium and caesium borate glasses with exceptionally high alkali content *Chim. Chron. New Ser.* **23** 309–14

[73] Shaw J, Werner-Zwanziger U and Zwanziger J 2006 Correlation of lead borate glass structure with photoelastic response *Phys. Chem. Glasses* **47** 513–7

[74] Michaelis V K, Aguiar P M and Kroeker S 2007 Probing alkali coordination environments in alkali borate glasses by multinuclear magnetic resonance *J. Non-Cryst. Solids* **353** 2582–90

[75] Bajaj A, Khanna A, Chen B, Longstaffe J G, Zwanziger U-W, Zwanziger J, Gómez Y and González F 2009 Structural investigation of bismuth borate glasses and crystalline phases *J. Non-Cryst. Solids* **355** 45–53

[76] Barney E R, Hannon A C and Holland D 2009 A multi-technique structural study of the tellurium borate glass system *Phys. Chem. Glasses* **50** 156–64

[77] Chen B, Werner-Zwanziger U, Nascimento M L, Ghussn L, Zanotto E D and Zwanziger J W 2009 Structural similarity on multiple length scales and its relation to devitrification mechanism: a solid-state NMR study of alkali diborate glasses and crystals *J. Phys. Chem. C* **113** 20725–32

[78] Saini A, Khanna A, Michaelis V K, Kroeker S, González F and Hernández D 2009 Structure–property correlations in lead borate and borosilicate glasses doped with aluminum oxide *J. Non-Cryst. Solids* **355** 2323–32

[79] Smedskjaer M M, Mauro J C, Sen S and Yue Y 2010 Quantitative design of glassy materials using temperature-dependent constraint theory *Chem. Mater.* **22** 5358–65

[80] Martin V, Wood B, Werner-Zwanziger U and Zwanziger J 2011 Structural aspects of the photoelastic response in lead borate glasses *J. Non-Cryst. Solids* **357** 2120–5

[81] Raguenet B, Tricot G, Silly G, Ribes M and Pradel A 2011 Revisiting the 'mixed glass former effect'in ultra-fast quenched borophosphate glasses by advanced 1D/2D solid state NMR *J. Mater. Chem.* **21** 17693–704

[82] Wu J, Potuzak M and Stebbins J F 2011 High-temperature *in Situ* ^{11}B NMR study of network dynamics in boron-containing glass-forming liquids *J. Non-Cryst. Solids* **357** 3944–51

[83] Christensen R, Olson G and Martin S W 2013 Structural studies of mixed glass former 0.35 Na_2O+0.65[xB_2O_3+(1–x) P_2O_5] glasses by Raman and ^{11}B and ^{31}P magic angle spinning nuclear magnetic resonance spectroscopies *J. Phys. Chem. B* **117** 2169–79

[84] Laorodphan N 2012 Structural studies of thallium containing germanate and borate glasses and crystalline phases (University of Warwick) (available at: http://webcat.warwick.ac.uk/record=b2685731~S1)

[85] Larink D, Eckert H, Reichert M and Martin S W 2012 Mixed network former effect in ion-conducting alkali borophosphate glasses: structure/property correlations in the system $[M_2O]_{1/3}$ $[(B_2O_3)_x(P_2O_5)_{1-x}]_{2/3}$ (M= Li, K, Cs) *J. Phys. Chem. C* **116** 26162–76

[86] Khanna A, Saini A, Chen B, González F and Pesquera C 2013 Structural study of bismuth borosilicate, aluminoborate and aluminoborosilicate glasses by ^{11}B and ^{27}Al MAS NMR spectroscopy and thermal analysis *J. Non-Cryst. Solids* **373** 34–41

[87] Hasan M S, Werner-Zwanziger U and Boyd D 2015 Composition-structure-properties relationship of strontium borate glasses for medical applications *J. Biomed. Mater. Res. A* **103** 2344–54

[88] Maldonis J, North J, Ramm A, Starkenburg D, Hopkins K, Wiese-Moore E, Rasmussen P, Delgado D, Affatigato M and Feller S 2014 Structure studies of caesium and lithium borovanadate glass systems *Phys. Chem. Glasses* **55** 85–96

[89] Trégouët H, Caurant D, Majérus O, Charpentier T, Cormier L and Pytalev D 2014 Spectroscopic investigation and crystallization study of rare earth metaborate glasses *Proc. Mater. Sci.* **7** 131–7

[90] Wu J and Stebbins J F 2014 Cation field strength effects on boron coordination in binary borate glasses *J. Am. Ceram. Soc.* **97** 2794–801

[91] Kaur N, Khanna A, Gónzález-Barriuso M, González F and Chen B 2015 Effects of Al^{3+}, W^{6+}, Nb^{5+} and Pb^{2+} on the structure and properties of borotellurite glasses *J. Non-Cryst. Solids* **429** 153–63

[92] LaComb M and Stebbins J F 2015 Tricluster oxygen atoms in crystalline and glassy SrB_4O_7: high resolution ^{11}B and ^{17}O nuclear magnetic resonance analysis *J. Non-Cryst. Solids* **428** 105–11

[93] Larink D and Eckert H 2015 Mixed network former effects in tellurite glass systems: structure/property correlations in the system $(Na_2O)_{1/3}[(2TeO_2)_x(B_2O_3)_{1-x}]_{2/3}$ *J. Non-Cryst. Solids* **426** 150–8

[94] Saitoh A, Tricot G, Rajbhandari P, Anan S and Takebe H 2015 Effect of B_2O_3/P_2O_5 substitution on the properties and structure of tin boro-phosphate glasses *Mater. Chem. Phys.* **149** 648–56

[95] MacDonald K, Hanson M A and Boyd D 2016 Modulation of strontium release from a tertiary borate glass through substitution of alkali for alkali earth oxide *J. Non-Cryst. Solids* **443** 184–91

[96] Masai H, Koreeda A, Fujii Y, Ohkubo T and Kohara S 2016 Photoluminescence of Sn^{2+}-centre as probe of transient state of supercooled liquid *Opt. Mater. Express* **6** 1827–36

[97] Svenson M N, Youngman R E, Yue Y, Rzoska S J, Bockowski M, Jensen L R and Smedskjaer M M 2016 Volume and structural relaxation in compressed sodium borate glass *Phys. Chem. Chem. Phys.* **18** 29879–91

[98] Funke L M, Bradtmüller H and Eckert H 2017 Recoupling dipolar interactions with multiple I=1 quadrupolar nuclei: a ^{11}B {^{6}Li} and ^{31}P {^{6}Li} rotational echo double resonance study of lithium borophosphate glasses *Solid State Nucl. Magn. Reson.* **84** 143–50

[99] Kim Y and Morita K 2017 Temperature dependence and cation effects in the thermal conductivity of glassy and molten alkali borates *J. Non-Cryst. Solids* **471** 187–94

[100] Masai H, Okumura S, Ohkubo T and Yanagida T 2017 Luminescence of Sn^{2+} center in oxide glass with a tendency toward phase separation *Opt. Mater. Express* **7** 2993–3002

[101] Torimoto A, Masai H, Okada G, Kawaguchi N, Yanagida T and Ohkubo T 2017 Emission properties of Ce^{3+} centers in barium borate glasses prepared from different precursor materials *Opt. Mater.* **72** 52–57

[102] Storek M, Adjei-Acheamfour M, Christensen R, Martin S W and Böhmer R 2016 Positive and negative mixed glass former effects in sodium borosilicate and borophosphate glasses studied by ^{23}Na NMR *J. Phys. Chem. B* **120** 4482–95

[103] Zhang R, de Oliveira M, Wang Z, Fernandes R G, de Camargo A S, Ren J, Zhang L and Eckert H 2017 Structural studies of fluoroborate laser glasses by solid state NMR and EPR spectroscopies *J. Phys. Chem. C* **121** 741–52

[104] Curtis B, Hynek D, Kaizer S, Feller S and Martin S W 2018 Composition dependence of the short range order structures in $0.2Na_2O+0.8[xBO_{3/2}+(1\text{-}x)\ GeO_2]$ mixed glass formers *J. Non-Cryst. Solids* **500** 61–69

[105] de Oliveira M Jr, Oliveira J S, Kundu S, Machado N M P, Rodrigues A C M and Eckert H 2018 Network former mixing effects in ion-conducting lithium borotellurite glasses: structure/property correlations in the system $(Li_2O)_y[2(TeO_2)_x(B_2O_3)_{1-x}]_{1-y}$ *J. Non-Cryst. Solids* **482** 14–22

[106] Fernandes H R, Kapoor S, Patel Y, Ngai K, Levin K, Germanov Y, Krishtopa L, Kroeker S and Goel A 2018 Composition-structure-property relationships in Li_2O–Al_2O_3–B_2O_3 glasses *J. Non-Cryst. Solids* **502** 142–51

[107] Jin T, Bernard G M, Miskolzie M, Terskikh V V and Michaelis V K 2018 A ^{11}B and ^{31}P MAS NMR study of the impact of Ca^{2+} and Sr^{2+} network modifying cations on the structure of borate and borophosphate glasses *Phys. Chem. Glasses* **59** 174–80

[108] Kapoor S, Youngman R E, Zakharchuk K, Yaremchenko A, Smith N J and Goel A 2018 Structural and chemical approach toward understanding the aqueous corrosion of sodium aluminoborate glasses *J. Phys. Chem. B* **122** 10913–27

[109] Paterson A L, Hannon A C, Werner-Zwanziger U and Zwanziger J W 2018 Structural differences between the glass and crystal forms of the transparent ferroelectric nanocomposite, $LaBGeO_5$, from neutron diffraction and NMR spectroscopy *J. Phys. Chem. C* **122** 20963–80

[110] Torimoto A, Masai H, Okada G, Kawaguchi N, Yanagida T and Ohkubo T 2018 Correlation between emission properties, valence states of Ce and chemical compositions of alkaline earth borate glasses *J. Lumin.* **197** 98–103

[111] Tsuryu K, Ohkubo T, Kakihara T and Iwadate Y 2018 Structural roles of V and Mo in borate and silicate glasses by solid state NMR and Raman spectroscopies *Phys. Chem. Glasses* **59** 234–40

[112] Doucet J, Tonkopi E, Nuschke A, Tremblay M, Brewer K, Beyea S, Filiaggi M, Abraham R, Werner-Zwanziger U and Boyd D 2019 Multi-modal imageability and degradation characteristics of high-borate glass systems for transient embolization *J. Non-Cryst. Solids* **510** 26–35

[113] Januchta K, Youngman R E, Jensen L R and Smedskjaer M M 2019 Mechanical property optimization of a zinc borate glass by lanthanum doping *J. Non-Cryst. Solids* **520** 119461

[114] Masuno A, Iwata T, Yanaba Y, Sasaki S, Inoue H and Watanabe Y 2019 High refractive index La-rich lanthanum borate glasses composed of isolated BO_3 units *Dalton Trans.* **48** 10804–11

[115] Lepry W C and Nazhat S N 2020 The anomaly in bioactive sol–gel borate glasses *Mater. Adv.* **1** 1371–81

[116] Lee A C and Lee S K 2021 Effect of composition on structural evolution and NMR parameters of quadrupolar nuclides in sodium borate and aluminoborosilicate glasses: a view from high-resolution ^{11}B, ^{27}Al, and ^{17}O solid-state NMR *J. Non-Cryst. Solids* **555** 120271

[117] Lee S K, Lee A C and Kweon J J 2021 Probing medium-range order in oxide glasses at high pressure *J. Phys. Chem. Lett.* **12** 1330–8

[118] Ruckman A, Beckler G, Guthrie W, Jesuit M, Boyd M, Slagle I, Wilson R, Barrow N, Tagiara N S and Kamitsos E I 2021 Lithium ion sites and their contribution to the ionic conductivity of RLi_2O-B_2O_3 glasses with $R \leqslant 1.85$ *Solid State Ion.* **359** 115530

[119] Chatzipanagis K I, Tagiara N S, Kamitsos E I, Barrow N, Slagle I, Wilson R, Greiner T, Jesuit M, Leonard N and Phillips A 2022 Structure of lead borate glasses by Raman, ^{11}B MAS, and ^{207}Pb NMR spectroscopies *J. Non-Cryst. Solids* **589** 121660

[120] Saini R, Kapoor S, Neuville D R, Youngman R E, Cerrutti B M, McCloy J S, Eckert H and Goel A 2022 Correlating sulfur solubility with short-to-intermediate range ordering in the structure of borosilicate glasses *J. Phys. Chem. C* **126** 655–74

[121] Topper B, Tsekrekas E M, Greiner L, Youngman R E, Kamitsos E I and Möncke D 2022 The dual role of bismuth in Li_2O–Bi_2O_3–B_2O_3 glasses along the orthoborate join *J. Am. Ceram. Soc.* **105** 7302–20

[122] Yang J and Sohn I 2022 Compositional dependence of thermophysical properties in binary alkaline earth borate melts: insights from structure in short-range and intermediate-range order *J. Mater. Sci. Technol.* **131** 195–203

[123] Sukenaga S, Unozawa H, Chiba Y, Tashiro M, Kawanishi S and Shibata H 2023 Incorporation limit of MoO_3 in sodium borosilicate glasses *J. Am. Ceram. Soc.* **106** 293–305

[124] Swanson R, Stebbins J, Yeo T, Xu Y, Hung I, Gan Z, McCormack S and Sen S 2023 Structure and fragility of normal and invert lanthanum borate glasses: results from ^{11}B and ^{17}O NMR Spectroscopy and calorimetry *J. Non-Cryst. Solids* **603** 122119

[125] Topper B, Möncke D, Youngman R E, Valvi C, Kamitsos E I and Varsamis C P 2023 Zinc borate glasses: properties, structure and modelling of the composition-dependence of borate speciation *Phys. Chem. Chem. Phys.* **25** 5967–88

[126] Sharma S, Middha S, Khanna A, Chen B and Chen B 2024 Comparative study of Eu^{3+} doped calcium borate glasses and crystalline calcium hexaborate phosphors *J. Mater. Sci., Mater. Electron.* **35** 152

[127] Song L, Feller S, Hawbaker H, Yin W, Li W, Hannon A C, Zhou Y, Xu J and Zhu F 2024 Unveiling the structure of calcium borate glass by neutron diffraction, MAS-NMR, Raman and first-principles calculations *Ceram. Int.* **50** 6634–47

[128] Silver A H 1958 *Nuclear Quadrupole Effects in Boron Compounds* (Rensselaer Polytechnic Institute)

[129] Greenblatt S and Bray P 1967 A discussion of fraction of 4-Co-ordinated boron atoms present in borate glasses *Phys. Chem. Glasses* **8** 213

[130] Taylor P and Friebele E 1974 On the nature of unique boron sites in borate glasses *J. Non-Cryst. Solids* **16** 375–86

[131] Dell W and Bray P 1982 The determination of phase relations in the system MgO-B_2O_3 at the metaborate composition using B^{11} NMR *Phys. Chem. Glasses* **23** 126–8

[132] Bray P J, Lui M L and Hintenlang D E 1982 NMR studies of structure and ion motion in glasses *Wiss. Z.* **32** 409–26

[133] Imre A W, Voss S and Mehrer H 2004 Ionic conduction, diffusion and glass transition in $0.2[XNa_2O{\cdot}(1-X)Rb_2O]{\cdot}0.8B_2O_3$ *J. Non-Cryst. Solids* **333** 231–9

[134] Nijhawan S 2003 Glass transition temperature of the sodium borosilicate system and an analysis of the structure of rubidium borate glasses using NMR spectroscopy and transition temperatures *Honors Thesis* Coe College, Physics Department

[135] Moeller A, Olesiak M, Gao J, Giri S, Affatigato M, Feller S and Kodama M 2003 A solution approach to high potassium content borate glasses *Phys. Chem. Glasses* **44** 237–40

[136] Michaelis V K 2011 *Nuclear Magnetic Resonance Studies of Disorder and Local Structure in Borate and Germanate Materials* (University of Manitoba)

[137] Raguenet B, Tricot G, Silly G, Ribes M and Pradel A 2012 The mixed glass former effect in twin-roller quenched lithium borophosphate glasses *Solid State Ion.* **208** 25–30

[138] Christensen R 2012 The mixed glass former effect in 0.35 Na_2O+0.65[xB_2O_3+(1-x) P_2O_5] Glasses (available at: https://doi.org/10.31274/etd-180810-2218)

[139] Pytalev D, Caurant D, Majérus O, Trégouët H, Charpentier T and Mavrin B 2015 Structure and crystallization behavior of $La_2O_3{\cdot}3B_2O_3$ metaborate glasses doped with Nd^{3+} or Eu^{3+} ions *J. Alloys Compd.* **641** 43–55

[140] Tricot G, Saitoh A and Takebe H 2015 Intermediate length scale organisation in tin borophosphate glasses: new insights from high field correlation NMR *Phys. Chem. Chem. Phys.* **17** 29531–40

[141] Wang W, Christensen R, Curtis B, Hynek D, Keizer S, Wang J, Feller S, Martin S W and Kieffer J 2017 Elastic properties and short-range structural order in mixed network former glasses *Phys. Chem. Chem. Phys.* **19** 15942–52

[142] Zielniok D, Cramer C and Eckert H 2007 Structure/property correlations in ion-conducting mixed-network former glasses: solid-state NMR studies of the system Na_2O–B_2O_3– P_2O_5 *Chem. Mater.* **19** 3162–70

[143] Takaishi T, Jin J, Uchino T and Yoko T 2000 Structural study of PbO–B_2O_3 Glasses by X-ray diffraction and ^{11}B MAS NMR techniques *J. Am. Ceram. Soc.* **83** 2543–8

[144] Aguiar P M 2007 *Multinuclear Magnetic Resonance Investigations of Structure and Order in Borates and Metal Cyanides* (University of Manitoba)

[145] Nanba T, Nishimura M and Miura Y 2004 A theoretical interpretation of the chemical shift of ^{29}Si NMR peaks in alkali borosilicate glasses *Geochim. Cosmochim. Acta* **68** 5103–11

[146] Sasaki S, Masuno A, Yanaba Y, Inoue H and Ohkubo T 2024 Survival of fragmented BO_4 units in highly modified rare-earth-rich borate glasses *Inorg. Chem.* **63** 23131–40

[147] Youngman R E and Zwanziger J W 1995 On the formation of tetracoordinate boron in rubidium borate glasses *J. Am. Chem. Soc.* **117** 1397–402

[148] Brow R K, Tallant D R and Turner G L 1997 Polyhedral arrangements in lanthanum aluminoborate glasses *J. Am. Chem. Soc.* **80** 1239–44

[149] Youngman R E and Zwanziger J W 1996 Network modification in potassium borate glasses: structural studies with NMR and Raman spectroscopies *J. Phys. Chem.* **100** 16720–8

[150] Mustarelli P, Quartarone E and Benevelli F 1997 A ^{11}B and ^{7}Li MAS-NMR study of sol-gel lithium triborate glass subjected to thermal densification *Mater. Res. Bull.* **32** 679–87

[151] Terashima K, Shimoto T H and Yoko T 1997 Structure and nonlinear optical properties of PbO-Bi_2O_3-B_2O_3 glasses *Phys. Chem. Glasses* **38** 211–7

[152] Terashima K, Uchino T, Hashimoto T and Yoko T 1997 Structure and nonlinear optical properties of BaO-TiO_2-B_2O_3 glasses *J. Ceram. Soc. Japan* **105** 288–93

[153] Grishchuk E V, Efryushina N P, Dotsenko V P and Gubanova E R 1998 Structural study of fluoroborate glasses by NMR and IR-spectroscopy *Neorg. Mater.* **34** 520–2

[154] Wang S and Stebbins J F 1998 On the structure of borosilicate glasses: a triple-quantum magic-angle spinning ^{17}O nuclear magnetic resonance study *J. Non-Cryst. Solids* **321** 286–90

[155] Jung J K, Song S K, Noh T H and Han O H 2000 ^{11}B NMR investigations in xV_2O_5–B_2O_3 and xV_2O_5–B_2O_3–PbO glasses *J. Non-Cryst. Solids* **270** 97–102

[156] Wang D, Zhang J, Zhang D, Wan S, Zhang Q, Sun D and Yin S 2013 Structural investigation of Li_2O–B_2O_3–MoO_3 glasses and high-temperature solutions: toward understanding the mechanism of flux-induced growth of lithium triborate crystal *CrystEngComm* **15** 356–64

[157] Chialanza M R, Keuchkerian R, Cárdenas A, Olivera A, Vazquez S, Faccio R, Castiglioni J, Schneider J F and Fornaro L 2015 Correlation between structure, crystallization and thermally stimulated luminescence response of some borate glass and glass-ceramics *J. Non-Cryst. Solids* **427** 191–8

[158] Tokuda Y, Takahashi Y, Masai H, Kaneko S, Ueda Y, Fujimura S and Yoko T 2015 Local structure of alkalis in mixed-alkali borate glass to elucidate the origin of mixed-alkali effect *J. Asian Ceram. Soc.* **3** 412–6

[159] Osipov A A, Eremyashev V E, Mazur A S, Tolstoi P M and Osipova L M 2016 Coordination state of aluminum and boron in barium aluminoborate glass *Glass Phys. Chem.* **42** 230–7

[160] Song L, Wang Y, Zhai T, Sun B, Du Y, Feller S, Yin W, Xu J, Hannon A C and Zhu F 2025 Revealing the microstructure and structural origin of glass-forming range of magnesium borate glass *Ceram. Int.* **51** 18966–77

[161] Jellison G Jr and Bray P 1978 A structural interpretation of B^{10} and B^{11} NMR spectra in sodium borate glasses *J. Non-Cryst. Solids* **29** 187–206

[162] Yun Y and Bray P J 1981 B^{11} nuclear magnetic resonance studies of Li_2O-B_2O_3 glasses of high Li_2O content *J. Non-Cryst. Solids* **44** 227–37

[163] Terashima K, Hashimoto T, Uchino T, Kim S-H and Yoko T 1996 Structure and nonlinear optical properties of Sb_2O_3-B_2O_3 binary glasses *J. Ceram. Soc. Japan* **104** 1008–14

[164] Button D P, Tandon R, King C, Veléz M H, Tuller H L and Uhlmann D R 1982 Insights into the structure of alkali borate glasses *J. Non-Cryst. Solids* **49** 129–42

[165] Button D P, Tandon R P, Tuller H L and Uhlmann D R 1980 Fast Li^+ ion conduction in chloro-borate glasses *J. Non-Cryst. Solids* **42** 297–302

[166] Zhong J 1988 *Structural Aspects of Several Oxide Glasses as Elucidated by Multinuclear NMR* (Brown University)

[167] Voss S, Berkemeier F, Imre A W and Mehrer H 2004 Mixed-alkali effect of tracer diffusion and ionic conduction in Na-Rb borate glasses as a function of total alkali content *Z. Phys. Chem.* **218** 1353–74

[168] Christensen R, Byer J, Olson G and Martin S W 2012 The glass transition temperature of mixed glass former $0.35Na_2O + 0.65[xB_2O_3 + (1 - x)P_2O_5]$ glasses *J. Non-Cryst. Solids* **358** 826–31

[169] Trégouët H, Caurant D, Majérus O, Charpentier T, Lerouge T and Cormier L 2017 Exploration of glass domain in the SiO_2-B_2O_3-La_2O_3 system *J. Non-Cryst. Solids* **476** 158–72

[170] Jellison G E Jr. 1977 *Structural Determinations of Boron Oxide and Sodium Borate Glasses* (Brown University)

[171] Zhong J, Wu X, Liu M L and Bray P J 1988 Structural modeling of lithium borosilicate glasses via NMR studies *J. Non-Cryst. Solids* **107** 81–87

[172] Ring P J 1964 *A Nuclear Magnetic Resonance Study of Some Vitreous and Crystalline Lithium-Borates* (Brown University)

[173] Greenblatt S and Bray P 1967 Nuclear magnetic resonance investigations of system BaO-B_2O_3 *Phys. Chem. Glasses* **8** 190–3

[174] Park M and Bray P 1981 Determination of the structure of glasses in the MnO-B_2O_3 system using B^{11} NMR *J. Korean Phys. Soc.* **14** 67–74

[175] Harris I Jr and Bray P 1984 B^{11} NMR studies of zinc borate compounds and glasses *Phys. Chem. Glasses* **25** 69–75

[176] Yongxing T, Zhonghong J and Xiuyu S 1989 NMR, IR and raman spectra study of the structure of borate and borosilicate glasses *J. Non-Cryst. Solids* **112** 131–5

[177] Ratai E, Chan J C and Eckert H 2002 Local coordination and spatial distribution of cations in mixed-alkali borate glasses *Phys. Chem. Chem. Phys.* **4** 3198–208

[178] Aguiar P M and Kroeker S 2007 Boron speciation and non-bridging oxygens in high-alkali borate glasses *J. Non-Cryst. Solids* **353** 1834–9

[179] Feller S, Mullenbach T, Franke M, Bista S, O'Donovan-Zavada A, Hopkins K, Starkenberg D, McCoy J, Leipply D and Stansberry J 2012 Structure and properties of barium and calcium borosilicate glasses *Phys. Chem. Glasses* **53** 210–8

[180] Funke L M and Eckert H 2016 Charge compensation in sodium borophosphate glasses studied by ^{11}B $\{^{23}Na\}$ and ^{31}P $\{^{23}Na\}$ rotational echo double resonance spectroscopy *J. Phys. Chem. C* **120** 3196–205

[181] Ratai E-M, Janssen M, Epping J, Chan J and Eckert H 2003 Local and medium range order in alkali borate glasses: an overview of recent solid state NMR results *Phys. Chem. Glasses* **44** 45–53

[182] Harris I Jr and Bray P 1984 B^{11} nuclear magnetic resonance studies of borate glasses containing tellurium dioxide *Phys. Chem. Glasses* **25** 44–51

[183] Reser M K (ed) 1964 *Phase Diagrams for Ceramists* (The American Ceramic Society)

[184] Reser M K (ed) 1975 *Phase Diagrams for Ceramists (1975 Supplement)* (The American Ceramic Society)

[185] Sastry B S R and Hummel F A 1959 Studies in lithium oxide systems: v, Li_2O-$Li_2O{\cdot}B_2O_3$ *J. Am. Ceram. Soc.* **42** 216–8

[186] Yu H, Jin Z, Chen Q and Hillert M 2000 Thermodynamic assessment of the lithium-borate system *J. Am. Ceram. Soc.* **83** 3082–8

[187] Morey G W and Merwin H E 1936 Phase equilibrium relationships in the binary system, sodium oxide-boric oxide, with some measurements of the optical properties of the glasses *J. Am. Ceram. Soc.* **58** 2248–54

[188] Milman T and Bouaziz R 1968 Contribution à l'étude des borates de sodium *Ann. Chim.* **3** 311–2 as cited Reser M K (ed) 1975 *Phase Diagrams for Ceramists (1975 Supplement)* (The American Ceramic Society)

[189] Utlak S A and Besmann T M 2019 Thermodynamic assessment of the Na_2O-Al_2O_3-SiO_2-B_2O_3 pseudo-binary and -ternary systems *J. Chem. Thermodyn.* **130** 251–68

[190] Rollet A P 1935 Sur les borates de potassium: Étude du système K_2O-B_2O_3 *C. R. Hebd. Séances Acad. Sci.* **200** 1763–5

[191] Rollet A P 1936 Sur le polymorphisme du pentaborate de potassium $5B_2O_3.K_2O$ *C. R. Hebd. Séances Acad. Sci.* **202** 1863–6

[192] Toledano P 1964 Borates of potassium and rubidium *Rev. Chim. Miner.* **1** 353–413
as cited in Shaw R R and Uhlmann D R 1968 Subliquidus immiscibility in binary alkali borates *J. Am. Ceram. Soc.* **51** 377–82

[193] Kocher J 1966 Study of rubidium and cesium borates *Rev. Chim. Mineral.* **3** 209 as cited in Reser M K (ed) 1975 *Phase Diagrams for Ceramists (1975 Supplement)* (The American Ceramic Society)

[194] Bubnova R S, Polyakova I G, Filatov S K and Krzhizhanovskaya M G 1997 Crystal structure and thermal behavior of rubidium borates *Proc. 2nd Int. Conf. on Borate Glasses, Crystals, and Melts* (The Society of Glass Technology) pp 120–7

[195] Krogh-Moe J 1958 Some new compounds in the system cesium oxide-boron oxide *Ark. Kemi* **12** 247–9

[196] Rockett T J and Foster W R 1965 Phase relations in the system boron oxide–silica *J. Am. Ceram. Soc.* **48** 75–80

[197] Chen H M, Chen J M, Wang S, Li W T, Meng F G, Chen W J, Li L and Yao S J 2014 Thermodynamic assessment of B_2O_3-SiO_2 binary system *Appl. Mech. Mater.* **628** 68–72

[198] Baret G R, Madar R and Bernard C 1991 Silica-based oxide systems: I. Experimental and calculated phase equilibria in silicon, boron, phosphorus, germanium, and arsenic oxide mixtures *J. Electrochem. Soc.* **138** 2830–5

[199] Kocher J and Sadeghi N 1967 Sur les borates anhydres d'argent *C. R. Acad. SC. Paris C* **17** 1481–4

[200] Geller R F and Bunting E N 1937 The system PbO-B_2O_3 *J. Res. Natl Bur. Stand.* **18** 585–93

[201] Levin E M and McDaniel C L 1962 The system Bi_2O_3-B_2O_3 *J. Am. Ceram. Soc.* **45** 355–60

[202] Levin E M 1970 Liquid immiscibility in oxide systems *Phase Diagrams: Materials Science and Technology, Volume III* ed A M Alper (Academic) pp 143–270

[203] Davis H M and Knight M A 1945 The System Magnesium Oxide-Boric Oxide *J. Am. Ceram. Soc.* **28** 97–102

[204] Carlson E T 1932 The system CaO-B_2O_3 *J. Res. Natl Bur. Stand.* **9** 825–32

[205] Polyakova I G and Litovchik E O 2008 Crystallization of glasses in the SrO-B_2O_3 system *Glass Phys. Chem.* **34** 369–80

[206] Witzmann H and Beulich W 1963 Zur Bildung wasserfreier Strontiumborate. Ein Beitrag zum Zustandsdiagramm des Systems SrO-B_20_3 *Z. Phys. Chem.* **225** 336–41
as cited in Polyakova I G and Litovchik E O 2008 Crystallization of glasses in the SrO-B_2O_3 system *Glass Phys. Chem.* **34** 369–80

[207] Pam X M, Wang C and Jin Z P 2004 Assessment of the thermodynamics and phase diagram of the SrO-B_2O_3 system *Int. J. Mater. Res.* **95** 40–44

[208] Harrison D E and Hummel F A 1956 Phase equilibria and fluorescence in the system zinc oxide-boric oxide *J. Electrochem. Soc.* **103** 491–8

[209] Dimitriev Y and Kashchieva E 1975 Immiscibility in the TeO_2-B_2O_3 system *J. Mater. Sci.* **10** 1419–24

[210] Levin E M, Robbins C R and Waring J L 1961 Immiscibility and the system lanthanum oxide–boric oxide *J. Am. Ceram. Soc.* **44** 87–91

[211] Subbarao E C and Hummel F A 1956 The system cadmium oxide-boric oxide: I. Phase equilibria *J. Electrochem. Soc.* **103** 29–33

[212] Kim Y and Jung I 2015 Thermodynamic evaluation and optimization of the MnO-B_2O_3 and MnO-B_2O_3-SiO_2 systems and its application to oxidation of high-strength steels containing boron *Metall. Mater. Trans. A* **46A** 2736–47

[213] Penin N, Seguin L, Gérand B, Touboul M and Nowogrocki G 2001 β-$Tl_2B_4O_7$: compound containing a new three-dimensional borate anion *J. Solid State Chem.* **160** 139–46

[214] Wong J and Angell C A 1976 *Glass: Structure by Spectroscopy* (Marcel Dekker Inc.)

[215] Kamitsos E 2015 Infrared spectroscopy of glasses *Modern Glass Characterization* ed M Affatigato (The American Ceramic Society and John Wiley & Sons, Inc.) pp 32–73

[216] Almeida R M and Santos L F 2015 *Raman Spectroscopy of Glasses. In Modern Glass Characterization* ed M Affatigato (The American Ceramic Society and John Wiley & Sons, Inc) pp 74–106

[217] Weir C and Lippincott E R 1961 Infrared studies of aragonite, calcite, and vaterite type structures in the borates, carbonates, and nitrates *J. Res. Natl Bur. Stand.* **65** 173–83

[218] Hart P and Smallwood S 1962 An examination of the infra-red spectra of borate anions *J. Inorg. Nucl. Chem.* **24** 1047–56

[219] Weir C and Schroeder R 1964 Infrared spectra of the crystalline inorganic borates *J. Res. Natl Bur. Stand.* **68** 465–87

[220] Rulmont A and Almou M 1989 Vibrational spectra of metaborates with infinite chain structure: $LiBO_2$, CaB_2O_4, SrB_2O_4 *Spectrochim. Acta* **45** 603–10

[221] Chryssikos G D, Kapoutsis J, Patsis A and Kamitsos E 1991 A classification of metaborate crystals based on raman spectroscopy *Spectrochim. Acta* **47** 1117–26

[222] Anderson S, Bohon R L and Kimpton D D 1955 Infrared spectra and atomic arrangement in fused boron oxide and soda borate glasses *J. Am. Ceram. Soc.* **38** 370–7

[223] Jellyman P and Procter J 1955 Infrared reflection spectra of glasses *J. Soc. Glass Technol.* **39** 173–92T

[224] Moore H 1956 A study of glasses consisting of the oxides of elements of low atomic weight. Part II. The absorption characteristics of certain of the experimental glasses *J. Soc. Glass Technol.* **40** 97T–138T

[225] Parsons J and Milberg M 1960 Vibrational spectra of vitreous $B_2O_3.xH_2O$ *J. Am. Ceram. Soc.* **43** 326–30

[226] Krogh-Moe J 1965 Interpretation of infrared spectra of boron oxide and alkali borate glasses *Phys. Chem. Glasses* **2** 46–54

[227] Krogh-Moe J 1969 The structure of vitreous and liquid boron oxide *J. Non-Cryst. Solids* **1** 269–84

[228] Goubeau J and Keller H 1953 Raman-Spektren Und Struktur von Boroxol-Verbindungen *Z. Anorg. Allg. Chem.* **272** 303–12

[229] Bril T 1976 Raman spectroscopy of crystalline and glassy borates *Philips Res. Rep.* **2** 1–114

[230] Galeener F L, Lucovsky G and Mikkelsen J Jr 1980 Vibrational spectra and the structure of pure vitreous B_2O_3 *Phys. Rev. B* **22** 3983–90

[231] Windisch C F Jr and Risen W M Jr 1982 Vibrational Spectra of oxygen-and boron-isotopically substituted B_2O_3 glasses *J. Non-Cryst. Solids* **48** 307–23

[232] Konijnendijk W L and Stevels J 1975 The structure of borate glasses studied by Raman scattering *J. Non-Cryst. Solids* **18** 307–31

[233] Tatsumisago M, Takahashi M, Minami T, Tanaka M, Umesaki N and Iwamoto N 1986 Structural investigation of rapidly quenched Li_2O-B_2O_3 glasses by Raman spectroscopy *Yogyo Kyokaishi* **94** 464–9

[234] Kamitsos E, Karakassides M and Chryssikos G D 1987 Vibrational spectra of magnesium-sodium-borate glasses. 2. Raman and mid-infrared investigation of the network structure *J. Phys. Chem.* **91** 1073–9

[235] Kamitsos E I, Patsis A, Karakassides M and Chryssikos G D 1990 Infrared reflectance spectra of lithium borate glasses *J. Non-Cryst. Solids* **126** 52–67

[236] Kamitsos E I and Chryssikos G D 1991 Borate glass structure by Raman and infrared spectroscopies *J. Mol. Struct.* **247** 1–16

[237] Möncke D, Tricot G, Winterstein-Beckmann A, Wondraczek L and Kamitsos E I 2015 On the connectivity of borate tetrahedra in borate and borosilicate glasses *Phys. Chem. Glasses* **56** 203–11

[238] Griscom D L 1978 Borate glass structure *Borate Glasses: Structure, Properties, Applications* ed L D P Plenum, V D Frechette and N J Kreidl (Springer) pp 11–149

[239] Minami T and Tanaka M 1980 Structure and ionic transport of superionic conducting glasses in the system AgI-Ag_2O-MoO_3 *J. Non-Cryst. Solids* **38** 289–94

[240] Merzbacher C I and White W B 1988 Structure of Na in aluminosilicate glasses; a far-infrared reflectance spectroscopic study *Am. Mineral.* **73** 1089–94

[241] Merzbacher C I and White W B 1991 The structure of alkaline earth aluminosilicate glasses as determined by vibrational spectroscopy *J. Non-Cryst. Solids* **130** 18–34

[242] Liu C and Angell C 1990 Mid-and far-infrared absorption of alkali borate glasses and the limit of superionic conductivity *J. Chem. Phys.* **93** 7378–86

[243] Berreman D 1963 Infrared absorption at longitudinal optic frequency in cubic crystal films *Phys. Rev.* **130** 2193–8

[244] (a) Varsamis C, Kamitsos E I and Chryssikos G D 1999 Structure of fast-ion-conducting AgI-doped borate glasses in bulk and thin film forms *Phys. Rev. B* **60** 3885–98
(b) Kamitsos E I, Dussauze M, Varsamis C P E, Vinatier P and Hamon Y 2007 Thin film amorphous electrolytes: structure and composition by experimental and simulated infrared spectra *J. Phys. Chem. C* **111** 8111–9

[245] Amma S, Luo J, Pantano C G and Kim S H 2015 Specular reflectance (SR) and attenuated total reflectance (ATR) infrared (IR) spectroscopy of transparent flat glass surfaces: a case study for soda lime float glass *J. Non-Cryst. Solids* **428** 189–96

[246] Kamitsos E I, Patsis A and Chryssikos G D 1993 Infrared reflectance investigation of alkali diborate glasses *J. Non-Cryst. Solids* **152** 246–57

[247] Chryssikos G D, Kapoutsis J, Kamitsos E, Patsis A and Pappin A 1994 Lithium-sodium metaborate glasses: structural aspects and vitrification chemistry *J. Non-Cryst. Solids* **167** 92–105

[248] Chatzipanagis K, Tagiara N S, Möncke D, Kundu S, Rodrigues A and Kamitsos E I 2020 Vibrational study of lithium borotellurite glasses *J. Non-Cryst. Solids* **540** 120011

[249] Feller S A 1980 *Lithium-7, Boron-10, Boron-11, and Oxygen-17 Nuclear Magnetic Resonance Studies of Lithium Borate Glasses and Related Compounds* (Brown University)

[250] Feller S A, Dell W J and Bray P J 1982 ^{10}B NMR studies of lithium borate glasses *J. Non-Cryst. Solids* **51** 21–30

[251] Tatsumisago M, Shinkuma Y, Saito T and Minami T 1992 Formation of frozen α-AgI in superionic glass matrices at ambient temperature by rapid quenching *Solid State Ion* **50** 273–9

[252] Kowada Y, Adachi H, Tatsumisago M and Minami T 1998 Electronic states of Ag ions in AgI-based superionic conducting glasses *J. Non-Cryst. Solids* **232–234** 497–501

[253] Kapoutsis J A 1997 A structural study of silver borate glasses by infrared reflectance and Raman spectroscopies *Proc. 2nd Int. Conf. on Borate Glasses, Crystals and Melts* (*Sheffield, UK*) ed A C Wright, S A Feller and A C Hannon pp 303–12

[254] Wright A C, Sinclair R N, Stone C E, Shaw J L, Feller S A, Kiczenski T, Williams R B, Berger H A, Fischer H E and Vedishcheva N M 2012 A neutron diffraction study of $2M_2O.5B_2O_3$ (M = Li, Na, K, Rb, Cs & Ag) and $2MO.5B_2O_3$ (M= Ca & Ba) glasses *Phys. Chem. Glasses* **53** 191–204

[255] Yiannopoulos Y D, Kamitsos E I, Chryssikos G D and Kapoutsis J A 1997 A vibrational spectroscopic study of alkaline earth borate glasses *Proc. 2nd Int. Conf. on Borate Glasses, Crystals and Melts* (*Sheffield, UK*) ed A C Wright, S A Feller and A C Hannon pp 514–21

[256] Yiannopoulos Y, Chryssikos G D and Kamitsos E 2001 Structure and properties of alkaline earth borate glasses *Phys. Chem. Glasses* **42** 164–72

[257] Ohtori N, Takase K, Akiyama I, Suzuki Y, Handa K, Sakai I, Iwadate Y, Fukunaga T and Umesaki N 2001 Short-range structure of alkaline-earth borate glasses by pulsed neutron diffraction and molecular dynamics simulation *J. Non-Cryst. Solids* **293** 136–45

[258] Alderman O L G, Benmore C, Holland D and Weber J 2023 Boron coordination change in barium borate melts and glasses and its contribution to configurational heat capacity, entropy, and fragility *J. Chem. Phys.* **158** 224501

[259] (a) Dietzel A 1942 Die Kationenfeldstärken Und Ihre Beziehungen Zu Entglasungsvorgängen, Zur Verbindungsbildung Und Zu Den Schmelzpunkten von Silicaten *Z. Elektrochem. Angew. Phys. Chem.* **48** 9–23
(b) Dietzel A H 1983 On the So-called mixed alkali effect *Phys. Chem. Glasses* **24** 172–180

[260] Shannon R D 1976 Revised effective ionic radii and systematic studies of interatomic distances in halides and chalcogenides *Acta Crystallogr. A* **32** 751–67

[261] Lv P, Wang C, Stevensson B, Yu Y, Wang T and Eden M 2022 Impact of the cation field strength on physical properties and structures of alkali and alkaline-earth borosilicate glasses *Ceram. Int.* **48** 18094–107

[262] Makris N, Varsamis C and Kamitsos E I 2008 Structural investigation of lead borate glasses by infrared reflectance spectroscopy *Proc. 24th Panhellenic Conf. in Solid State Physics* pp 44–45

[263] Vedishcheva N, Shakhmatkin B, Wright A, Sinclair R and Grimley D 1992 A combined thermodynamic and neutron scattering investigation of glasses in the system PbO-B_2O_3 *Bol. Soc. Esp. Ceram. V* **31-C** 41–46

[264] Ushida H, Iwadate Y, Hattori T, Nishiyama S, Fukushima K, Ikeda Y, Yamaguchi M, Misawa M, Fukunaga T and Nakazawa T 2004 Network structure of B_2O_3–PbO and B_2O_3–PbO–$PbBr_2$ glasses analyzed by pulsed neutron diffraction and Raman spectroscopy *J. Alloys Compd.* **377** 167–73

[265] Krishnamurthy A, Wren J E, Michaelis V K and Kroeker S 2024 Composition-dependent structural role of lead in aluminoborate and galloborate glasses: a solid-state NMR study *J. Am. Ceram. Soc.* **107** 4522–35

[266] Möncke D, Kamitsos E I, Palles D, Limbach R, Winterstein-Beckmann A, Honma T, Yao Z, Rouxel T and Wondraczek L 2016 Transition and post-transition metal ions in borate glasses: borate ligand speciation, cluster formation, and their effect on glass transition and mechanical properties *J. Chem. Phys.* **145** 124501

[267] Ganguli M and Rao K 1999 Studies on the effect of Li_2SO_4 on the structure of lithium borate glasses *J. Chem. Phys.* **103** 920–30

[268] Liu H, Shen G, Wang X, Wei J and Shen D 2000 Viscosity and IR investigations in the Li_2O-B_2O_3 system *Prog. Cryst. Growth Charact. Mater.* **40** 235–41

[269] Kashif I, Salem S, Soliman A, Farouk H, Mostafa A, Salah S and Sanad A M 2006 Infrared and magnetic susceptibility studies of iron sodium borate glasses doped by sulphur *J. Phys. Chem. Solids* **67** 2370–5

[270] Doweidar H and Saddeek Y B 2009 FTIR and ultrasonic investigations on modified bismuth borate glasses *J. Non-Cryst. Solids* **355** 348–54

[271] Gaafar M, Abd El-Aal N, Gerges O and El-Amir G 2009 Elastic properties and structural studies on some zinc-borate glasses derived from ultrasonic, FT-IR and x-ray techniques *J. Alloys Compd.* **475** 535–42

[272] Pascuta P 2010 Structural investigations of some bismuth–borate–vanadate glasses doped with gadolinium ions *J. Mater. Sci., Mater. Electron.* **21** 338–42

[273] Kaur A, Khanna A, Bhatt H, Gónzález-Barriuso M, González F, Chen B and Deo M 2017 BO and TeO speciation in bismuth tellurite and bismuth borotellurite glasses by FTIR, ^{11}B MAS-NMR and Raman spectroscopy *J. Non-Cryst. Solids* **470** 19–26

[274] Kaur R, Khanna A, González-Barriuso M, González F and Chen B 2018 Structural, optical and thermal properties of glass and anti-glass phases in strontium tellurite and borotellurite systems doped with europium *Mater. Res. Bull.* **106** 288–95

[275] Osipova L, Osipov A and Osipov A 2019 The structure of binary and iron-containing ZnO–B_2O_3 glass by IR, Raman, and Mössbauer spectroscopy *Glass Phys. Chem.* **45** 182–90

[276] Ihara R, Honma T, Benino Y, Fujiwara T and Komatsu T 2004 Second-order optical nonlinearities of metastable $BiBO_3$ phases in crystallized glasses *Opt. Mater.* **27** 403–8

[277] Dong M, Sayyed M, Lakshminarayana G, Ersundu M Ç, Ersundu A, Nayar P and Mahdi M 2017 Investigation of gamma radiation shielding properties of lithium zinc bismuth borate glasses using XCOM program and MCNP5 code *J. Non-Cryst. Solids* **468** 12–16

[278] Varsamis C-P E, Makris N, Valvi C and Kamitsos E I 2021 Short-range structure, The Role Of Bismuth and property–structure correlations In Bismuth borate glasses *Phys. Chem. Chem. Phys.* **23** 10006–20

[279] (a) Stehle C, Vira C, Hogan D, Feller S and Affatigato M 1998 Optical and physical properties of bismuth borate glasses related to structure *Phys. Chem. Glasses* **39** 83–86
(b) George H, Vira C, Stehle C, Meyer J, Evers S, Hogan D, Feller S and Affatigato M A 1999 Structural analysis of the physical properties of bismuth and lead based glasses *Phys. Chem. Glasses* **40** 326–32

[280] Topper B, Tagiara N S, Herrmann A, Kamitsos E I and Möncke D 2022 Yttrium and rare-earth modified lithium orthoborates: glass formation and vibrational activity *J. Non-Cryst. Solids* **575** 121152

[281] Lower N P, Mcrae J L, Feller H A, Betzen A R, Kapoor S, Affatigato M and Feller S A 2001 Physical properties and alkaline-earth and alkali borate glasses prepared over an extended range of composition *J. Non-Cryst. Solids* **293–295** 669–75

[282] Kamitsos E I and Karakassides M 1989 Structural studies of binary and pseudo binary sodium borate glasses of high sodium content *Phys. Chem. Glasses* **30** 19–26

[283] Zhong J and Bray P J 1986 NMR study of structure of sodium boroaluminate glass at high sodium content *J. Non-Cryst. Solids* **84** 17–25

[284] (a) Yano T, Kunimine N, Shibata S and Yamane M 2003 Structural investigation of sodium borate glasses and melts by Raman spectroscopy.: I. Quantitative evaluation of structural units *J. Non-Cryst. Solids* **321** 137–46
(b) Yano T, Kunimine N, Shibata S and Yamane M 2003 Structural investigation of sodium borate glasses and melts by Raman Spectroscopy. II. Conversion between BO_4 and BO_2O^- units at high temperature *J. Non-Cryst. Solids* **321** 147–56

[285] Chryssikos G D, Kamitsos E I and Karakassides M A 1990 Structure of borate glasses. Part 2: the alkali-induced network modification schemes in terms of structure and properties *Phys. Chem. Glasses* **31** 109–16

[286] Araujo R 1983 Statistical mechanics of chemical disorder: application to alkali borate glasses *J. Non-Cryst. Solids* **58** 201–8

[287] Stebbins J F and Ellsworth S E 1996 Temperature effects on structure and dynamics in borate and borosilicate liquids: high-resolution and high-temperature NMR results *J. Am. Ceram. Soc.* **79** 2247–56

[288] Akagi R, Ohtori N and Umesaki N 2001 Raman spectra of K_2O–B_2O_3 glasses and melts *J. Non-Cryst. Solids* **293** 471–6

[289] Osipova L, Osipov A and Bykov V 2007 Structure of high-alkali melts in the lithium borate system from vibrational spectroscopic data *Glass Phys. Chem.* **33** 486–91

[290] Cormack A and Park B 2000 Molecular dynamics simulations of borate glasses *Phys. Chem. Glasses* **41** 272–7

[291] Varsamis C-P E, Vegiri A and Kamitsos E I 2002 Molecular dynamics investigation of lithium borate glasses: local structure and ion dynamics *Phys. Rev. B* **65** 104203

[292] Majérus O, Cormier L, Calas G and Beuneu B 2003 Temperature-induced boron coordination change in alkali borate glasses and melts *Phys. Rev. B* **67** 024210

[293] Cormier L, Majérus O, Neuville D and Calas G 2006 Temperature-induced structural modifications between alkali borate glasses and melts *J. Am. Ceram. Soc.* **89** 13–19

[294] Alderman O L, Benmore C J, Lin A, Tamalonis A and Weber J R 2018 Borate melt structure: temperature-dependent B–O bond lengths and coordination numbers from high-energy x-ray diffraction *J. Am. Ceram. Soc.* **101** 3357–71

[295] Alderman O L G, Benmore C and Weber J 2020 Consequences of sp^2–sp^3 boron isomerization in supercooled liquid borates *Appl. Phys. Lett.* **117** 131901

[296] Warren B 1934 The diffraction of x-rays in glass *Phys. Rev.* **45** 657

[297] Warren B 1940 X-ray diffraction study of the structure of glass *Chem. Rev.* **26** 237–55

[298] Biscoe J, Pincus A, Smith C Jr and Warren B 1941 X-ray study of lime-phosphate and lime-borate glass *J. Am. Ceram. Soc.* **24** 116–9

[299] Green R L 1942 X-ray diffraction and physical properties of potassium borate glasses *J. Am. Ceram. Soc.* **25** 83–89

[300] Mozzi R and Warren B 1969 The structure of vitreous silica *J. Appl. Crystallogr.* **2** 164–72

[301] Mozzi R L and Warren B 1970 The structure of vitreous boron oxide *J. Appl. Crystallogr.* **3** 251–7

[302] Neuefeind J and Poulsen H 1995 Diffraction on disordered materials using "neutron-like" photons *Phys. Scr.* **1995** 112

[303] Poulsen H, Neuefeind J, Neumann H-B, Schneider J and Zeidler M 1995 Amorphous silica studied by high energy x-ray diffraction *J. Non-Cryst. Solids* **188** 63–74

[304] Yasui I, Hasegawa H and Saito Y 1988 Structure of borate glasses containing Tl and Ba oxide *J. Non-Cryst. Solids* **106** 30–33

[305] Yasui I, Hasegawa H, Saito Y and Akasaka Y 1990 Structure of borate glasses containing heavy metal ions *J. Non-Cryst. Solids* **123** 71–74

[306] Vedishcheva N M, Shakhmatkin B A, Wright A C, Grimley D I, Etherington G and Sinclair R N 1993 Structural order in lead borate glasses: a test of recent thermodynamic predictions *In Fundamentals of Glass*

Science and Technology; Stazione Sperimentale del Vetro: Murano, Venice, 1993 459–62
[307] Wright A, Sinclair R, Crimley D, Hulme R, Vedishcheva N, Shakhmatkin B, Hannon A, Feller S, Meyer B and Royle M 1996 Borate glasses, superstructural units and the random network theory 1 *Glass Phys. Chem.* **22** 268–78
[308] Kita Y, Misawa M, Umesaki N, Kirihara T, Fukunaga T and Iida T 1993 Structural analysis of Na_2O-B_2O_3 melts by pulsed neutron total scattering method and molecular dynamics simulation *ISIJ Int.* **33** 188–94
[309] Herms G, Sakowski J, Gerike W and Stachel D 1998 Structural changes in two different types of oxide glass melts: borates and metaphosphates *Z. Naturforsch. A* **53** 874–82
[310] Herms G and Sakowski J 2000 X-ray diffraction studies of structural changes in molten borate glasses *Phys. Chem. Glasses* **41** 309–12
[311] Alderman O L G, Liska M, Machacek J, Benmore C, Lin A, Tamalonis A and Weber J 2016 Temperature-driven structural transitions in molten sodium borates Na_2O–B_2O_3: x-ray diffraction, thermodynamic modeling, and implications for topological constraint theory *J. Phys. Chem. C* **120** 553–60
[312] Alderman O L G, Benmore C J, Reynolds B, Royle B, Feller S and Weber R J 2023 Liquid fragility maximum in lithium borate glass-forming melts related to the local structure *Int. J. Appl. Glass. Sci.* **14** 52–68
[313] Hoppe U, Walter G, Barz A, Stachel D and Hannon A 1998 The PO bond lengths in vitreous P_2O_5 probed by neutron diffraction with high real-space resolution *J. Phys.: Condens. Matter* **10** 261
[314] Brown I D and Altermatt D 1985 Bond-valence parameters obtained from a systematic analysis of the inorganic crystal structure database *Acta Crystallogr. B* **41** 244–7
[315] Alderman O L G, Ferlat G, Baroni A, Salanne M, Micoulaut M, Benmore C, Lin A, Tamalonis A and Weber J 2015 Liquid B_2O_3 up to 1700 K: x-ray diffraction and boroxol ring dissolution *J. Phys.: Condens. Matter* **27** 455104
[316] Suzuya K, Yoneda Y, Kohara S and Umesaki N 2000 High energy X-ray study of the structure of vitreous B_2O_3 *Phys. Chem. Glasses* **41** 282–5
[317] Gurr G, Montgomery P, Knutson C and Gorres B 1970 The crystal structure of trigonal diboron trioxide *Acta Crystallogr. B* **26** 906–15
[318] Warren B, Krutter H and Morningstar O 1936 Fourier analysis of x-ray patterns of vitreous SiO_2 and B_2O_2 *J. Am. Ceram. Soc.* **19** 202–6
[319] Sugiyama K, Nomura K and Kimura S 1995 X-ray diffraction study on the structure of liquid Li_2O-B_2O_3 *High Temp. Mater. Process.* **14** 131–6
[320] Kajinami A, Kotake T, Deki S and Kohara S 2003 The structural analysis of manganese borate glass by high-energy x-ray diffraction measurement *Nucl. Instrum. Methods Phys. Res. B* **199** 34–37
[321] Brazhkin V, Katayama Y, Trachenko K, Tsiok O, Lyapin A, Artacho E, Dove M, Ferlat G, Inamura Y and Saitoh H 2008 Nature of the structural transformations in B_2O_3 glass under high pressure *Phys. Rev. Lett.* **101** 035702
[322] Johnson P A, Wright A C and Sinclair R N 1982 A neutron diffraction investigation of the structure of vitreous boron trioxide *J. Non-Cryst. Solids* **50** 281–311
[323] Misawa M 1990 Structure of vitreous and molten B_2O_3 measured by pulsed neutron total scattering *J. Non-Cryst. Solids* **122** 33–40
[324] Hannon A C, Barney E R and Holland D 2009 The structure of tin borate based glasses *Phys. Chem. Glasses* **50** 271–83
[325] Zeidler A, Wezka K, Whittaker D A, Salmon P S, Baroni A, Klotz S, Fischer H E, Wilding M C, Bull C L and Tucker M G 2014 Density-driven structural transformations in B_2O_3 glass *Phys. Rev. B* **90** 024206
[326] Alderman O L G 2025 Boroxol ring dissolution in molten and glassy B_2O_3 by neutron and x-ray diffraction difference methods *J. Chem. Phys.* **162** 054502
[327] Lelong G, Cormier L, Hennet L, Michel F, Rueff J-P, Ablett J M and Monaco G 2021 Lithium borates from the glass to the melt: a temperature-induced structural transformation viewed from the boron and oxygen atoms *Inorg. Chem.* **60** 798–806
[328] Wright A C, Sinclair R N, Stone C E, Shaw J L, Feller S A, Williams R B, Fischer H E and Vedishcheva N M 2014 A neutron diffraction study of sodium, rubidium and cæsium borate glasses *Phys. Chem. Glasses* **55** 74–84
[329] Swenson J, Börjesson L and Howells W 1995 Structure of borate glasses from neutron-diffraction experiments *Phys. Rev. B* **52** 9310
[330] Cormier L, Calas G and Beuneu B 2009 Quantification of boron coordination changes between lithium borate glasses and melts by neutron diffraction *Phys. Chem. Glasses* **50** 195–200
[331] Suzuki Y, Ohtori N, Takase K, Handa K, Itoh K, Fukunaga T and Umesaki N 2003 Pulsed neutron diffraction studies of $RO.xB_2O_3$ glasses: r=Ca, Sr and Ba; X=2, 3 and 4 *Phys. Chem. Glasses* **44** 150–4
[332] Handa K, Kita Y, Kohara S, Suzuya K, Fukunaga T, Misawa M, Iida T, Iwasaki H and Umesaki N 1999 Structure of M_2O–B_2O_3 (M: na and K) glasses and melts by neutron diffraction *J. Phys. Chem. Solids* **60** 1465–71
[333] Cormier L, Calas G and Beuneu B 2007 Structure of single and mixed alkali Li–Rb borate glasses by neutron diffraction *J. Non-Cryst. Solids* **353** 1779–84
[334] Shaw J, Wright A, Sinclair R, Frueh J, Williams R, Nelson N, Affatigato M, Feller S and Scales C 2003 A neutron diffraction investigation of the structure of caesium borate glasses *Phys. Chem. Glasses* **44** 256–9
[335] Kajinami A, Harada Y, Inoue S, Deki S and Umesaki N 1999 The structural analysis of zinc borate glass by laboratory EXAFS and x-ray diffraction measurements *Jpn. J. Appl. Phys.* **38** 132
[336] Youngman R E, Cornelius L K, Koval S E, Hogue C L and Ellison A J 2009 Structure–property studies of $SrBr_2$–SrO–B_2O_3 glasses *Phys. Chem. Glasses* **50** 175–82
[337] Matsumura S, Watanabe M, Mizuno A and Kohara S 2007 Supercooled barium boric oxide melts: x-ray diffraction measurements and glass formation *J. Am. Ceram. Soc.* **90** 742–5
[338] Gejke C, Swenson J, Delaplané R and Börjesson L 2002 Neutron diffraction study of microscopic structure of SnB_2O_4 glass *Phys. Rev. B* **65** 212201
[339] Holland D, Smith M, Howes A, Davies T and Barrett L 2003 Influence of the borate anomaly on the Sn (II) environment in tin borate glasses *Phys. Chem. Glasses* **44** 59–63
[340] Hayashi A, Nakai M, Tatsumisago M and Minami T 2002 Structure and properties of glasses in the system Li_2O–SnO–B_2O_3 *C. R. Chim.* **5** 751–7
[341] Wright A C, Etherington G, Feller S A, Gnappi G, Grimley D, Montenero A, Sinclair R N and Stone C 2002 Neutron diffraction studies of binary network glasses containing PbO and Bi_2O_3 *Glass Sci. Technol.* **75** 139–44
[342] Orman R G 2010 Characterisation of novel antimony (III) oxide-containing glasses (University of Warwick) (available at: https://pugwash.lib.warwick.ac.uk/record=b2334501~S15)
[343] Stone C, Wright A, Sinclair R, Feller S, Affatigato M, Hogan D, Nelson N, Vira C, Dimitriev Y and Gattef E

2000 Structure of bismuth borate glasses *Phys. Chem. Glasses* **41** 409–12
[344] (a) Tagiara N S, Palles D, Simandiras E D, Psycharis V, Kyritsis A and Kamitsos E I 2017 Synthesis, thermal and structural properties of pure TeO_2 glass and zinc-tellurite glasses *J. Non-Cryst. Solids* **457** 116–25
(b) Tagiara N S, Moayedi E, Kyritsis A, Wondraczek L and Kamitsos E I 2019 Short-range structure, thermal and elastic properties of binary and ternary tellurite glasses *J. Phys. Chem. B* **123** 7905−18
(c) Papadopoulos A G, Tagiara N S, Simandiras E D and Kamitsos E I 2020 On the absence of doubly bonded Te=O groups in TeO_2 glass *J. Phys. Chem. B* **124** 5746−53
[345] Milberg M and Meller F 1959 Structure of vitreous $B_2O_3 \cdot {}^1/_3H_2O$ *J. Chem. Phys.* **31** 126–9
[346] Meller F and Milberg M 1960 The structure of some B_2O_3-H_2O glasses *J. Am. Ceram. Soc.* **43** 353–6
[347] Brüning R and Patterson S 2003 Thermal and structural properties of B_2O_3–H_2O glasses *J. Mater. Res.* **18** 2494–500
[348] Brüning R, Galbraith J B, Braedley K E, Johnstone J, Robichaud J, Balaji S and Djaoued Y 2010 X-ray diffraction and micro-raman study of structural transformations in $(B_2O_3)_{1-x}(H_2O)_x$ glasses and liquids *J. Am. Ceram. Soc.* **93** 3745–51
[349] Wright A C 2018 The structural chemistry of B_2O_3 *Phys. Chem. Glasses* **59** 65–87
[350] Sen S 1999 Temperature induced structural changes and transport mechanisms in borate, borosilicate and boroaluminate liquids: high-resolution and high-temperature NMR results *J. Non-Cryst. Solids* **253** 84–94
[351] Alderman O L G 2018 Borate melt structure: a short review *Phys. Chem. Glasses* **59** 1–10
[352] Li D, Bancroft G, Fleet M, Hess P and Yin Z 1995 Coordination of B in K_2O-SiO_2-B_2O_3-P_2O_5 glasses using BK-edge XANES *Am. Mineral.* **80** 873–7
[353] Fleet M and Muthupari S 1999 Coordination of boron in alkali borosilicate glasses using XANES *J. Non-Cryst. Solids* **255** 233–41
[354] Yamamoto K, Fujita M, Tsuji J, Kojima K, Wada N, Taniguchi K, Ikeda S and Perera R 2001 Boron K-edge x-ray absorption and emission spectroscopic studies in sodium borate glasses *Mem. SR Cent. Ritsumeikan Univ.* **3** 15–20
[355] Lee S K, Eng P J, Mao H and Shu J 2008 Probing and modeling of pressure-induced coordination transformation in borate glasses: inelastic x-ray scattering study at high pressure *Phys. Rev. B* **78** 214203
[356] Lee S K, Eng P J, Mao H, Meng Y and Shu J 2007 Structure of alkali borate glasses at high pressure: B and Li K-edge inelastic x-ray scattering study *Phys. Rev. Lett.* **98** 105502
[357] Brazhkin V, Farnan I, Funakoshi K, Kanzaki M, Katayama Y, Lyapin A and Saitoh H 2010 Structural transformations and anomalous viscosity in the B_2O_3 melt under high pressure *Phys. Rev. Lett.* **105** 115701
[358] Buscemi M 2019 *Investigation of Boro-Germanate and Germanium Disulfide Glasses: Relation between Structure and Properties* (University of Bath)
[359] Sasaki S, Masuno A, Ohara K, Yanaba Y, Inoue H, Watanabe Y and Kohara S 2020 Structural origin of additional infrared transparency and enhanced glass-forming ability in rare-earth-rich borate glasses without B–O networks *Inorg. Chem.* **59** 13942–51
[360] Shannon R T and Prewitt C 1970 Revised values of effective ionic radii *Acta Crystallogr. B* **26** 1046–8
[361] Shannon R T and Prewitt C T 1969 Effective ionic radii in oxides and fluorides *Acta Crystallogr. B* **25** 925–46
[362] Dronskowski R 2006 Computational chemistry of solid state materials *Mater. Today* **9** 53
[363] Barney E R, Hannon A C, Laorodphan N and Holland D 2011 Influence of lone-pair cations on the germanate anomaly in glass *J. Phys. Chem. C* **115** 14997–5007
[364] Hannon A C, Vaishnav S, Alderman O L G and Bingham P A 2021 The structure of sodium silicate glass from neutron diffraction and modeling of oxygen-oxygen correlations *J. Am. Ceram. Soc.* **104** 6155–71
[365] Hoppe U, Walter G, Kranold R and Stachel D 2000 Structural specifics of phosphate glasses probed by diffraction methods: a review *J. Non-Cryst. Solids* **263** 29–47
[366] Baugher J and Bray P 1972 B^{11} NMR in germanium borate glasses *Phys. Chem. Glasses* **13** 63
[367] Schurko R W 2013 Ultra-wideline solid-state NMR spectroscopy *Acc. Chem. Res.* **46** 1985–95
[368] Pell A J, Pintacuda G and Grey C P 2019 Paramagnetic NMR in solution and the solid state *Prog. Nucl. Magn. Reson. Spectrosc.* **111** 1–271
[369] Pell A J and Pintacuda G 2015 Broadband solid-state MAS NMR of paramagnetic systems *Prog. Nucl. Magn. Reson. Spectrosc.* **84** 33–72
[370] Stebbins J F, McCarty R J and Palke A C 2018 Toward the wider application of ^{29}Si NMR spectroscopy to paramagnetic transition metal silicate minerals and glasses: Fe (II), Co (II), and Ni (II) Silicates *Am. Mineral.* **103** 776–91
[371] Zhu F, Bowron D T, Gärtner S, Fang C, Zhou Y, Liu H and Hannon A C 2023 Structural analysis of potassium borate solutions *Phys. Chem. Chem. Phys.* **25** 12207–19
[372] Laorodphan N, Pooddee P, Kidkhunthod P, Kunthadee P, Tapala W and Puntharod R 2016 Boron and pentavalent vanadium local environments in binary vanadium borate glasses *J. Non-Cryst. Solids* **453** 118–24
[373] Vedishcheva N M and Wright A C 2014 *Glass: Selected Properties and Crystallization* ed J W P Schmelzer (de Gruyter) pp 269–99
[374] Lee S K, Kim H N, Lee B H, Kim H I and Kim E J 2010 Nature of chemical and topological disorder in borogermanate glasses: insights from B-11 and O-17 solid-state NMR and quantum chemical calculations *J. Phys. Chem. B* **114** 412–20